Explorations of Neurobiology with Analogue Integrated Circuits: Ion Channels and Intraneuronal Adaptation

Catherine J. Breslin

Thesis submitted for the degree of

Doctor of Philosophy

The University of Edinburgh

September 1998

Declaration

I declare that this thesis has been composed by myself and that, except where indicated to the contrary, the research documented is my own.

Catherine Breslin

Abstract

One method for exploring neurobiology is to build analogue integrated circuits which are then used as models for developing and testing theories of the brain. The original motivation for the use of analogue integrated circuits was the concept of a physical equivalence between field-effect transistors operating in the weak-inversion region and ion channels permitting ion conductance through the neuronal membrane. The concept of physical equivalence is examined, with respect to both the physical processes occurring in ion channels and transistors and the equivalences that can be found between neurobiology and models of neurobiology. Changes in ion conductance are the basis for the transmission of electrical impulses in neurons and nervous systems. For the transmission to benefit, or at least not harm, the chances of survival for the organism's genetic material, it must be capable of adapting to changing environment. It has been suggested that ion channels undergoing electrokinesis along the neuronal membrane are a component of intraneuronal adaptation. Analogue integrated circuitry is built to represent the neuronal membrane, a population of dendritic N-type Ca^{++} channels and intraneuronal adaptation. This is used to link the electrokinesis theory with recent observations of ion channel behaviour, specifically the ion channel gating mechanism, gating modes and transitions between them. The effect of gating in ion channels on the overall output of a neuron is examined and the circuitry is shown to perform a simple adaptation task. The conclusions drawn from the work include support for adhering to the concept of physical equivalence in analogue integrated circuit design for exploring neurobiology and the possibility

Acknowledgements

Firstly, I would like to acknowledge the Engineering and Physical Sciences Research Council for providing funding for my work, both here, and away from here. And I would definitely like to thank my parents, Judith and Derek, for repeatedly supplementing that funding and, along with my brothers, Matt, Simon and John, for thinking well of whatever I might have done.

I would like to thank my supervisors, Alan Murray, for encouraging me to take up the work and for providing a neural niche in the electrical engineering environment and David Willshaw, whose guidance and support throughout was, and still is, immensely appreciated. From my time at ETH, Zurich, I wish to thank Rodney Douglas for inviting me to work at the Institute for Neuroinformatics, Kevan Martin for giving me food and shelter and Susanne Still and John Breslin for taking care of my well-being during that time. I would very much like to thank the many individuals who gave a considerable amount of their time to helping me, including Christoph Rasche, and most remarkably, those I have never met, especially, Anthony Bell, formerly of the Salk Institute and John Lazzaro of the University of California at Berkeley.

The Centre for Neural Systems and the Centre for Cognitive Science have the most friendly and lively academic environments I have ever experienced. Among those responsible for this are Alistair Reid, Volker Steuber, Bruce Graham and Andrew Gillies, who need also to be thanked for ensuring my understanding of neurobiology didn't go too far astray, and Padraic Monaghan for the lion's share of the friendliness. There are individuals in the Department of Electronics and

Electrical Engineering to whom I am greatly indebted, firstly, Robin Woodburn, for invaluable and extremely enjoyable conversations and for making the first year much less tricky. Dot Drummond, Clive Reeves, Susan Kivlin and David Stewart for technical support. Marcus Alphey, for a disturbing amount of information, and Kostis Papathanasiou, Bill Buchan and John Breslin for help and advice with many, many parts of the chip design process, not to mention the truth behind the voyage of the Argonauts, cardboard rocketships and electric giraffes. From these last days, I would like to thank Leslie Smith and Simon Collin for reading and commenting on the thesis and Harry Newton for the fridge magnets.

Finally, the thanks that are the most difficult to express. To Misha Mahowald, for that long conversation in December. And to my husband, John Breslin, for making it such that, after days of thinking, i'm still no closer to being able to thank him enough for all the things, so i would like to thank him for just one – the hundreds of rabbits he's going to let me keep.

"and on we went again into the silence, along empty reaches, round the still bends, between the high walls of our winding way, reverberating in hollow claps the ponderous beat of the stern-wheel. Trees, trees, millions of trees, massive, immense, running up high; and at their foot, hugging the bank against the stream, crept the little begrimed steamboat, like a sluggish beetle crawling on the floor of a lofty portico. It made you feel very small, very lost, and yet it was not altogether depressing, that feeling."

Heart of Darkness, Joseph Conrad, 1901

Table of Contents

List of Figures

List of Tables

Chapter 1

Explorations of Neurobiology with Analogue ICs – Introduction

Many methods have been used to make explorations of neurobiology. This thesis describes the use of analogue integrated circuits to investigate neurobiological phenomena and to make predictions about these phenomena that can be directly verified by physiological experimentation. This method for exploring neurobiology is known as neuromorphic engineering. How and why this method came about is described in Chapter 2 of this thesis, but perhaps the most intuitive way of introducing it is to describe what it is *not*.

- It is not about constructing artificial neural networks. It is considered that explorations of this new branch of statistics are not well-matched with analogue integrated circuit implementation. More significantly, it is believed that artificial neural networks are not well-matched with explorations of neurobiology.

- It is not about applications-driven electrical engineering, though this possibility is not precluded.

- It is not about proposing that what the brain *does* is analogue computation, or any other form of mathematics, even if this emerges as a convenient way to *describe* it.

The particular area of neurobiology being explored is that of nonsynaptic ion channel behaviour – the intraneuronal, or intrinsic properties of a neuron.

1.1 Ion Channels and Intraneuronal Adaptation

The movement of ions through ion channels is the primary source of alterations in the membrane potential of a neuron.[3] These alterations are the basis of a neuron's behaviour, whether that behaviour be extracting signals from noise,[4] performing logical operations,[5] placing an organism's nervous system on the brink of dynamic instability,[6] or any of the other behaviours talked of in the introductions to neuroscientific texts. For all of these behaviours, it is agreed that a neuron needs somehow to establish and maintain a population of ion channels with distribution and densities most appropriate for the present environment, and to adapt to any future environment. Whilst adaptation and learning are traditionally looked at on an *inter*neuronal level, there is sufficient evidence for *intra*neuronal processes such as ion channel adaptation occurring, to make it a reasonable topic for research.

This research requires a model of ion channels that is dependent on the most recent structural and physiological evidence, and these findings are incorporated into analogue integrated circuitry, as much as this medium will allow. Specifically, the nature of ion channel gating is included. This model is then placed within

the "channel space" framework proposed by Bell[7,8] – the primary hypothesis here being that ion channels can move laterally in the membrane, in a manner dependent on their gating state. In addition, the proximity of ion channels to each other can influence the gating state. This framework of gating and lateral diffusion provides a mechanism for ion channel adaptation. This framework is then linked to recent electrophysiological findings that certain ion channels possess at least three distinct gating modes[2],[1] and suggests that this observation is the result of the lateral diffusion of neighbouring ion channels.

Analogue integrated circuitry was designed to implement these phenomena. Based upon the 1991 Mahowald and Douglas "Silicon Neuron"[9], this IC represents the activation, inactivation and time-dependent variables of ion channel conductances according to the Hodgkin-Huxley formalism.[10] The first stage was the redesign of the silicon neuron for an alternative fabrication process and the second was to design and fabricate novel circuitry to represent ion channels with gating modes and the capacity to adapt from a non-conducting to a conducting membrane.

The significance of this work is threefold:

- Firstly, it provides support for the feasibility of alterations in ion channel gating affecting the overall behaviour of a neuron, and for this to be a mechanism for intraneuronal adaptation.

- Secondly, it demonstrates that it is feasible to implement ion channels in analogue integrated circuitry, using data from neurophysiological studies, to a level of detail sufficient to investigate the process of intraneuronal adaptation.

- Thirdly, that explorations of neurobiology with analogue integrated circuitry allow predictions to be made that can be experimentally verified.

Chapter 2 – Ion Channels and Physically Equivalent Devices

Chapter 2 introduces the neuromorphic engineering field, providing examples of work, from that of Carver Mead in the mid-1980's[11], to work presented at a 1997 European Workshop on Neuromorphic Systems.[12] It discusses one of the motivations Mead cites for his work – the notion of field-effect transistors as physically equivalent to ion channels, and the extent to which this is the case. Though none of the examples presented in this chapter adheres strictly to the notion of physical equivalence, it is a recurring theme throughout this thesis and one to which the thesis returns at the conclusion.

Chapter 3 – Neurobiological Description: Levels of Equivalence

Chapter 3 introduces the possibility of equivalences other than the physical. This requires discussion of levels of description, as proposed by the psychologist David Marr,[13] and others subsequently.[14,15] Explicit reference to the notion of levels within the neuromorphic engineering community is rarely made.[16] There are definite advantages to working within formal and semi-formal frameworks such as this. These are described, and an example of such a framework provided. Some disadvantages are also mentioned – there is still debate over whether formalisation is either necessary or desirable. Whatever conclusions are drawn, it is considered beneficial at least to articulate the considerations before embarking on the modelling and implementation itself.

Chapter 4 – Neurobiological and Silicon Neurons

Several varieties of neuron model are presented, including a description of the

Hodgkin-Huxley model for neuronal membrane conductance and its *in silico* instantiation – the Mahowald and Douglas "Silicon Neuron" design. Models that incorporate a dendritic structure are then presented, and finally Chapter 4 describes the development of ion channel models, from the minimal account of them as selectively permeable pores in the membrane, to models with gating structure and physiology. These are the features to be incorporated in the neuromorphic ion channels described in this thesis.

Chapter 5 – Ion Channel Gating and Adaptation

This chapter presents electrophysiological experiments that revealed the gating modes of N-type Ca^{++} channels. It discusses how these gating modes are described, by classical kinetics, structural description and, more recently, by nonlinear dynamics.[17] It then presents experiments that revealed the lateral diffusion, or electrokinesis of ion channels in the neuronal membrane and discusses the significance of these findings. Bell's "Channel Space" framework is introduced and here the phenomenon of gating modes is linked with that of electrokinesis.

Chapter 6 – Silicon Neurons: Experimental Work and Application

This chapter describes the first stage of implementing neuromorphic ion channels. It was necessary to fabricate silicon neurons with the fabrication process available which was different from the fabrication process used by Mahowald and Douglas.[9] Results from simulation and implementation are presented. The thesis then explores the possibility of using the neurons to control, via central pattern generation, locomotor gaits and gait transition in a simple quadruped robot.[18] Some ways in which intraneuronal adaptation could be relevant to this work are suggested.

Chapter 7 – Neuromorphic Ion Channels: Experimental Work

This chapter describes the main part of the experimental work - The design and implementation of novel circuits to represent gated ion channel circuitry and results from simulation and implementation of these circuits.[19] This includes a simple adaptation task, outlined by Bell.[7] The chapter concludes with a discussion of the results, the predictions made possible by this work and suggestions for further work.

Chapter 8 - Explorations of Neurobiology with Analogue ICs - Conclusions

The final chapter provides a summary of conclusions from the previous chapters, and possibilities for further work, on ion channels, adaptation and explorations of neurobiology with analogue integrated circuitry.

Appendix A - Modification of AnaLOG for the Mietec 2.4μm Process

This appendix describes the simulation tool, AnaLOG[20], and how it was modified for the Mietec 2.4μm fabrication process.

Appendix B - Technical Details: Silicon Neurons

This appendix describes the technical details required to fabricate silicon neurons in the Mietec 2.4μm process. It includes circuit diagrams and layout plans for each of the subcells, and details of the test circuitry and experimental setup.

Appendix C - Technical Details: Neuromorphic Ion Channels

This appendix describes the technical details required to fabricate adaptable ion channel circuits in the Mietec 2.4μm process. It includes circuit diagrams and layout plans for the channel circuits, their summation and adaptation.

Chapter 2

Ion Channels and Physically Equivalent Devices

2.1 Introduction

The chapter begins with a brief introduction to neuromorphic engineering as synthetic neurobiology and then discusses physical equivalence and adaptive properties. The earliest direct ancestor of the work described in this thesis is that carried out by Carver Mead's group at Caltech during the mid to late 1980's.[11] The original motivation for Mead's work is the notion that field-effect transistors are subject to the same physical processes, namely those described by Boltzmann's distribution, as ion channels in the neuronal membrane. The chapter discusses this physical equivalence; the extent to which it is the case and the implications for neuromorphic engineering in general. This chapter concludes by presenting the work of this thesis, along with other descendants of the Caltech group's work, in the form of an "evolutionary tree" diagram. This, by no means exhaustive, collection of neuromorphic engineering examples, helps place the work in context with the rest of the field.

2.2 Synthetic Neurobiology

It is not the intention of this thesis to explore the philosophical basis for the methodology of neuromorphic engineering, except to acknowledge that a methodology should be aware of issues in the philosophy of science, such as epistemologies and paradigms. This thesis does not claim that the work described herein could only be carried out using a neuromorphic (hardware-based) methodology, but only that arguments do exist for the validity of the approach. One argument, adapted from Harnad[21], is outlined as follows:

- Neuromorphic engineering is an example of *synthetic* neurobiology,[22] whereas software-based modelling is an example of *virtual* neurobiology.

- Virtual neurobiology is an arbitrary, ungrounded symbol system.[1] This is an objection that synthetic neurobiology does not have to address. The only question that remains is how close an equivalence is required in order for synthetic neurobiology to "capture" neurobiology.

- Equivalence is a matter of physics. In the case of neuromorphic engineering, is there a physical process in silicon that is equivalent to one in neurobiology?

- Neurobiological life has adaptive properties. Therefore synthetic neurobiological life must have adaptive properties.

---

[1] According to Harnad, an ungrounded system is one in which the connection between symbols and what they are about is dependent on an external interpreter.

Harnad's notion of equivalence is what Mead believed he had found between the processes occurring in field-effect transistors and the processes occurring in ion channels.[2] Equivalence and adaptive properties are discussed in the following two sections.

2.3 Physical Equivalence

Mead makes several claims for the appropriateness of silicon analogue VLSI as a medium for representing, investigating and applying neurobiology. This thesis will not discuss his claims relating to power consumption, fault tolerance and other pragmatic considerations[23], as these have not yet come to fruition. The discussion of motivations is restricted to the following statement of Mead's, appearing in his 1989 book[11]. This is said to provide *"A simple, unifying perspective within which the function of either technology [neurobiology or silicon] can be visualized, described and analyzed."*:

"The operation of elementary devices in both technologies can be described by the aggregate behaviour of electrically charged entities interacting with energy barriers. In both cases, the rate at which dynamic processes take place is determined by the energy due to random thermal motion of the charged entities, which is accurately described by the Boltzmann distribution."

The discussion is restricted to this statement because it is the only one that

---

[2]Of course, electrical circuit theory and electrically equivalent circuits have been used for a long time in neurobiology to describe the basic electrical properties of neurons. Mead's equivalence, however, exists at a less abstract level.

includes the notion of equivalence. The formal significance of this is described in Chapter 3. Here, the physical basis of the statement is explored. The following subsection is adapted from Mead's book.[11]

2.3.1 Particles in Motion

In both neurobiological and electronic systems, the movement of an individual particle is determined by thermal motion. Particles will experience collisions at random intervals. The average time between collisions is the *mean free time.* After a collision, the particle moves in a random direction with a random velocity. If the particle is subject to some force, it will accelerate towards or away from that source. The acceleration will cause a *net change in the position* of the particle. The *drift* of a collection of particles is the net change in position per mean free time. Again, in both neurobiological and electronic systems, there are spatial gradients in the concentrations of particles. *Diffusion* describes the movement of particles from regions of higher density to regions of lower density, at a rate proportional to the gradient. The distribution of particles within a neuron or a transistor is the result of a balance: particles will tend to drift in the direction of electrostatic attraction, creating a potential gradient, whilst diffusion will tend to move to counteract this accumulation of particles.

Particles in Ion Channels

In neurons, the membrane potential at which particles (ions) are at equilibrium is known as the Nernst potential. This involves Na^+, K^+ and Cl^- ions. These ions diffuse in the direction of the chemical gradient and drift in the direction of the

electrical gradient. Eventually, the membrane reaches a potential at which the chemical gradient of the ions balances the electrical gradient. The *Boltzmann distribution* describes the exponential decrease in the density of particles in thermal equilibrium with the potential gradient, in this case, between extra- and intracellular spaces. The membrane potential alters the permeability of the membrane to ions in such a way that the diffusion of ions through the membrane is an exponential function of the membrane potential.[3]

Particles in Field-Effect Transistors

Silicon can be doped with elements that are donors or acceptors of electrons, producing regions that contain charge carriers. These make up the source and drain of a transistor. They are separated by a material, known as the channel, on top of which is a control electrode that forms the gate region. Particles (charge carriers) diffuse from the source to the drain. At the same time, should particles be added to the gate region, electrostatic effects will result in drift away from the channel, allowing more particles to diffuse from the source to the drain. As in the case of the neuron, the Boltzmann distribution describes the exponential decrease in the density of particles in thermal equilibrium with the potential gradient, in this case, in the channel region and, also like the neuron, the diffusion through the channel is an exponential function of a potential, in this case, the gate potential. In classical electronics, this all occurs below the threshold for conduction of the main "population" of charge carriers in the channel. This operating region is therefore known as subthreshold, or weak inversion. Figure 2–1 shows a cross-

[3]It can also be a function of the intracellular Ca^{++} concentration, mechanical deflection or light intensity

section of an n-type MOSFET. It shows the source and drain regions connected by the conducting channel.

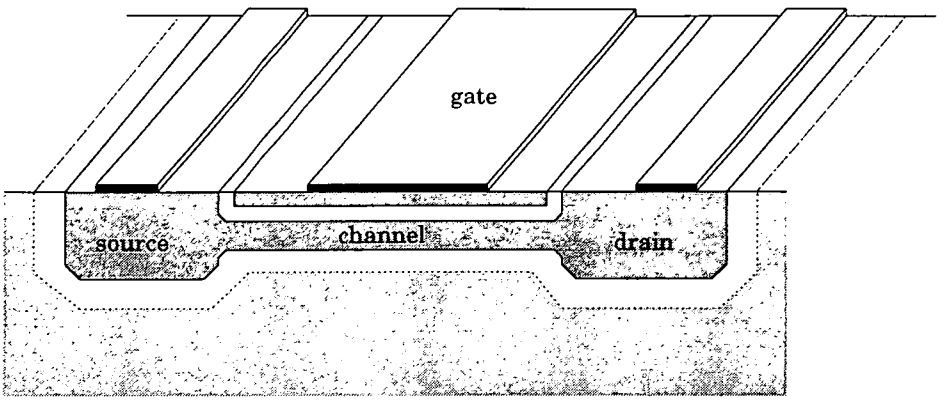

Figure 2–1: *Cross-section of an n-type MOSFET*

There are some ways in which the processes described above, for transistors and neurobiological membranes, differ from each other. The exponential function of ion channels is steeper than that of transistors, the reasons for this are explained in Chapter 4. It is the current through a population of ion channels that is an exponential function of the membrane potential.

A Nonlinear Dynamical Explanation

Before moving on to the topic of adaptive properties, it is worthwhile to mention that there is an alternative way to describe the processes of drift and diffusion in neurobiological membranes and transistors, and that is as nonlinear dynamical systems. In this account, the ion channel protein, and hence the channel of the transistor, can be characterised by a potential energy function. This energy is a measure of drift and diffusion. Stable ion channel protein structures correspond to a local minimum in the energy. When an ion channel switches between states

(open and closed), it rises out of the energy minimum of one state, crosses an energy barrier, and descends into the energy minimum of the other state. Likewise, charge in the source and drain regions of a transistor correspond to local minima, and charge flowing through the transistor channel crosses an energy barrier. The height of the energy barrier is determined by the membrane voltage and the gate voltage of neurons and transistors, respectively. Whilst the energy structure of transistors has been fully characterised and can be found in textbooks of electronic engineering[24], the energy structure of ion channel proteins is unknown. For example, are there few or many local minima and, if there are many, can they be traversed in any order? These points become relevant when the detailed structure of ion channels is discussed in Chapters 4 and 5. The fact of transistors being more fully characterised than ion channel proteins, reappears in the following chapter, with reference to the validity of the neuromorphic engineering approach.

2.4 Adaptive Properties

Arguments for the validity of the synthetic or neuromorphic approach, also included the statement that *"Neurobiological life has adaptive properties."*. In fact Harnad cites adaptive properties as a criterion for life. Put simply, environments change, so organisms must adapt to survive, in order that genetic material be passed on.[4] Adaptation can be explored at many levels, from mechanosensory systems to cognitive processes. This thesis considers intraneuronal or *intrinsic*

[4]This includes the development of the organism, to get it to a stage at which it can begin to survive.

adaptation, using ion channels as the elements of adaptation. Though much work on adaptation is carried out at an *inter*neuronal level, there are organisms that adapt successfully using only ion channels.[25]

2.5 Neuromorphic Engineering

The examples shown in figure 2–2 have been drawn from the time of the work of Mead's group to the work presented at the most recent conference on neuromorphic engineering – the First European Workshop on Neuromorphic Systems held at the University of Stirling in August of 1997.[12] In addition, all examples of neuromorphic and near-neuromorphic work mentioned in this thesis are included in order to provide a common frame of reference. It does not claim to be exhaustive. For example, there are numerous papers on optical motion sensors, though only that of Tanner and Mead is included, but incorporates enough examples to demonstrate evolution and divergence from Mead's work and perhaps indicate future trends.

Figure 2–2 shows that much neuromorphic work has diverged from using the physical equivalence between transistors and ion channels. Only those examples located on the rightmost branch have this feature; the silicon neurons, dendrites and ion channels. The middle branch shows examples of central pattern generation and locomotion controller work, whilst the leftmost branch shows neuromorphic sensorimotor systems. The divergence from physically equivalent neuromorphisms is discussed in the following chapter. Adaptive properties have been explored by Westermann, Northmore and Elias, in the context of off-chip

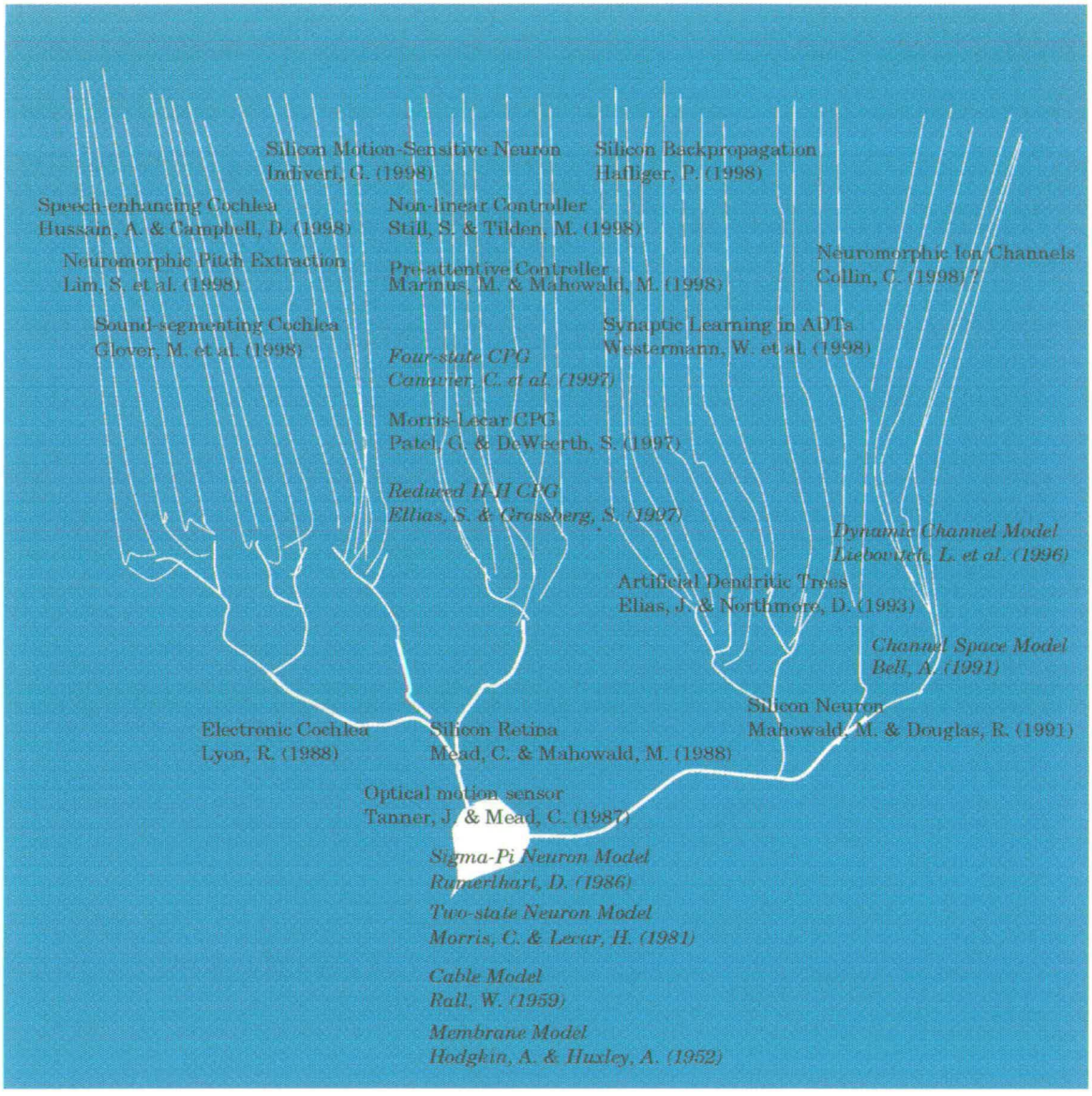

Figure 2–2: *An evolutionary tree of neuromorphic engineering. Unitalicised lettering indicates neuromorphic or near-neuromorphic work, italicised lettering indicates theoretical models used in the neuromorphic work.*

storage of synaptic "weights". Of adaptation, they comment: *"Ideally, weight storage and adaptation capability would be combined in a single small device. For example, floating gates, or programmable amorphous silicon resistors [...]. However, we may find that effective adaptation requires more complex interactions which cannot be reproduced by a simple device. The next best approach might be to use conventional MOSFET design techniques [...]."*[26] On a more general note, Douglas, Mahowald and Martin comment: *"It seems that the cortex is not designed in the highly specified style of a Pentium, but rather depends on local adaptive mechanisms to draw its components into calibration with respect to one another."*[27][p. S26] This places the work of this thesis on the rightmost branch – a descendant of the Mahowald and Douglas Silicon Neuron. It is applied to an area thus far unexplored by neuromorphic engineering – ion channels and intraneuronal adaptation.

Chapter 3

Neurobiological Description: Levels of Equivalence

3.1 Introduction

In the previous chapter, Mead's original motivation for embarking on neuromorphic engineering was taken to be the physical equivalence between transistors and individual, or a population of, ion channels. The *physical* half of physical equivalence was discussed from two very different perspectives – as the movement of particles, and as the basis for creating a synthetic approach to representing neurobiology. This chapter discusses the *equivalence* half of physical equivalence. It does this by introducing levels of equivalence other than the physical and demonstrating how these levels can be placed into a formal framework. It is possible to use this framework to assess examples of neuromorphic engineering. The implications and conclusions from this assessment are presented. Finally, reasons why such a framework may have undesirable features are discussed.

3.2 The History of Formalisation

The philosophy of formalisation, initiated by Frege in the final decades of the nineteenth century, was concerned, at the time, with demonstrating that arithmetic could be formalised without the use of any non-logical notions or rules.[28] It has since provided the foundations for Computer Science and Artificial Intelligence and work in Cognitive Science and Computational Neuroscience. Specifically, the *computational metaphor* or paradigm is that a mapping is performed from the states of the world onto the brain, and further, from states of the brain onto states of an algorithm that solves a computational problem. This would suggest that formalisation of neuromorphically-engineered elements and systems is possible.[1] The advantage of formalisation is that it can make discussion more precise and also relates the work in neuromorphic engineering to the literature on models of computation and representation.

3.3 The Language of Formalisation

Formalisation is *representation in a formal language.* In this framework it is assumed that there is a domain of discourse. Traditionally, this is formally treated as a *model.* Given a model, the formalisation exists in some *language.* For example, propositional or predicate language. These include a set of symbols with rules of composition that define what it is to be a well-formed proposition. For

[1]This does not mark a return to describing the brain's computation by symbolic logic, rather, the formalisation is applied at a more abstract level.

instance, given a vocabulary $\{ a, b, \wedge, \vee, \neg \}$, a subset of propositional calculus, if a, b are well-formed formulae, so are $a \wedge b$, $a \vee b$, $\neg a$. The propositional letters can be used to represent many things. In addition, there are standard recursive definitions for formal logics that define interpretations of composite expressions relative to the interpretations of their basic components. The goal of logic is to be *sound* in its determination of theorems with respect to the model and *complete* (all true facts represented somewhere). The possible benefits of formalising the relationship between neurobiological phenomena and neuromorphically-engineered models of the phenomena is that the formalisation will have well-defined mathematical properties, including a correspondence with the standard model of computation, the Turing Machine. However, since the benefits of such a correspondence are not immediately apparent, only an outline of a formalisation is provided here.

3.4 Levels of Description

As evident from figure 2–2 in Chapter 2, neuromorphic devices can be constructed for many different aspects of neural organisation, and over a wide range of spatio-temporal scales. Currently, and in the past, work with computer simulation (virtual neurobiology) has led to debate over how much data (or constraints on the model) to incorporate.[29] It is generally considered to be the case that, when a model is too under-constrained, it will not be able to produce reliable data, in other words, it will have no predictive power, while a model that is too over-constrained will become an alternative realisation of neurobiology – a model in which the incorporated detail is too complex (or possibly too medium-dependent) for it to contribute anything to the understanding of the system. For the most

part, neuromorphic engineers have made a pragmatic use of neurobiological data. One way to determine how much data should be incorporated is to consider at what *level* the modelling is taking place.

This chapter presents a summary of David Marr's theory of levels.[13] This theory is familiar to most neurobiologists. It is also considered because it provides a semi-formal framework. Marr suggests three levels of description for complex systems:

- The *computational*, at which the nature of the computation to be performed is expressed.
- The *algorithmic*, at which the procedure for carrying out the computation is formulated.
- The *implementational*, the level of hardware.

At the computational level, equivalence depends on similarity of output. For example, a neuron that produces action potential spikes and a chip that produces action potential spikes are computationally equivalent. The algorithmic level provides an explanation of how the system being modelled, and the model itself can produce the appropriate output from the given input. There may be more than one possible algorithm for any given computation. Some neuromorphisms implement precisely that algorithm by which the computation is performed in the neurobiological system. Others implement the most pragmatic of the possible algorithms. For example, whilst a neuron produces spikes by altering a membrane voltage that is maintained by a number of conductances, a chip may produce spikes by means of a simple oscillator, or, it may produce spikes by representing

the membrane voltage and the conductances in the way that the biological neuron does. This is the case for the Mahowald and Douglas silicon neuron [9]. And this latter case can be said to be algorithmically equivalent whilst the example of the oscillator is not. At the implementational, or *physical level*, if the chip produces spikes as a direct result of transistors undergoing the same physical processes, described in Chapter 2, as ion channels, then it can be said to be implementationally, or physically equivalent.

Marr's framework remains the most relevant for neurobiological modelling in the computational paradigm. However, theories of levels are not confined to neurobiology. Allen Newell's framework for physical symbol systems[14,15] is presented to see if it sheds any light on the analogue VLSI side of things. This framework emerged as digital computers developed. The levels are:

- The *knowledge level*
- The *configuration level*
- The *symbol level*, whose medium is symbolic expressions.
- The *register-transfer sub-level*, whose medium is bit vectors.
- The *logic circuit sub-level*, whose medium is single bits.
- The *circuit level*, which has as its medium current and voltage
- The *device level*, which has as its medium electrons and magnetic domains.

A level consists of a medium that is to be processed, components that provide primitive processing elements, laws of composition that permit components to

be assembled into systems, and laws of behaviour that determine how system behaviour depends on the component behaviour and the structure of the system. There are some gaps in this framework, for example, Newell comments that levels are realised by *technologies*, that the environment has a say in whether a technology can exist, but he does not provide much justification for this stance. Neither does his framework provide a way of describing this environment in which the physical system resides. Some attempt has been made to fill in these gaps in the framework described here.

3.5 An Example of a Formalisation

Described here is an outline of a formalisation that incorporates aspects of both Marr's and Newell's levels with the intention of providing a coherent framework for considering the implications of neuromorphic implementations of neurobiological systems. Doubtless many aspects of neuromorphic engineering and VLSI technology will have been neglected in this outline. However, it is believed that such an outline has not previously been articulated, and that it is necessary for a framework, though not necessarily of this form, to be developed if neuromorphic engineering is to continue fruitfully.

The parameters in this framework include structure and input, upon which neurobiological constraints act to produce an output. The parameter set could be expanded as required, to include, for example, the environment in which the production of output occurs. Different possible environments yield potentially different

output.[2] For example, in a high-altitude environment, the environmental mapping of the same structure and inputs would yield a significantly different output. The other "half" of the framework would also include structure and input, but upon which a technology would act to produce an output. This would correspond with Newell's notion of *technologies*. To complete the framework, a parameter is required to represent the interpretation of the technology, i.e *how* it maps structure and inputs to output. This parameter would be concerned with, for example, whether action potentials are produced by a simple oscillator, or differential pairs and low-pass filters, or single transistors behaving as ion channels.

This framework can then be used to reexamine the neurobiological theory of levels. When considering whether a piece of brain and a chip are *computationally* equivalent, only the output need be examined. The technology could be a number of things, a digital simulation, for example. There might be pragmatic reasons for using analogue VLSI, such as speed, but analogue VLSI would not be *necessary* to make the framework complete at this level. To examine the *algorithmic* level would involve examining the *interpretation* of the technology and demonstrating that the interpretation that maps analogue VLSI structures and inputs to output, is a *reasonable* one. However, the only way to be certain of this, is to engineer at the implementational, or physical, level.

---

[2]So it would be possible to use the framework to express the neurobiological constraints imposed by the environment (see previous comment by Newell).

3.6 Implications and Conclusions

It is suggested that the framework would provide a formal way of articulating the following:

- Many of the traditional justifications for neuromorphic engineering, for example, sharing such characteristics as limited space, imprecision, redundancy of single elements, are pragmatic and not directly concerned with the interpretation.

- There may be a formal way of determining whether the neurobiological algorithm and the neuromorphic algorithm are equivalent,[3] but the only way to be certain of equivalence is to engineer at the physical level.

- Only if equivalence exists, will the neuromorphism have predictive power. That is the model will be capable of predicting what will be the case for the neurobiological phenomenon. This is possible by virtue of the fact that the technology used is usually epistemologically more fully characterised than neurobiology.

The implication of this is that there are three ways to ensure the fruitfulness of neuromorphic engineering. One is to use the physical equivalence between transistors and ion channels. Another is to try to prove that there is algorithmic

---

[3] A proof of equivalence that is sensitive to notions of levels of description was begun, but not completed, by Carol Foster[30], though without reference to a specific medium or technology such as analogue VLSI.

equivalence between the neurobiology and the neuromorphic device. And another is to build a device at the algorithmic level and demonstrate that it has predictive power. This thesis follows the third of these approaches, but acknowledges that they are all equally valid.

In the introduction to this chapter, it was suggested that the framework had some undesirable features. This begins with its sensitivity to levels and ends with a problem of incompatibility with the entire computational paradigm. Below, are listed three potential problems with the framework.

- Levels may have infinite depth – It may not be possible to determine how deep a level it is necessary to go to obtain even sufficient physical equivalence. For example, is it necessary to neuromorphically engineer ion channels at a genetic level?

- There may be a level at which synthetic modelling becomes impossible and only virtual modelling is possible. If this were the case, it would remove all justification for (non-applications based) neuromorphic engineering at the outset.

- If the computational paradigm is overturned, this may remove the need for a formal framework of levels of equivalence altogether.

The first two of these potential problems offer some support for neuromorphic engineering at an algorithmic level and demonstrating predictive power, rather than engineering at the physical level or trying to prove algorithmic equivalence by formal methods. The last problem involves nonlinear dynamics. It has been suggested that the appearance of levels in neurobiology has only to do with

shared dynamics at different scales of observation, and that nonlinear dynamics is about *level-independent* principles. A discussion of nonlinear dynamical paradigms versus computational ones is not the topic of this thesis. It is worthwhile reflecting that whilst one of these paradigms may be more appropriate than the other for *describing* the brain, we still need to know *what* to describe and building a predictive device to tell us this, from within either paradigm, is an entirely valid approach. The following two chapters begin to tell us what there is to describe about ion channels.

Chapter 4

Neurobiological and Silicon Neurons

4.1 Introduction

The last chapter established that engineering at the algorithmic level and demonstrating predictive power was a valid method for exploring neurobiology. Chapter 1 explained why ion channels and intraneuronal adaptation were a reasonable topic for research. This chapter begins to describe models of the structure and function of ion channels, by discussing how neuron models in general have developed. This includes a description of the Hodgkin-Huxley model for conduction and excitation in axons,[10] and how the silicon neuron design of Mahowald and Douglas[9] is an instantiation of this model. This chapter also includes some discussion of the development of dendritic models and subsequent instantiation[31] and finally, discussion of the development of models of ion channels as independent units. This, along with the Chapter 5, provides the background to the work described in Chapter 6 – the analogue VLSI instantiation of neurons and Chapter 7 – neurons with independent ion channel units.

4.2 Development of Neuron Models

Some of the illustrations in figure 4–1 (adapted from Mel[32]), originally drawn by Ramon Y Cajal, are almost ninety years old. These clearly show neurons with extremely intricate structures, and the discussion of the Hodgkin-Huxley model will show that by the 1950s they were known also to have extremely intricate functions, yet many neuron models, and most instantiations, abstract significantly from this. Collectively, they can be known as reduced Hodgkin-Huxley models.

4.2.1 Reduced Hodgkin-Huxley Models

The minimal model incorporates one internal variable – the membrane potential – which increases monotonically with the total amount of positive input and decreases with negative input. These models are capable of input integration and output pulse production, they are incapable of allowing specific inputs or input combinations priority over others. A variation on this minimal model is one that treats the membrane potential as the result of two processes – a long period of input integration and a very brief period of output pulse production. The equations that describe them are known as Fitzhugh-Nagumo equations. This is known as an *integrate-and-fire* model. One further variation of this model is a *leaky* integrate-and-fire model, which is capable of output pulse production only when the input is strong enough to overcome a leak. Another is the inclusion of an additional variable to represent intracellular Ca^{++} concentration. This provides an indication of the neuron's recent activity. The Fitzhugh-Nagumo model has been implemented in numerous places[33,34,35], and there are a number of implement-

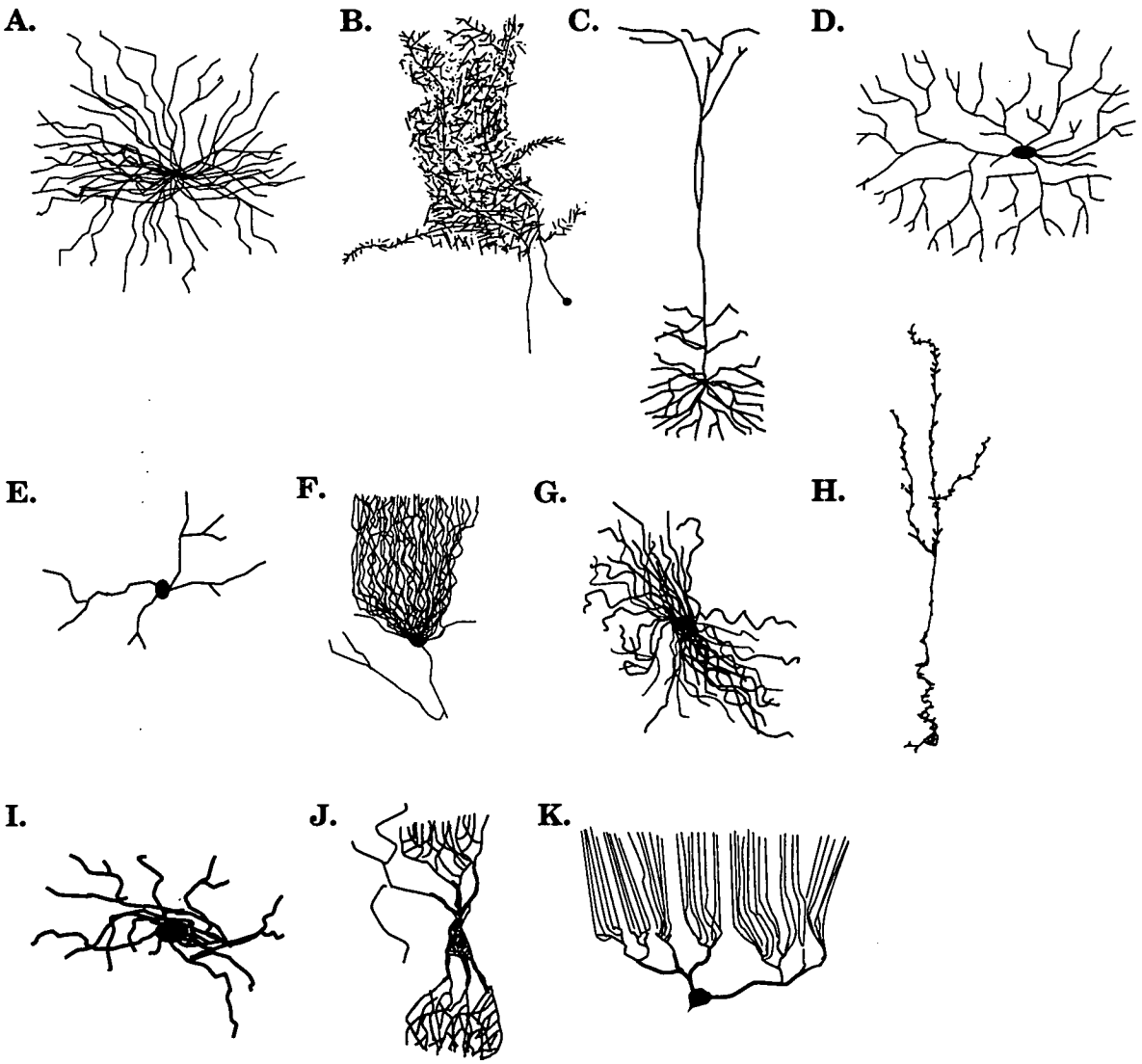

Figure 4–1: *Neurons from nervous systems: A. Alpha motorneurons in spinal cord of cat, B. Spiking interneuron in mesothoracic ganglion of locust, C. Layer 5 neocortical pyramidal neuron in rat, D. Retinal ganglion neuron in cat, E. Amacrine neuron in retina of larval tiger salamander, F. Cerebellar Purkinje neuron in human, G. Relay neuron in ventrobasal thalamus of rat, H. Granule neuron from olfactory bulb of mouse, I. Spiny projection neuron in rat striatum, J. Neuron from the Nucleus of Burdach in human foetus, K. Purkinje neuron in mormyrid fish*

ations that incorporate one or more additional variables to represent intracellular Ca^{++}.[36,37,38] In terms of the framework described, these models would be too underconstrained to have predictive power about neurobiology. However, they can be useful in other ways, some of which are mentioned in Chapter 6.

4.2.2 The Hodgkin-Huxley Model

One of the most significant advances in neurobiology was the analysis by Hodgkin and Huxley (1952) of the initiation and propagation of the action potential in the squid giant axon. The following description is an account of their findings. The experiments were carried out using a voltage-clamp technique. This allows voltage-gated channels to open or close in response to imposed alterations in membrane potential, but prevents the effects from altering the membrane potential. The conductance of the membrane to different ions can then be measured as a function of membrane potential. In the resting axon, the electrical gradient created by Na^+ and K^+ ions flowing through nongated channels is balanced by the chemical gradient, so that the membrane potential is constant. Ion flow through nongated channels is known as the leak conductance. This process was described in Chapter 2. A transient depolarising potential causes some voltage-gated Na^+ channels to open, and the resultant increase in membrane Na^+ permeability allows Na^+ influx to outstrip K^+ efflux. Thus a net influx of positive charge flows through the membrane and positive charge accumulates inside the cell, causing further depolarisation. This produces the rising phase of the action potential. Two processes repolarise the membrane, terminating the action potential. First, as the depolarisation continues, it inactivates the voltage-gated Na^+ channels. The second repolarising process results from the delayed opening of voltage-gated

K^+ channels. As K^+ channels begin to open, K^+ efflux increases. This is known as the delayed rectifier current. (K_D) The delayed increase in K^+ efflux combines with a decrease in Na^+ influx to produce a net efflux of positive charge from the cell, which continues until the cell has repolarised to its resting value. This produces the falling phase of the action potential. In most neurons, action potentials are followed by a transient hyperpolarisation. This brief decrease in membrane potential occurs because the K^+ channels that open in the later phase of the action potential close some time after the membrane potential has repolarised.

The experimental work of Hodgkin and Huxley yielded a set of equations, containing six experimentally-derived voltage-dependent functions that describe the total conductance associated with any particular population of channels. This can be expressed as a general equation in which the total conductance of a patch of membrane at a particular time is the maximal conductance of the patch, G_{max_X} (which is given by the conductance of a single channel in its open state, multiplied by the channel density), multiplied by the fraction of all channels that are open. This fraction is determined by the hypothetical activation and inactivation variables q and u. Activation is the process of ion channel opening, whilst inactivation is the process of ion channel closing.

E_{N_X} is the Nernst potential for ion species X.

$$I_X = ((G_{max_X}.u^a)q^b)(V - E_{N_X}) \tag{4.1}$$

q and u have the kinetic form

$$\frac{\delta x(t,V)}{\delta t} = \frac{x_\infty(V) - x(t,V)}{\tau_x(V)} \tag{4.2}$$

τ_x is the time constant of activation or inactivation.

Figure 4–2, adapted from Hodgkin and Huxley, 1952, shows their numerical solution for the components of an action potential. Figure 4–3 allows a comparison of their numerical solution with a recorded action potential.[1]

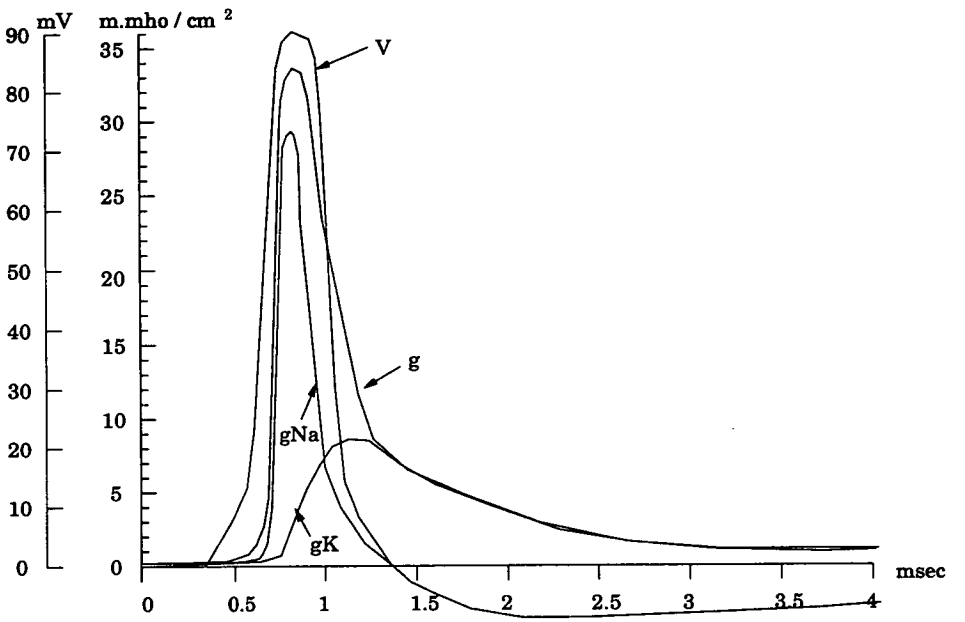

Figure 4–2: *Numerical solution showing components of membrane conductance (g) during propagated action potential (V). V is measured relative to the resting potential.*

4.2.3 Implementation of the Hodgkin-Huxley model

The Mahowald and Douglas silicon neuron can represent any patch of neuronal membrane with ion channels, according to the Hodgkin-Huxley model. It is necessary to represent the following variables:

---

[1] In the Hodgkin-Huxley model, the activation and inactivation variables are q^2u for Na^+ and q^4 for K^+

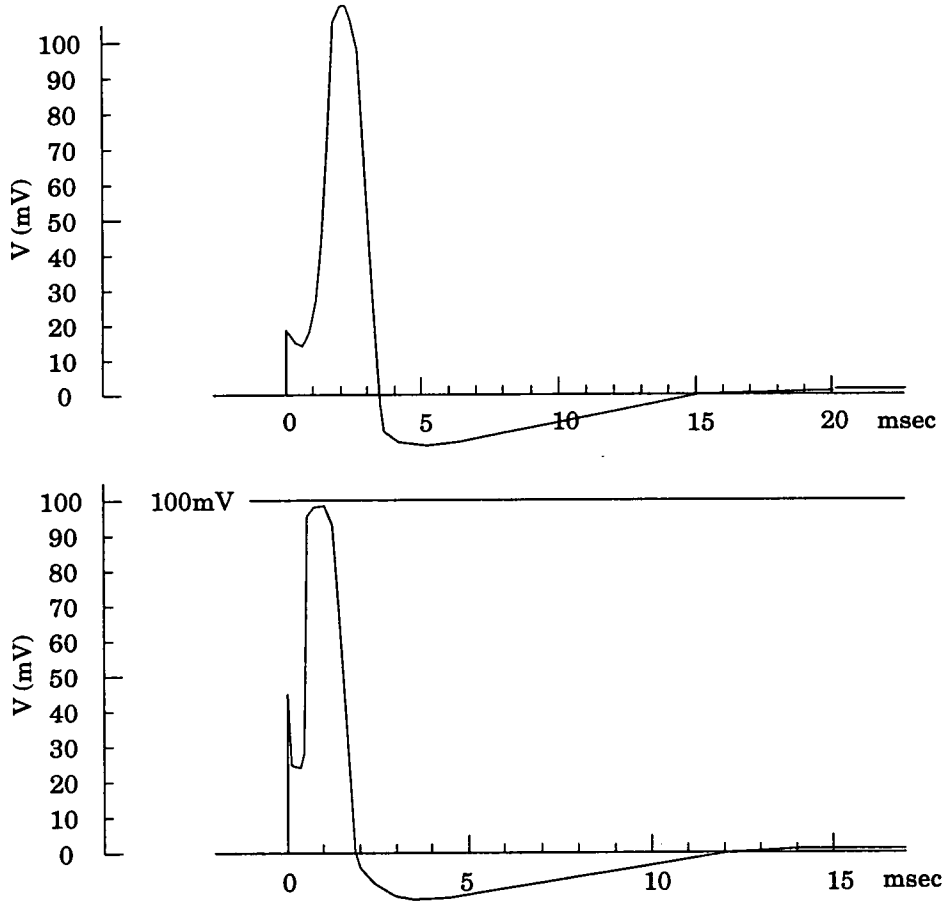

Figure 4–3: *Upper curve: numerical solution for initial depolarisation of 15mV, calculated for 6° C. Lower curve: tracing of membrane action potential recorded at 9.1° C. The vertical scales are the same in both curves. The horizontal scales differ by a factor appropriate to the temperature difference.*

1. Membrane capacitance, resistance and leak conductance

2. Conductance of ion X, G_{max_X}, where X is Na^+ and K^+.

3. Activation variables, q, for Na^+ and K^+

4. Inactivation variable, u, for Na^+. (K^+ has an infinite kinetic time variable of inactivation and is therefore not implemented.)

5. Time-dependent variables, τ_q and τ_u.

The Mahowald and Douglas silicon neuron represents these variables as described in the following subsections.

Membrane capacitance, resistance and leak conductance

Membrane capacitance is represented "simply" by a capacitor. Some considerations of capacitor design are outlined in Appendix B.

A transistor can operate as a resistor, since the current through the channel can be controlled (by the gate voltage). However, a single transistor acting as a resistor provides a varying resistance, depending on which of its source and drain regions is at a higher voltage. Placing two transistors in series ensures that even if source and drain region voltages switch, the resistance provided will remain constant. (Figure 4–4)

The leak conductance is represented by a wide-range transconductance amplifier. This is similar to the transconductance amplifiers used to represent the activation and inactivation variables. It likewise has a sigmoidal input-output transfer

function. The difference is that the transistors which control the gradient of the sigmoid are configured to produce a shallower slope.

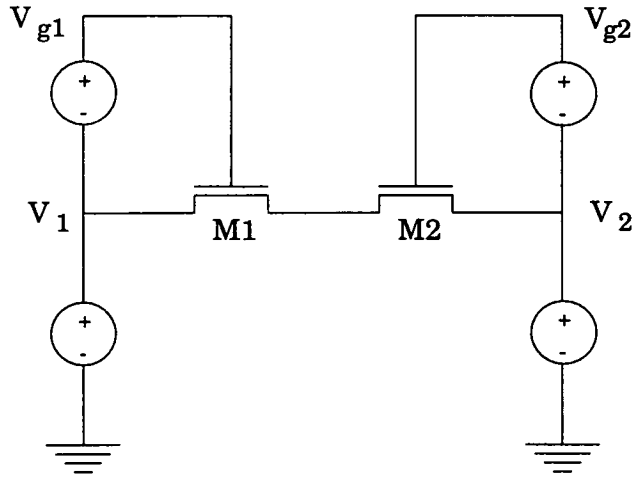

Figure 4–4: *Schematic of pass transistors representing membrane resistance*

Conductance of ion X

The conductance element for Na^+ and K^+ is implemented using a single transistor. The current through the channel, drain-source current, I_{ds}, represents the current of ion X. If this transistor is operated in the weak-inversion region, then the representation will be of the physically equivalent form explained in Chapter 2. The magnitude of this current depends on the voltage gradient across the transistor, V_{ds}, which in turn depends on the source voltage, V_s, which represents the Nernst potential for ion X, and the drain voltage, V_d, which represents the membrane potential. The magnitude of the current is modulated by the voltage on the gate of the transistor, which is the output of the activation/inactivation variables circuit further upstream.

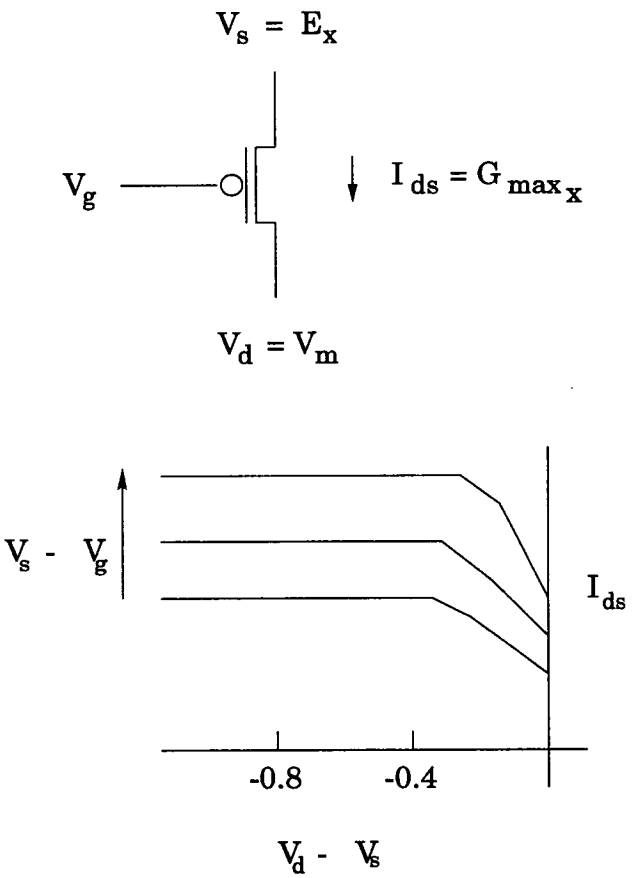

Figure 4–5: *Schematic of a transistor representing conductance*

Activation/inactivation variables

The Na^+ and K^+ conductances have a sigmoidal conductance-voltage relation which is similar to the current-voltage relation generated by the differential stage of a transconductance amplifier. With reference to figure 4–6, the output, which feeds into the gate of the conductance transistor, is the difference between the voltages V_m, the membrane potential, and onknee, a threshold voltage, subtracted by the voltage that is the difference between the voltage V_m and offknee, another threshold voltage. The voltage *qsat* controls the gradient of the sigmoid. Onknee is the threshold for activation and offknee is the threshold for inactivation. Therefore, the current through the q leg of the activation differential stage represents the degree of activation of ion channels, whereas the current through the u leg of the inactivation differential stage represents the degree of inactivation. The degree of inactivation u is subtracted from the degree of activation q to compute the final conductance.[2]

Time-dependence variables

The time dependence of the conductances is achieved using follower-integrators with variable time constants to act as low-pass filters for the membrane voltage. The filtered outputs then control the activation or inactivation transistors. The follower-integrator is constructed with an amplifier connected to a capacitor to form a low-pass filter. The current sourced into the capacitor is proportional to

---

[2]The u current of the inactivation transconductance amplifier and the q output current of the activation amplifier are summed into a current-mirror. The current-mirror half-wave rectifies the result of the subtraction, so that no matter what the values of q and u, the value of the conductance is never negative.

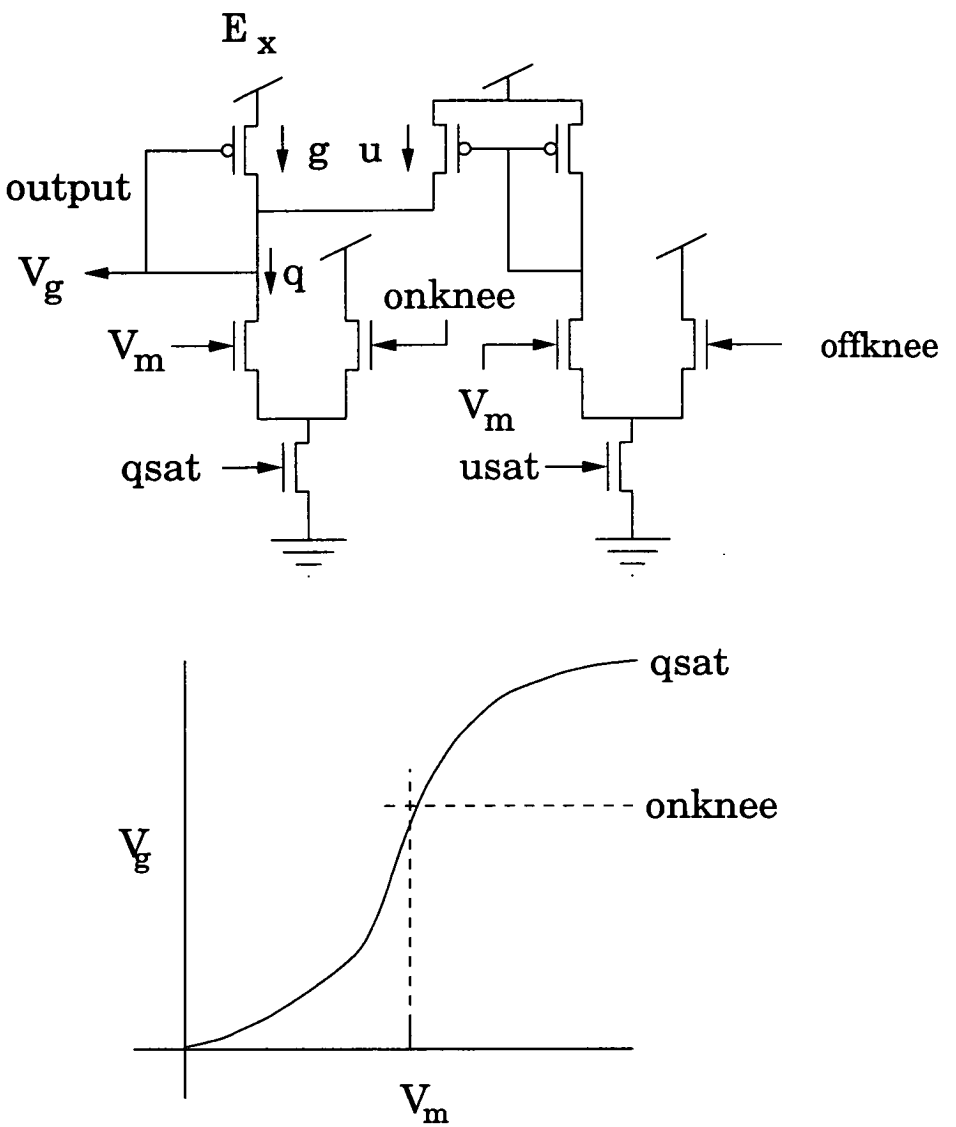

Figure 4–6: *Schematic of the differential pairs representing the activation/inactivation variables. The total degree of activation, g, is the difference between activation, q, and inactivation, u.*

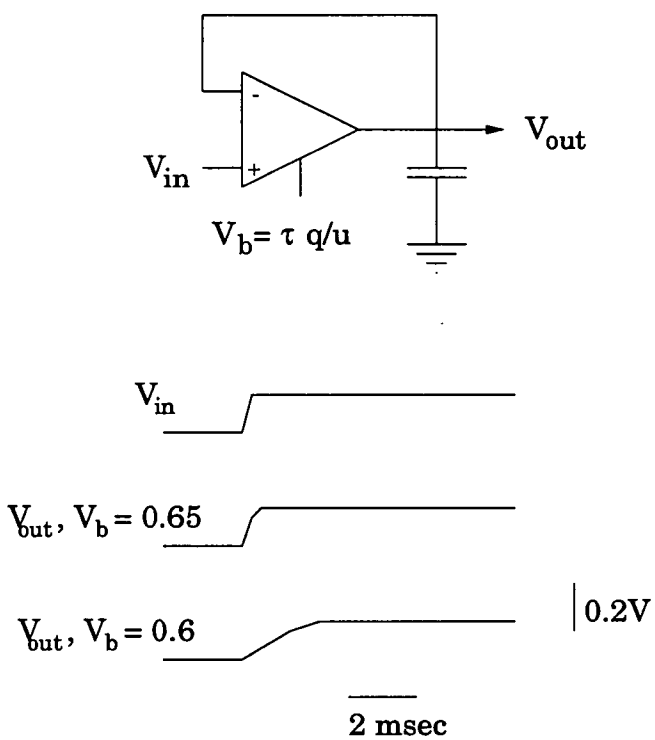

Figure 4–7: *Schematic of the low-pass filter representing the time dependencies*

the difference between V_{in} and V_{out}. The rate at which V_{out} is able to respond to changes in V_{in} is set by the transconductance of the amplifier.[3]

Calcium conductance

In addition, neurons may contain a calcium (Ca^{++}) current which requires a stronger depolarisation than Na^+ to activate and can provide a maintained influx for prolonged depolarisations, a calcium-dependent potassium current (K_{AHP}), that is activated by the accumulation of intracellular Ca^{++} and, during an action potential, contributes to the return of the membrane potential to the threshold for generating a subsequent action potential, and a potassium A-current (K_A), that is active during the hyperpolarisation and slows the return of the membrane potential to the threshold for generating a subsequent action potential.

In addition to Na^+ and K^+ conductances, the Mahowald and Douglas silicon neuron includes a Ca^{++} conductance. In neurons, during each spike, there is a Ca^{++} influx through voltage-gated Ca^{++} channels. Should the spike frequency be high, Ca^{++} cannot be cleared swiftly enough from the intracellular space, and therefore accumulates inside the neuron. This activates a K^+ after-hyperpolarisation (AHP) conductance, which has the effect of causing the spike frequency to decrease or adapt in the presence of continued input. In the Mahowald and Douglas silicon neuron, the accumulated Ca^{++} is represented by the voltage across a capacitor. Charge is added to the capacitor at every spike, and decays away at the interspike interval. The voltage is used as the activation input to the AHP conductance differential pair, which functions as for Na^+ and K^+.

---

[3]This device is not used for K^+ since its activation turns on very quickly.

Summary

A schematic of the Na^+ and K^+ conductance circuitry is shown in figure 4–8. Figure 4–9 shows circuit modules for the Na^+, K^+, Ca^{++} and leak conductances.

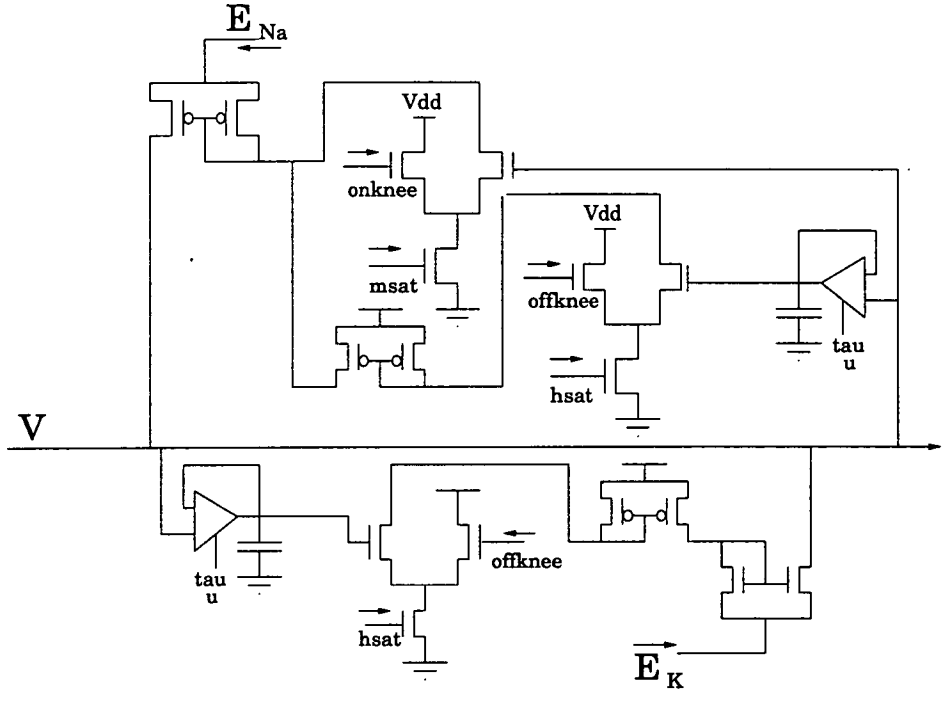

Figure 4–8: *Schematic of the Na^+ and K^+ conductance circuitry.*

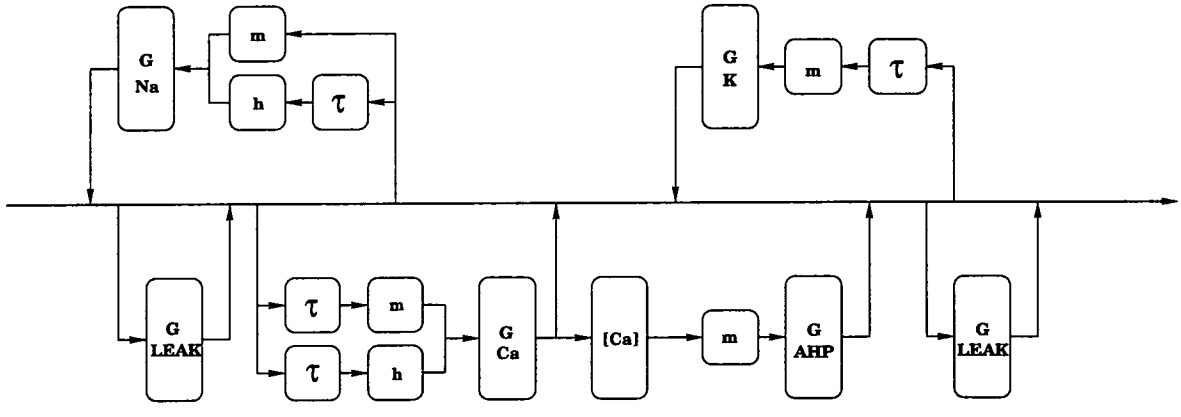

Figure 4–9: *Schematic of the Na^+, K^+ Ca^{++} and leak conductance circuit modules.*

In summary, the operation of the circuit is as follows: For K^+ the membrane potential, V_m is low-pass filtered by a follower-integrator whose output controls the activation transistor of a differential pair. In turn this is transformed into a voltage that controls the conductance transistor. This transistor drains the current from V_m, to the K^+ Nernst potential, E_K. With Na^+, there is additional circuitry for inactivation: again, V_m is low-pass filtered and controls the inactivation differential pair. Activation and inactivation signals combine to give the conductance control voltage. The Ca^{++} conductance operates in a similar manner. In addition, there is capacitance circuitry representing intracellular Ca^{++} concentration. The silicon neuron can be viewed as a soma. The dendrites, appearing in so many geometrical and functional forms, as evident from figure 4–1 are represented only by the load of the circuit. The following subsection outlines some of the properties of dendrites that affect the overall behaviour of neurons. This indicates only the very tip of the iceberg.

4.2.4 Dendrite Models

In the late 1950s, the "cable theory" of William Thomson (for transatlantic telegraph cable, 1855) was applied by Wilfred Rall to dendrites, in order to interpret intracellular microelectrode recordings.[39,40,41] Cable theory describes the passive process in dendrites which involves the conductive intracellular cytoplasm. John Elias and various collaborators have worked extensively on the signal processing capabilities of passive dendrites with spatially extensive structures.[31, 42,43,44,45] In addition to the passive process, it has been known for some time that the dendrites can also conduct via specific transmembrane ion channels.[46,

47,48,49,50] This constitutes the active process. Active dendrites have several important properties.

- The ability to generate action potentials, mediated by the influx of Ca^{++} ions.

- The ability to act in a nonlinear manner

  - Sublinear: When two neighbouring regions of dendrite are activated simultaneously, the combined alteration in membrane potential is less than twice as large as the alteration in membrane potential from a single region. This is because the increased conductance at each region also lowers the resistance in that region, siphoning off current that would otherwise contribute to the alteration in membrane potential.

  - Supralinear (amplification): Membrane potential alteration from distal regions can be amplified, such that they can become as effective as membrane potential alteration from proximal regions.

- The ability to carry a somatic action potential *back* into the dendrites (antidromic spike invasion), such that the firing of the neuron can have an effect on the distal regions of the dendrites.

4.2.5 Ion Channel Models

By the end of the nineteenth century, physiologists knew that cells are permeable to some ions and it was proposed that membranes contain channels through which these ions can flow. Ion channels were discovered to be glycoproteins that have

various conformational states. In some of these states, a central aqueous pore is formed that spans the membrane and allows specific ions to flow between the intracellular and extracellular spaces. In other states, this ion flow is not possible. This suggests that ion channels have a mechanism for selective permeability and a mechanism for permitting or preventing ion flow.[3,51,52] In 1975, Bertil Hille[53] proposed that ion channels have a narrow region known as a *selectivity filter* and it was proposed that ion channels possess some form of gating structure which is sensitive to the strength of the electric field across the membrane and can move under the influence of this field, causing channels to be open or closed to the flow of ions. This led to ion channel models of the form depicted in A. of figure 4–10. B. shows a more developed representation of the gating structure – the S4 transmembrane domain – an α helix that contains a large number of cationic residues. A change in the electric field causes the S4 helix to twist upwards, resulting in a movement of positive charge from the intracellular to the extracellular space. It is suggested that the movement of the S4 helix, is coupled to a change in the position of residues on other helices, causing the opening of the transmembrane pore. The cationic residues are known as the gating charge, or gating particles. With the development of patch-clamping, (Neher and Sakmann, 1976) a significant advance from the voltage clamp used by Hodgkin and Huxley that allows the measurement of single channel activity, more was discovered about the nature of the gating behaviour. With the development of ion channel cloning techniques, the channel protein was found to be arranged as four to six α-helices spanning the membrane, and the selectivity filter and gating structure could be located in the amino acid primary sequence.[54,55] In 1998, the first crystal structure of a K^+ channel was reported,[56] which revealed the selectivity filter as

an aqueous cavity with a hydrophobic lining and the point of gating as a bundle crossing of the helices lining the pore. This structural model is shown in C., of figure 4–10.

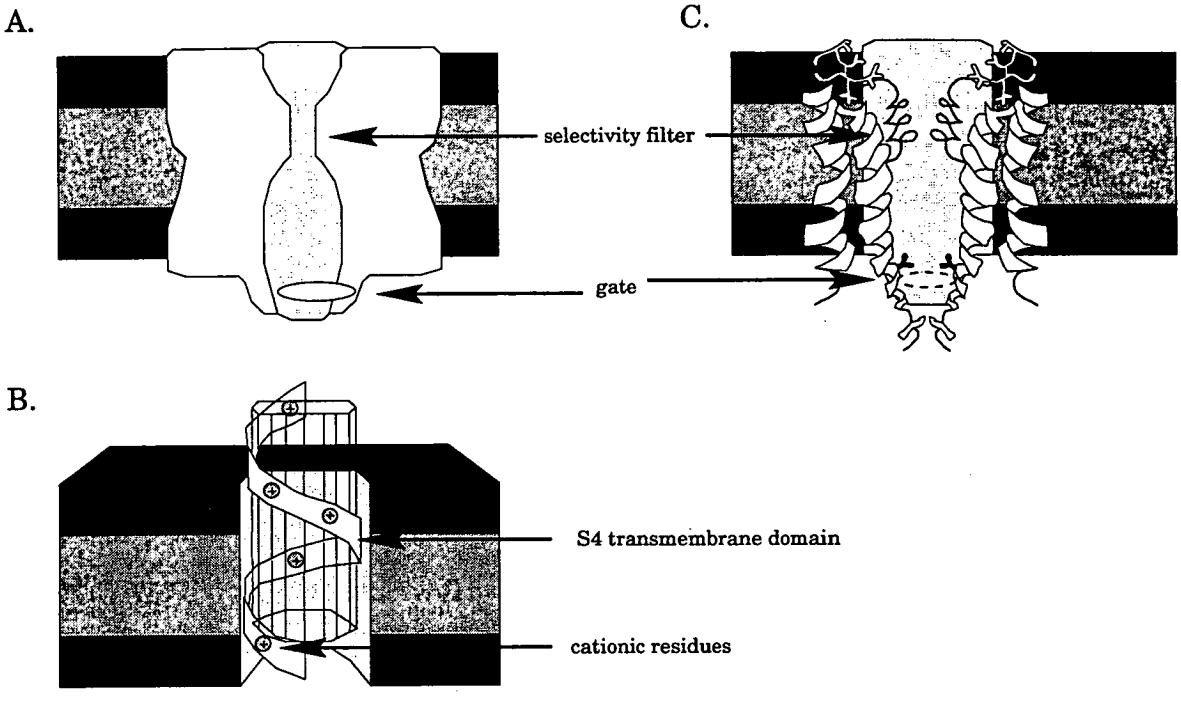

Figure 4–10: *A. shows a cartoon of a cross-section through an ion channel with selectivity filter and intracellular gate. B. shows the gating structure in more detail, with gating charges. C. shows the structure of a bacterial proton-gated K^+ channel, with a comparison of features. Only two of the four α-helices are depicted. (Adapted from Yellen, 1998)*

Calcium Channels

In Chapter 5, the gating mechanism of ion channels is explored in more depth. In order to do this, it is necessary to restrict the discussion to a specific type of ion channel. N-type [4] calcium channels have been selected for the following reasons:

---

[4]The N- prefix denotes "neither", a reference to comparison of the depolarisation it produces with two other Ca^{++} channel subtypes – L-type (long-lasting) and T-

- Ca^{++} channels may be the earliest form of ion channel to have evolved. In some organisms, all membrane potential alterations are a result of the flow of Ca^{++} ions through Ca^{++} channels.

- Although similar to Na^{+} and K^{+} ion channels with respect to voltage-dependent gating behaviour and selective permeability, they are more susceptible to modulation. Making them likely candidates for a role in intraneuronal adaptation.

- N-type Ca^{++} channel kinetics have been well-characterised. The equations used in the work described subsequently have come from physiological experiments with rat sensorimotor pyramidal neurons.

- The data on ion channel gating modes was taken from N-type Ca^{++} channels in frog sympathetic neurons.

- N-type Ca^{++} channels are found in the soma and dendrites of neurons. This makes it reasonable to consider them a unit of intraneuronal adaptation.

---

type (transient).[57,58,59] Recently, it has been taken to denote "neuronal", owing to evidence of its presence in the soma and dendrites.

Chapter 5

Ion Channel Gating and Intraneuronal Adaptation

5.1 Introduction

Chapter 4 described the development of neuron models and the inclusion of dendritic processes and ion channel behaviour. The description of ion channel models was left at the point where the selectivity filter and gating structure had been described. It remains to describe possible mechanisms by which ion channels contribute to intraneuronal adaptation. This chapter proceeds with an account of how single channel recording has recently demonstrated that, in addition to open and closed conformational states, ion channels possess at least three distinct *gating modes*, *within* which opening and closing occurs. Gating modes are characterised as a sudden change in the kinetic behaviour of an ion channel which is maintained for several seconds (the *dwell* time), in the absence of any alteration in test potential. These changes in kinetic behaviour result in alterations of overall ion flow, thereby affecting a neuron's behaviour. It is not yet known why or how these gating modes occur, but they provide ion channels with a mechanism for contributing to intraneuronal adaptation.

The chapter introduces the experimental work involved with discovering the existence of the three gating modes in N-type Ca^{++} channels, and outlines a model for describing gating and gating modes. It then introduces two suggestions for how the different gating modes occur. The experimentalists have suggested that the binding of G-proteins (guanine nucleotide binding proteins) to an ion channel may influence the occurrence of particular gating modes. An alternative suggestion is that the *proximity* of neighbouring ion channels is affecting the likelihood of particular gating modes occurring. This suggestion depends upon ion channels being capable of lateral, *electrokinetic* movement within the neuronal membrane. Electrokinesis of ion channels is proposed by Anthony Bell to be a mechanism for intraneuronal adaptation.[7,8] It should be noted that much of the content of sections on the electrokinesis of ion channels and ion channel-based adaptation of the neuron can be attributed to Bell and is of a speculative nature. However, the use of evidence for gating modes as support for his ideas is original, though also speculative. The chapter concludes with a discussion of some implications of G-protein binding and electrokinesis, and the role of gating modes in intraneuronal adaptation.

5.2 Conductance of N-type Ca^{++} Channels

It was explained at the close of Chapter 4, that to explore gating it was necessary to restrict the discussion to one subtype of ion channel, namely the N-type Ca^{++} channel. For the Mahowald and Douglas silicon neuron design, it was not necessary to specify a subtype of ion channel as the kinetic variables used were considered to be adequate for all cationic channels. However, to represent gat-

ing with the circuitry described in Chapter 7, such a specification is required. The equation for the N-type conductance is of the same form as the equation for generic channel conductance presented in the previous chapter, in equation 4.1.

$$I_{Ntype} = ((G_{Nmax_{Ca++}}.u)q^2)(V - E_{N_{Ca++}}) \tag{5.1}$$

where $G_{Nmax_{Ca++}}$ is the maximum permeability of Ca^{++} ions through N-type Ca^{++} channels in the membrane (0.73 x 10^{-12} cm^3 s^{-1}.)

$E_{N_{Ca++}}$ is the Nernst potential for Ca^{++} (+128mV).

q is the activation variable which describes the opening of the channel and,

u is the inactivation variable which describes the closing of the channel. As in equation 4.2, q and u have the kinetic form:

$$\frac{\delta x}{\delta t} = \frac{x_\infty - x}{\tau_x} \tag{5.2}$$

It is then possible to substitute into this equation real neurophysiological values taken from voltage-clamp and channel blocking experiments. The resulting equation can be found at the beginning of chapter 7, with details of the experimental procedure by which it was obtained.

5.3 Gating of N-type Ca^{++} channels

N-type Ca^{++} channels have been shown to display at least three patterns of gating, characterised as low-, medium- and high-p_o modes on the basis of open channel probability during depolarising pulses.[2,1] Open channel probability was calculated for each sweep, as in equation 5.3.

$$\frac{t_O}{t_O + t_C} \tag{5.3}$$

where t_O is the mean of all open times, and t_C is the mean of all closed times.

N-type Ca^{++} channels undergo hundreds or thousands of open-closed transitions in one mode, before switching to a different mode. Each mode has kinetics that differ from the other modes, e.g activation kinetics and voltage-dependence. The dwell time in each mode varies from patch to patch. This suggested to the experimentalists that gating modes maybe result from the binding to the channel by other substances, namely G-proteins. Generally, transitions from high- to low-p_o gating modes *reduce* overall Ca^{++} influx, and the binding of substances is suggested to favour the low-p_o gating mode. The experiments were carried out by removing intact sympathetic chains from adult bullfrogs (*Rana catesbeiana*) and cultured for up to 15 days. Then cell-attached patch recordings were carried out using a -10mV test potential. These particular neurons were used because they lack T-type channels, and the N-type channels significantly outnumber the L-type channels. Figure 5–1 shows a representation of the three gating modes. It is possible to detect the presence of modes by visual inspection.

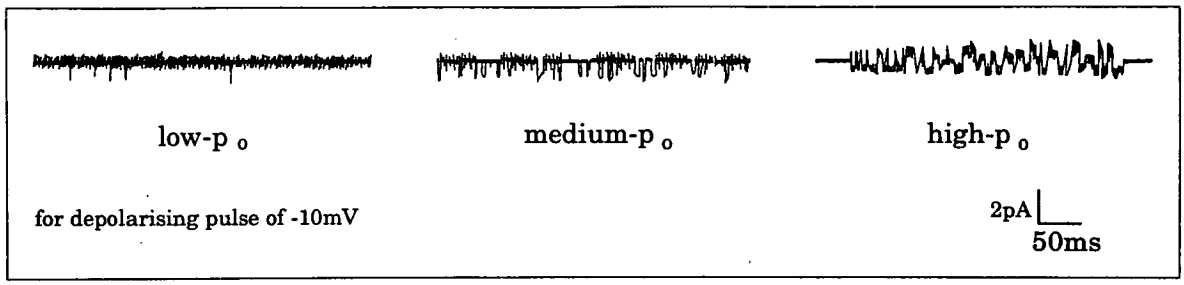

Figure 5–1: *The three gating modes of N-type Ca^{++} channels*

The three gating modes have the following general characteristics, (figure 5–2):

at -10mV:

low-p o	open ~ 0.3ms closed 10 - 20ms	↑ requires increasing depolarisation	↓ increasing voltage dependence	↓ increasing Ca ++ entry
medium-p o	open 1.5ms closed 3ms			
high-p o	open 3ms closed 1ms			

Figure 5–2: *Some general characteristics of the three gating modes*

Figure 5–3 is an abstract representation of the proportion of time spent in an open state for each of the gating modes.

5.4 Describing Gating and Gating Modes

Gating is most commonly described by analysing the rate constants between states and constructing a state diagram representing transitions between states.[3] A number of assumptions are made in the construction of these state diagrams:

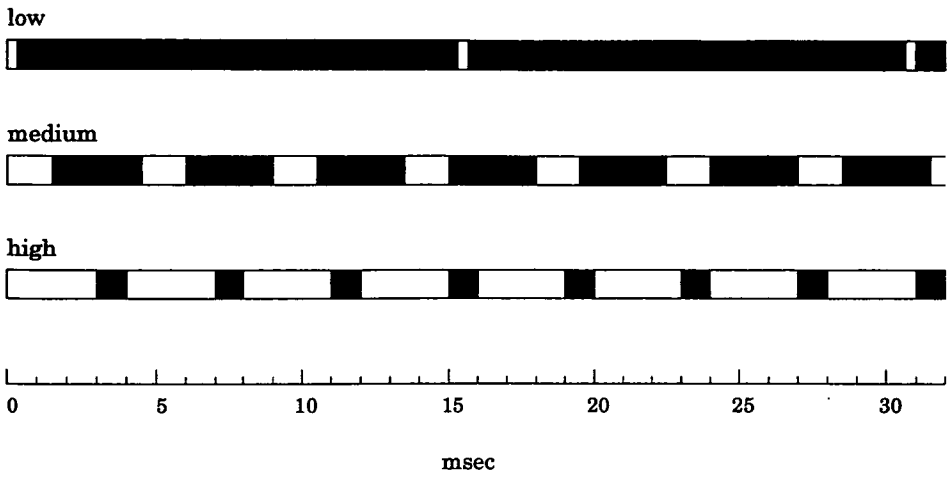

Figure 5–3: *The proportion of time spent in an open state for each of the three observed gating modes. White denotes an open state, whilst black denotes a closed state.*

- Transitions do not depend on how the system reached the state.

- Transitions are first-order – if a transition is multiexponential, then it must be subdivided into first-order, intermediate steps.

Excluding gating modes for the moment, a state diagram for an N-type Ca^{++} channel might be constructed in the following way: firstly, evidence suggests that, for Ca^{++} channels in general, four gating charges must move from the intracellular to the extracellular space for the channel to open. With reference to B. of figure 4–10 in Chapter 4, the gating charges are the cationic residues located in the S4 helix. This can be represented in the form shown in 5–4.

The binary numbers represent the gating charges, "0" indicating that the charge is in the "incorrect" (intracellular) position, and "1" indicating that the charge is in the "correct" (extracellular) position. Only when all four gating charges are in the correct position, is the ion channel open, "O". "C4", "C3" and "C2" indicate

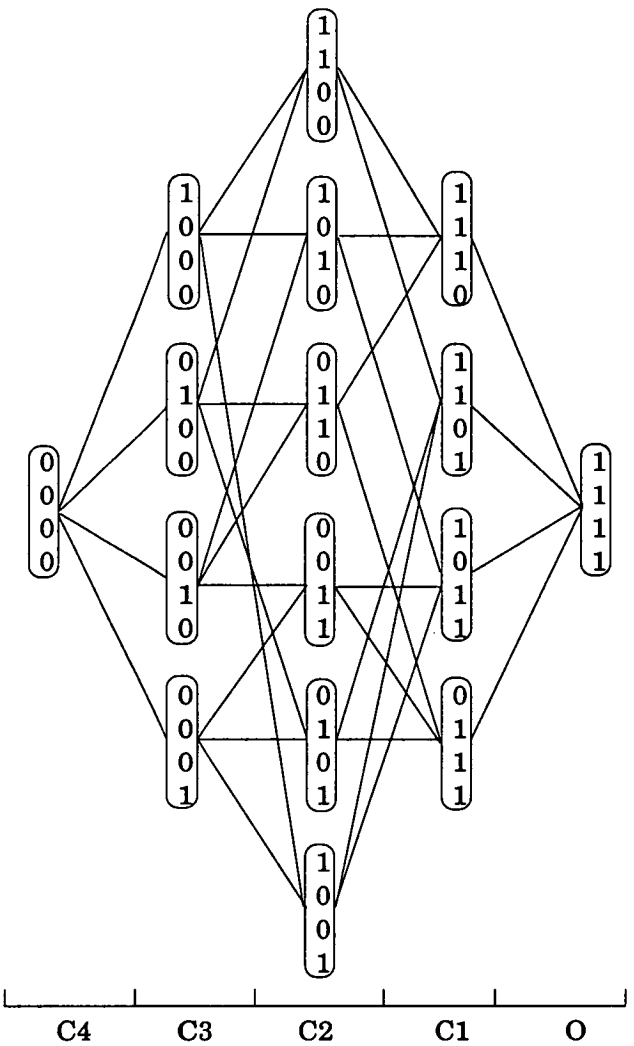

This can be simplified to:

$$C4 \underset{\beta}{\overset{\alpha}{\rightleftharpoons}} C3 \underset{\beta_1}{\overset{\alpha_1}{\rightleftharpoons}} C2 \underset{\beta_2}{\overset{\alpha_2}{\rightleftharpoons}} C1 \underset{\beta_3}{\overset{\alpha_3}{\rightleftharpoons}} O$$

Figure 5–4: *A Monod-Wyman-Changeux scheme for conformational state and transitions according to the movement of gating charges. This scheme – a set of first-order, independent states – was developed as part of the authors' 1965 theory of conformational states and transitions during the cooperative binding of ligands. (Adapted from Hille, 1984).*

closed and *inactivatable* conformations of the channel, with zero, one and two charges in the correct position, whilst "C1" indicates a closed and activatable conformation. "Activatable" and "inactivatable" relate to the time required for a channel to open after it has closed. In an activatable conformation, only one gating charge is in an incorrect position and the channel can, therefore, be opened more rapidly than from an inactivatable conformation. The simplified equation shows the conformational states and the rate constants between them. The rate constants are related to open probability in the following way: translating the rate constants into a voltage-dependent time constant, τ_q, gives the equation in 5.4

$$\tau_q = \frac{1}{\alpha_q + \beta_q} \tag{5.4}$$

where τ_q is the time constant of activation, i.e the time it takes for the fraction of channels that are going to be open at equilibrium, to open, α_q is the rate constant between C4 and O and β_q is the rate constant between O and C4. Therefore, in any given sweep, a more rapid time constant of activation will mean that the probability of finding the channels open will increase. As described previously, there are different probabilities of open and closed states *within* each of the three gating modes. It is therefore possible to construct a nested state diagram such as that shown in figure 5–5.

One argument against a state diagram representation of gating and gating modes is that the state and transition values are related to the timescale on which they are measured.[17] The implication is that, if more measurements were taken, at smaller timescales, more modes would be revealed. The experimentalists them-

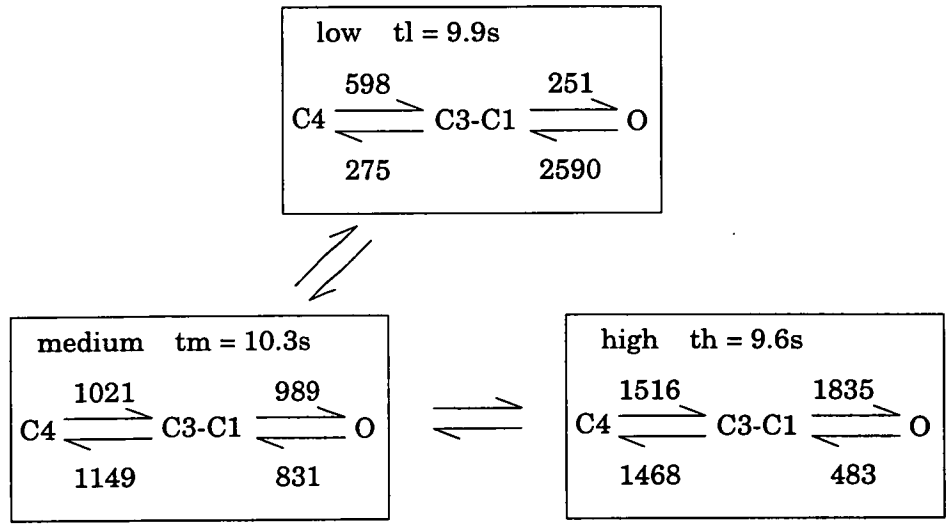

Figure 5–5: *The gating modes of N-type Ca^{++} channels as represented by a state diagram. This diagram represents the sets of C2-C1-O states, corresponding to each mode. The mean dwell times in each mode are indicated as $t_{l,m}$ and $_h$ and were derived from the experimental data. The rate constants (in s^{-1}) for the transitions between closed and open states are averaged over 13 experiments, (adapted from Delcour, 1993[1]).*

selves suggest that further subdivision of the gating modes may be necessary. Others, those endorsing nonlinear dynamical descriptions of neurobiological phenomena perhaps, would argue that a different model and methodology is required. Another argument is that ion channel processes are not independent but are weakly correlated with each other.[60] This would be contrary to the first assumption of the state diagrams described previously. However, if such a state diagram can adequately describe gating and gating modes, there may be no need to express underlying molecular, *microscopic* dependencies. Either way, these are arguments about how to describe ion channel gating and gating modes. It still remains to explain how they happen.

5.5 G-Protein Binding

G-proteins are heterotrimers (polymers formed from three different molecules) that move in the plane of the membrane, the alpha subunit of which can bind to ion channels, thereby modulating gating. The binding of G-proteins to N-type Ca^{++} channels has been proposed to down-modulate conductance by causing channels to make transitions to the low-p_o gating mode.[2,1] In cartoon form, this may take place in the way shown in figure 5–6. A, B. and C. depict high-, medium- and low-p_o gating, respectively. The effect of G-protein binding, shown in D, E. and F, is to restrict the degree to which the gating structure can move, or perhaps the speed at which it can move, consequently favouring low-p_o gating. It is only possible to use the cartoon ion channel. The manner in which a G-protein interacts with the helical structure shown in C. of figure 4–10 in Chapter 4 is not yet known.

Delcour et al. use a state diagram to describe this phenomenon. This is shown in figure 5–7.

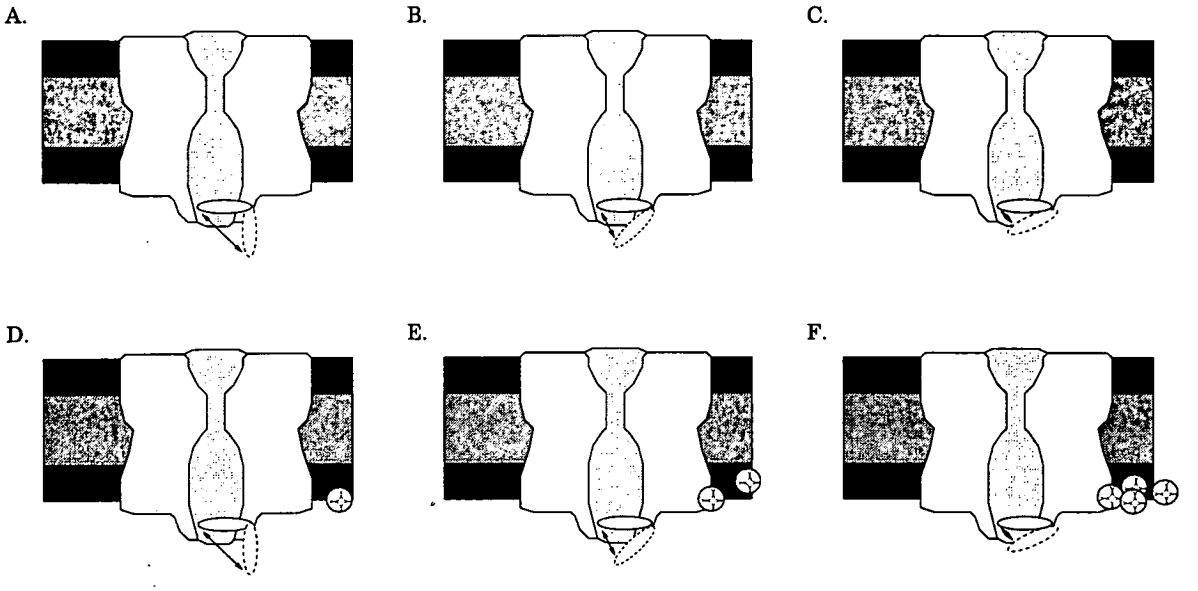

Figure 5–6: *A., B. and C. depict high-, medium- and low-p_o gating modes, respectively. D., E. and F. show the effect of G-protein binding.*

5.6 Electrokinesis of Ion Channels

Variation in patterns of spiking are made possible by a neuron's ion channel repertoire and distribution. It is more or less taken for granted that *regulation* of ion channel synthesis occurs during development and through the lifespan of the organism. In neurons, there is also the question of how these ion channels, which can be synthesised only in the soma, and in some neurons, in the primary dendrites, become distributed over the remaining surface of the neuron. This is carried out, in part, by axonal and vesicular transport mechanisms, but this may not account for the specific positioning of ion channels. If axonal and vesicular transport were responsible for the positioning of channels, an even distribution would be expected. Figure 5–8 provides some evidence that this is not the case.

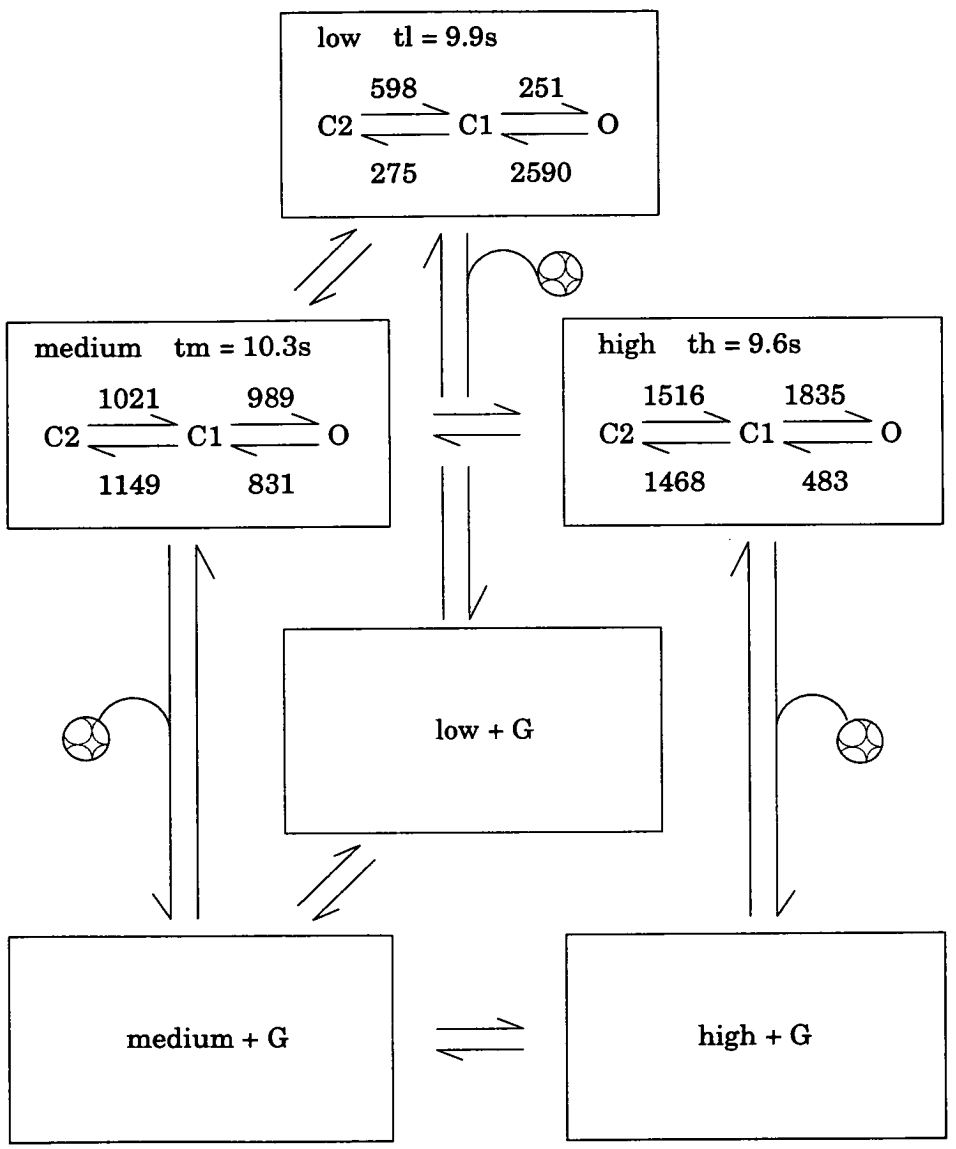

Figure 5–7: *A state diagram to represent G-protein binding to N-type Ca^{++} channels, and the effect upon gating mode, (adapted from Delcour, 1993[2]).*

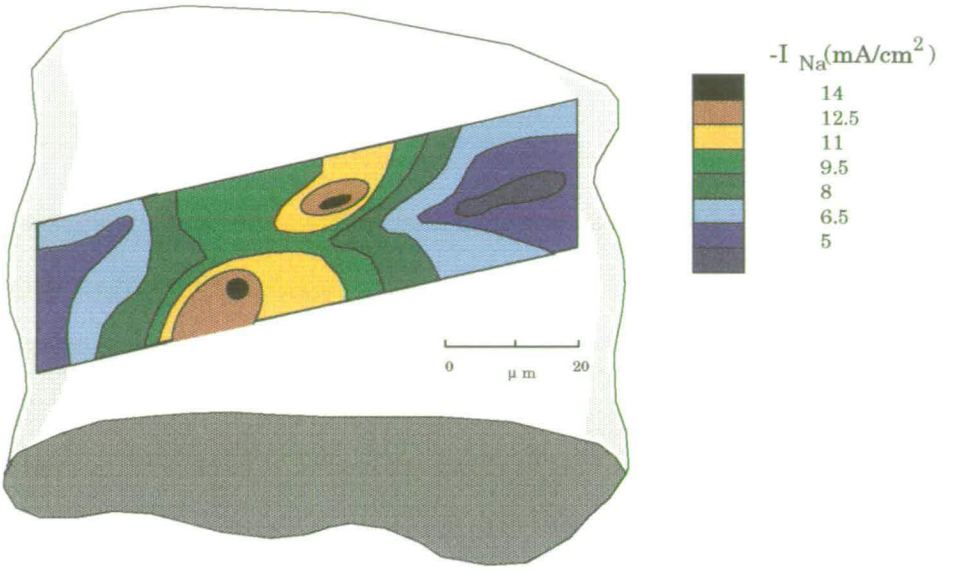

Figure 5–8: *A density distribution of peak Na^+ current, indicating an uneven distribution of (Na^+) channels on the surface of frog sartorius muscle fibre, (adapted from Hille, 1984).*

It has been known for over a decade that ion channels can move in the neuronal membrane. In the absence of any electrokinetic force, the average diffusion rate for N-type Ca^{++} channels is 3.7 x 10^{-10} m^2s^{-1}. Movement can be measured by labelling the ion channel proteins with a fluorescent tag and observing their distribution in a living neuron under a fluorescence microscope. Bell's hypothesis is that ion channels also move electrokinetically – that the degree and direction of movement is affected by the ion channel's own, and neighbouring ion channel's, open or closed state. This is significant, as it provides a mechanism for *activity-dependent* adaptation. The following section describes some features of ion channel-based (electrokinetic) adaptation. This is presented in greater depth in the "channel space" papers of Bell.[7,8]

5.7 Ion Channel-Based Adaptation of the Neuron

For the purposes of this work, it is assumed that only channels in an open state are susceptible to electrokinesis. This could arise for two reasons:

1. the intracellular end of the channel is at a different polarity as a result of the conformational change causing charge to move across the membrane. It therefore has a different susceptibility to the electric fields.

2. the flow of ions through the open channel also endows the channel with a different susceptibility.

In the case of N-type Ca^{++} channels, when open, the intracellular end of the channel will exist at a negative polarity as a result of the conformational change of the S4 region, (see B. of figure 4–10). However, the flow of Ca^{++} ions will result in an accumulation of positive charge at the intracellular face of the membrane. The overall effect is that N-type Ca^{++} channels will tend to move to regions where there is a depression in membrane potential. At a microscopic level, this will mean that individual ion channels will tend to move away from their neighbours. This has the effect of reducing the influence of the neighbours on the ion channels, and this in turn manifests itself as a transition to a lower gating mode. Lower gating modes have lower open probabilities as a result of slower time courses of closed to open state conformational change. For the purpose of the subsequent implementation, this is represented by the following model and by figure 5–9. It should be noted, however, that the outcome could equally be produced by a

G-protein mechanism, or some other factor that can cause alterations in gating mode.

The model consists of a neuron, with a patch of membrane that has a population of N-type Ca^{++} channels. Current injection is provided to the neuron, which behaves according to the Hodgkin-Huxley formalism, and exhibits spiking behaviour. Electrokinesis of ion channels is represented, and during adaptation, this is permitted to take place. The patch of membrane can be represented as a strip divided into six regions. It is assumed that, at the edges of the patch, the ion channel complement repeats and so it is useful to imagine that the strip wraps around itself. An ion channel can be located in any of the sextants. This allows three possible distributions. In A, all three ion channels are adjacent. This proximity results in the ion channel at X possessing a high open probability (as a result of a rapid closed – open transition). It is proposed that this is observed as a high-p_o gating mode. However, as a result of electrokinesis, ion channels will move away from neighbours with high open probability and towards areas of depleted potential in the membrane. The intermediate stage of this is shown in B. In B, two of the ion channels remain adjacent, whilst one moves away from its neighbour, the open probability of ion channel X decreases (a reduction in open probability as a result of a reduction in the speed of closed – open transition). This may be observed as a medium-p_o gating mode. Finally, the two remaining adjacent ion channels move apart, this results in the distribution shown in C. Ion channels have low open probability as a result of slow closed – open transition values and are observed to be in low-p_o gating mode and have moved to areas of depleted potential in the membrane patch as much as possible.

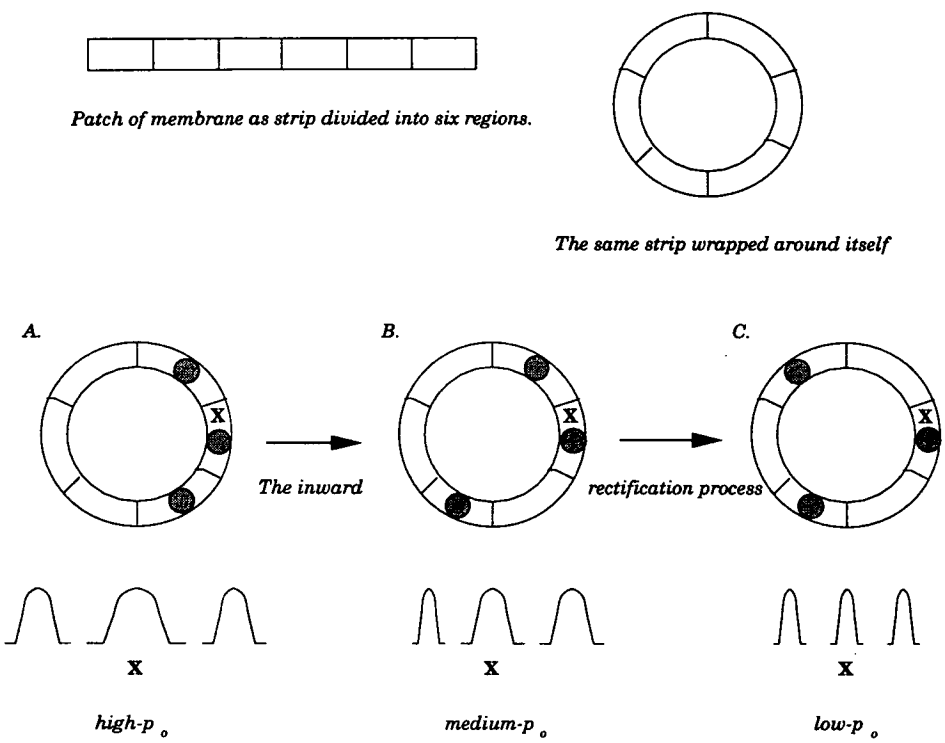

Figure 5–9: *Electrokinesis of channels, and how this could account for different gating modes.*

There are a number of possible outcomes for the membrane patch as a result of this particular channel movement. One neurobiologically plausible outcome is that if case A. represents a situation where the proximity of ion channels creates a high Ca^{++} conductance, preventing the membrane from conducting spikes, the electrokinetic movement will result in the distribution of case C., where channels are located in a way that allows the membrane to conduct spikes. This is an example of an adaptive process involving ion channels. It serves to demonstrate the effect that the distribution of individual ion channels can have on overall neuron behaviour.

5.8 Electrokinesis as a Cause of Gating Mode Transitions

The previous two sections explained the electrokinesis of ion channels and how this can be a mechanism for adaptation. Here, it is suggested that the electrokinesis also accounts for the observation of gating modes. As mentioned previously, there is evidence that ion channel processes are not independent, but are weakly correlated with each other.[60] The evidence comes from studies of the insertion of ion channel proteins into lipid bilayers[61], resulting in a supralinear increase in conductance of the population. In the words of the authors, the inserted ion channel *"creates some condition around itself that facilitates the construction or opening of the following ones."* It is suggested that this *condition* is an electrokinetic one. Figure 5–10 shows how this process might account for the observation of different gating modes, in a similar way as the figure drawn for a G-protein

mechanism. The vertical arrows denote the open probability. The horizontal arrows denote the lateral electrokinetic force on the ion channel.

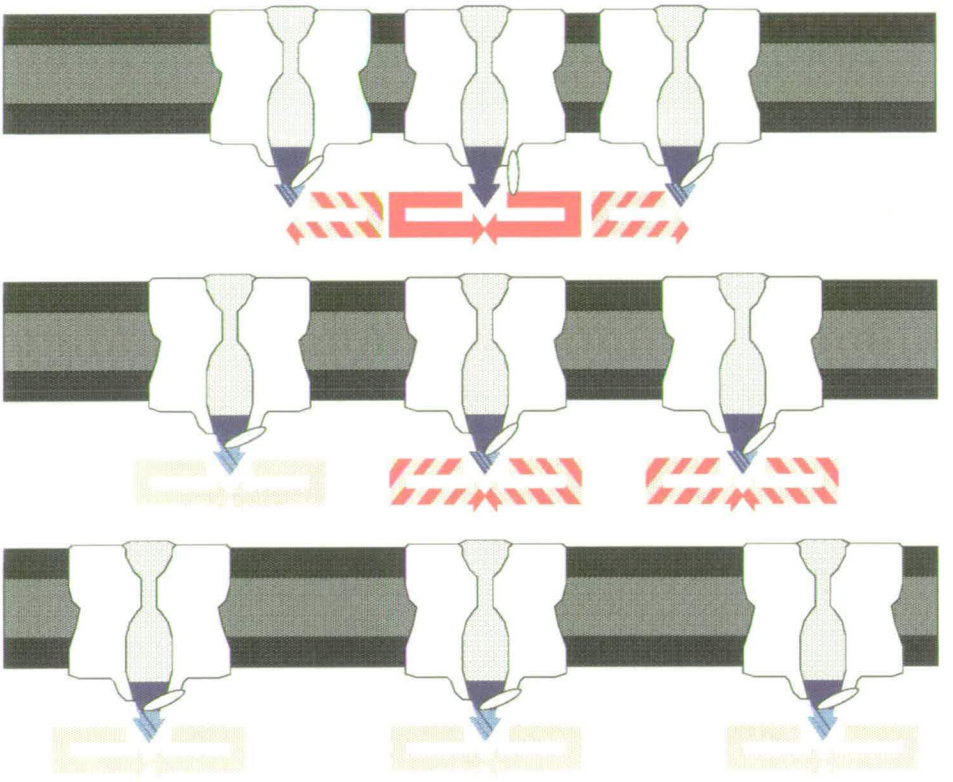

Figure 5–10: *How an electrokinetic process can account for the observation of the three gating modes. The vertical arrows denote the proportion of time spent in an open state. The horizontal arrows denote the lateral electrokinetic force on the channel*

This provides a qualitative description of electrokinesis as a cause for gating modes and gating mode transitions. The interdependency of ion channel proximity, electrokinetic force and ion channel kinetics would result in a negative feedback process. It would not be inconceivable to look for movement of ion channels alongside observation of gating modes. However, for the purpose of this thesis, it is sufficient to assume that G-protein binding or electrokinesis and chan-

nel kinetics are interdependent and that adaptation can occur as a result of this interdependency.

5.9 Discussion

This chapter concentrated on adaptation by N-type Ca^{++} channels, which are classified by Bell as inward rectifiers. According to Bell, there are other channel types; namely outwardly rectifying, depolarising and hyperpolarising. Depolarising and hyperpolarising channels are synaptic; potentiating and depressing respectively. It is therefore possible to extend the model to these other channel types. It is also possible to extend the model to macroscopic phenomena, such as synapse formation and learning[62,63,64] and structural morphogenesis, for example, dendritic spines[65,66,67,68] and collars.[69] The former may have relevance to the work of Elias and various collaborators, on neuromorphic synapses with correlative adaptation rules.[26]

A number of issues arise from the electrokinetic model. Electrokinesis can account for permanently closed ion channels – that there are no ion channels proximal enough to result in the opening of these channels. In the same way, electrokinesis can account for silent (non-adapted) neurons in a region of nervous system. The reverse of this is that electrokinesis can account for the experimentalists' statement that subdivision of the high-p_o mode is unnecessary. The high-p_o mode may represent the most physically proximal that two ion channels are capable of being. This could be experimentally verified. Whilst electrokinesis as a cause of distinct gating modes is merely a speculative suggestion, there are currently

no explanations in the literature for *why* ion channels can be observed to have different gating modes and to make apparently spontaneous transitions between them. This is not to claim that electrokinesis would be the only cause of gating mode transitions. Electrokinesis could occur in conjunction with G-protein binding, for example. Although in a recent review of G-protein modulation of Ca^{++} channels[70], the experimentalists comment that *"There is no easy explanation for the fact that some investigators observe receptor-mediated Ca^{++} channel inhibition when infusing nucleotide-free solutions into cells."* This may, or may not, be relevant to electrokinesis. Also, the models differ from each other in that much G-protein activity occurs as a result of neurotransmitter action, which means that it is not an intraneuronal mechanism, in the strictest sense. A prediction that follows from either the electrokinetic or the G-protein binding model, and again, assuming that case A, of figure 5–9 represents a high Ca^{++} conductance, is that dendritic N-type Ca^{++} channels will be observed in a low-p_o mode when actively conducting spikes. Analogue integrated circuitry can be designed to demonstrate this, and this is what is described in the subsequent two chapters. However, it can only be fully determined by direct experimental evidence. As mentioned previously, adapting to perform conduction is just one of many possible outcomes of alterations in ion channel gating and distribution by, as yet unknown, mechanisms. Chapter 6 provides some evidence for the significance of gating modes, specifically for the phenomenon of locomotion, whilst Chapter 7 demonstrates that it is possible to represent this in analogue integrated circuitry. At the conclusion of Chapter 7, a discussion begins as to whether, though possible, it is also *desirable* for gating modes to be represented in analogue integrated circuitry.

Chapter 6

Silicon Neurons – Experimental Work and Application

6.1 Introduction

Chapter 4 described the design of the Mahowald and Douglas (1991) "silicon neuron". As noted in Chapter 4, the Mahowald and Douglas silicon neuron incorporates the highest degree of neurobiological plausibility, or in the language of Chapter 3, the highest degree of *algorithmic equivalence*, of an implemented neuron at this time. It was shown that more abstract versions of silicon "neurons" exist, a subset of which reappear in this chapter, where they are used to achieve a particular applications goal, specifically, that of providing a central pattern generator for locomotion. This has been a mostly successful venture. The challenge for the work described in this chapter is to demonstrate that analogue integrated circuitry that implements the Hodgkin-Huxley model creates neurobiologically plausible central pattern generation and permits an additional set of behaviours that abstracted neurons are unable to provide. The chapter begins with a brief introduction to the neurobiology of locomotion, the half-centre model and associated phenomena.

Several simulations[33,71,72] and one implementation[37] of central pattern generators for quadrupeds exist in the literature. They incorporate varying degrees of neurobiological plausibility in their neuron models and can produce a range of locomotor behaviours, or gaits. The silicon neuron is shown to match the simulations cited above, with respect to neurobiological plausibility and repertoire of behaviours and has the advantage of having been designed with a specific implementation in mind. It is considerably more neurobiologically plausible than the cited implementation, and whilst both can function adequately as controllers, it is possible that the silicon neuron-controlled quadrupedal walking machine has the potential to exhibit more versatile behaviours, without requiring additional circuitry.

The silicon neuron chip was simulated using AnaLOG[20]. This provides an interactive graphical environment for schematic simulation and layout. It was developed in Caltech, in the late '80's, specifically for simulating circuits with transistors operating in the weak-inversion region, optimised for use with a MOSIS 2μm fabrication process. As explained in Chapter 2, the motivation for operating neuromorphic VLSI circuits in the weak-inversion region originates from the notion of physical equivalence between transistors operating in this region and ion channels. However, since most of the circuitry described in Chapter 4 is not designed to be physically equivalent to ion channels, this does not apply. The motivation for operating the transistors in this circuitry in the weak-inversion region is the consequent low-power consumption, although the advantages offered by this have not yet come to fruition.

The simulation of the weak-inversion region using standard tools, such as HSPICE, is notoriously difficult, since the relevant models are often unavailable. AnaLOG

uses the Enz, Krummenacher, Vittoz (EKV) model for CMOS devices in the weak-inversion region. The EKV approximation produces square-law behaviour for large values of its argument and exponential behaviour for small values. Thus, if the argument is a function of gate voltage, the result is source-drain current. And, unlike HSPICE, the transition from exponential to square-law is continuous. A recent version allows parameter values to be specified by the user for model fitting to alternative fabrication processes. AnaLOG has been adapted to allow the simulation of circuits in the weak-inversion region for the Mietec 2.4μm CMOS process. The technical details of the adaptation of AnaLOG for the Mietec 2.4μm process are to be found in Appendix A.

The intention was initially to simulate and compare the results for the two fabrication processes. The results were expected to be different, notably since the transistors were not resized to take the different scales of the fabrication processes into account. However, it was examined whether if, despite these expected disparities, the Mietec 2.4μm process-tuned neuron in simulation would produce action potentials of a qualitatively and quantitatively similar nature to that of a MOSIS 2μm process-tuned neuron. This would demonstrate that the circuit is robust to alterations in transistor size and variations in process parameters. It would also confirm that a silicon neuron could be fabricated using alternative processes from the original, without necessitating a radical redesign of the circuitry. Further simulations were then carried out for a network of two neurons, to demonstrate the effects of inhibitory coupling, and to determine plausible mechanisms for bursting, inhibition and fatigue. These phenomena are required if the silicon neurons are to be used as the central pattern generator in a controller for a walking machine.

The next two sections present results from simulation and implementation, for both single neuron and inhibitorily coupled neuron operation. The subsequent section describes the application of coupled neurons in the control of a quadrupedal walking machine. Finally, the chapter concludes with a discussion of the silicon neuron, with respect to the walking machine and the possiblities for implementing additional behaviours. Appendix B describes the technical details required to design and implement a silicon neuron in an alternative fabrication process to the one originally used. (The original was a MOSIS 2μm process, the work described here uses a Mietec 2.4μm process). The majority of this work involved resizing the transistors and redesigning the subcells to ensure that they complied with Mietec design rules. All capacitors were redesigned to have more symmetric structures in order to reduce mismatch between them. Several layout errors in the original design were corrected. Finally, the subcells were rearranged so that they made a more efficient use of silicon area. The technical specifications, layout plans and test circuitry are to be found in Appendix B.

6.2 The Neurobiology of Locomotion

Locomotion that involves steps taken by legs, requires a rhythmic alteration of antagonistic muscles; flexors and extensors. The step cycle has two phases: contraction of flexor muscles is responsible for the swing phase – when the foot is off the ground and flexing forward and contraction of extensor muscles is responsible for the stance phase – when the foot is planted and the leg is extending relative to the body. Flexor and extensor muscles are shown in figure 6–1, with the spinal cord circuitry explained in more depth subsequently.

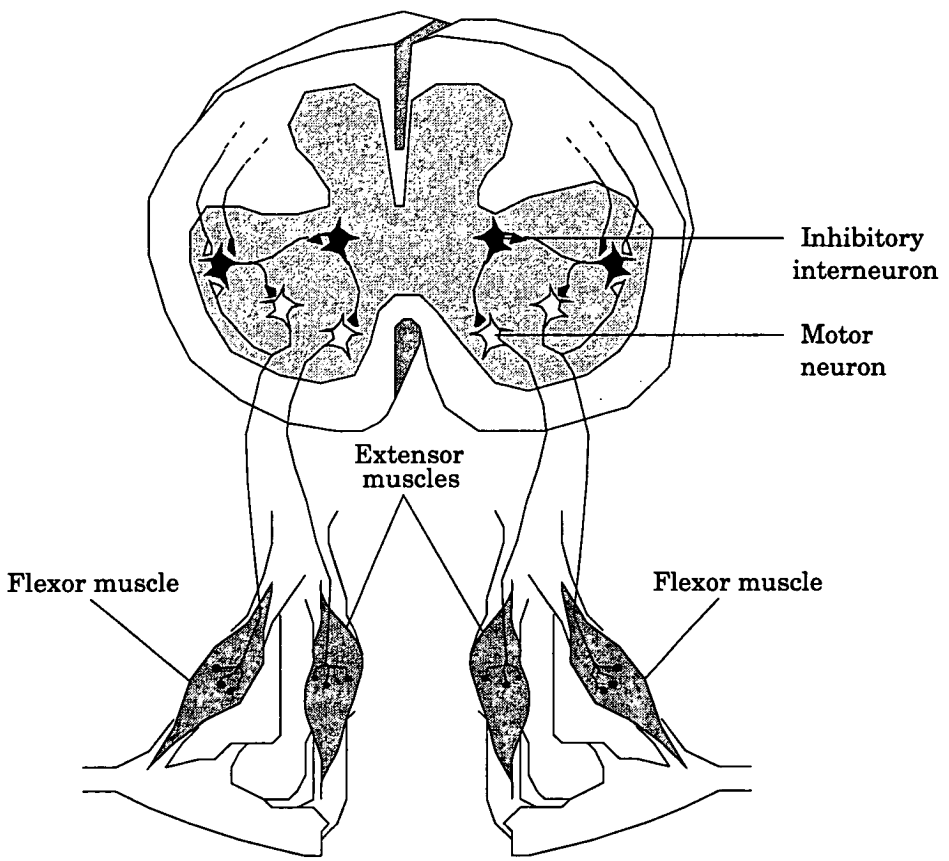

Figure 6–1: *The flexor and extensor muscles and spinal cord circuitry of a quadruped*

6.3 The Half-Centre Model

A hypothetical model of a small set of intraspinal neurons that produces rhythmic behaviour (a central pattern generator (CPG)) is called the half-centre model. The simplest form of this model proposes that interneurons controlling flexor and extensor motor neurons have reciprocal inhibitory connections. i.e when one is active, the other is inactive. (Figure 6–2).

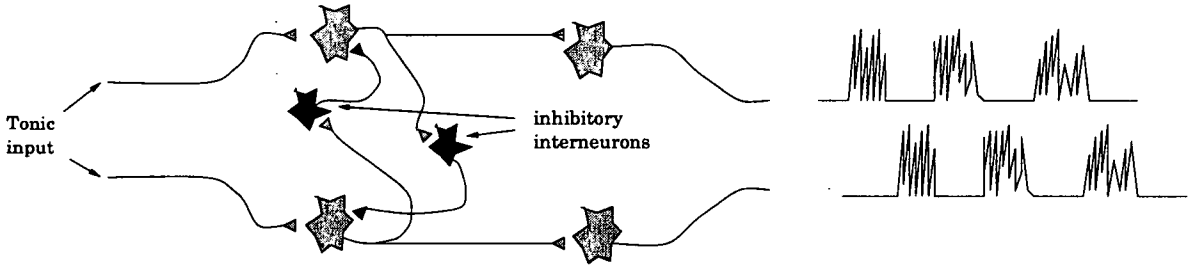

Figure 6–2: *The half-centre model of rhythmic alternating activity in the flexor and extensor motor neurons of the legs.*

6.3.1 Tonic and Phasic Spiking

The activity of the neurons is in the form of phasic spiking (bursts), rather than tonic spiking (the production of individual spikes). The mechanics of spiking were described in Chapter 4. To recap here, spikes are generated by the inward Na^+ current followed by the outward K^+ current. Ca^{++} also enters the neuron during the spike leading to activation of the K^+–after hyperpolarisation (KAHP) conductance. This contributes to the afterhyperpolarisation and slows the return of the membrane potential to the threshold for activation of a succeeding action potential. Phasic spiking occurs when the hyperpolarisation deinactivates the

KAHP conductance which increases the duration of the afterhyperpolarisation. The hyperpolarisation also deinactivates a low threshold Ca^{++} conductance. As the hyperpolarisation decreases, the membrane potential reaches threshold for activation of the low threshold Ca^{++} conductance, producing a long, slow depolarisation. During this long, slow depolarisation a brief series of spikes are generated. Ca^{++} ions enter with each spike, faster than the neuron can remove them, so $[Ca^{++}]_i$ gradually rises until, after a number of spikes, the Ca^{++}–dependent K^+ channels are activated. They hyperpolarise the neuron and shut off activity and Ca^{++} entry. Then the whole process repeats itself. The hyperpolarisation is therefore critical in the generation of phasic spiking. Neurons that are capable of producing phasic spiking can generate rhythmic behaviours. Many fundamental behaviours, such as breathing and walking require the continual rhythmic stimulation of a set of muscles. Also, neurons with phasic properties are used to secrete neurohormones into the circulation. An example is that of oxytocin-containing neurons that are located in the hypothalamus of mammals, used in the control of lactation. Phasic spiking results from a combination of conductance alterations, namely, sustained K^+ hyperpolarisation, accumulated Ca^{++} and deinactivated Ca^{++}-dependent K^+.

The rhythmic alternation of activity could occur as a result of a number of mechanisms, which may be dependent on, or independent of each other:

- *decay* of bursting as a result of the Ca^{++}-dependent K^+ conductances

- *fatigue* of inhibitory synapses, as a result of neurotransmitter depletion, which causes the strength of inhibition to decline with time. (Though the input neuron may still be producing bursts)

- *adaptation* of the neurons to phasic descending input, where response to a consistent input declines with time.

- *post-inhibitory rebound*, in which the threshold for excitation of a neuron decreases as a result of past inhibition.

6.4 Locomotor Gaits of Quadrupeds

There are at least eight possible quadruped locomotor gaits. They can be represented as a cycle in which the phase of the whole cycle is normalised to one, figure 6–3. This shows the delays between each of the legs for the various gaits.

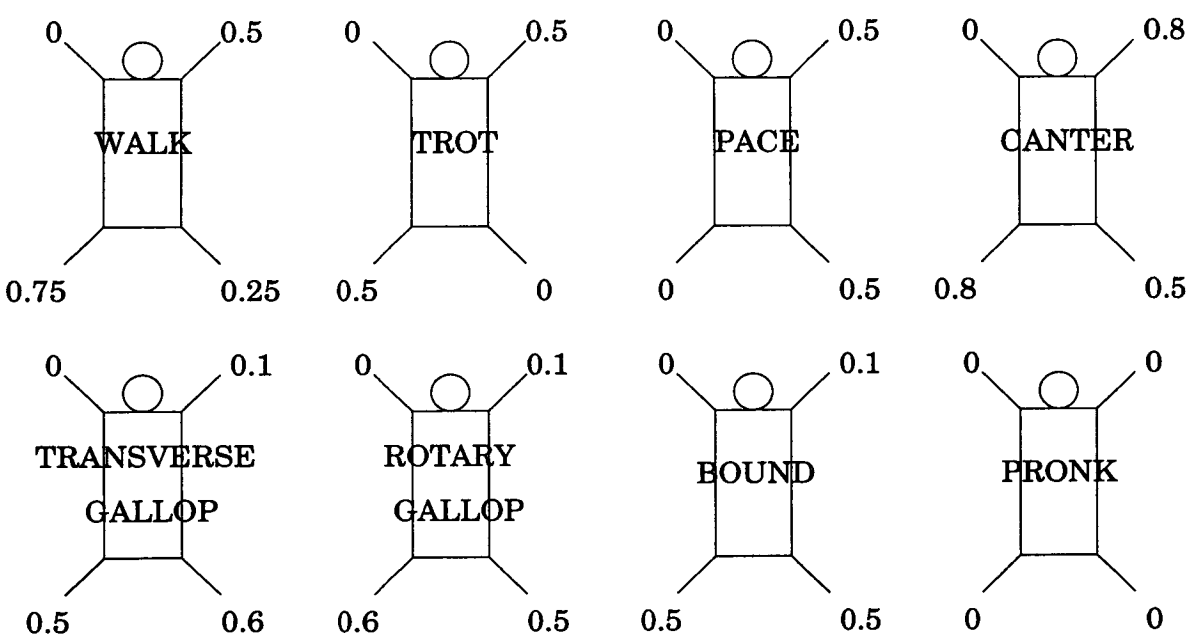

Figure 6–3: *The phase differences between the legs of a quadruped for eight locomotor gaits*

In order to reduce the problem faced by a silicon neuron-controlled walking machine, the work will concentrate on replicating only the walking and trotting

gaits. This can be done without any loss of neurobiological plausibility, since this less evolved method of locomotion – involving only lateral movement of the limbs (a sprawling posture) – and exhibiting only walking and trotting gaits, can be observed in salamanders and some other amphibians.[73,74,75]

6.5 A Discussion of the Relevant Literature

It has been demonstrated in several places in the literature [33,71] that a central pattern generator (CPG) can be constructed from four oscillators (of which the silicon neuron is an example), that can produce most, if not all, of the gaits shown in figure 6–3. Figure 6–4 is a table of three of the most relevant CPG models (those which retain some degree of neurobiological plausibility) and their features, with the model described in this chapter included for comparison. There are two principle features, which vary from model to model, the first is the connection architecture and the second is whether gait transitions are produced by intrinsic or extrinsic parameter alteration, i.e intraneuronal or interneuronal alteration.

The Patel and DeWeerth model is the least neurobiologically plausible, their approach is justified by asserting that any, more complex neurons, would require a large number of transistors to implement and that this would restrict its use in systems with a high number of nodes. This is characteristic of an intraneuronal vs interneuronal debate – researchers that use simplified models will therefore emphasise the importance of large architectures and connectivity. The Ellias-Grossberg model is neurobiologically plausible. Its only disadvantage is that it was not designed with a specific implementation in mind. The virtues of imple-

AUTHOR	Patel & DeWeerth 1997	Ellias & Grossberg 1997	Canavier et al. 1997	Collin & Still 1998
NEURON MODEL	Morris - Lecar	Hodgkin - Huxley	Reduced Hodgkin - Huxley	Hodgkin - Huxley
ANIMAL MODEL	None	Cat	Cat, horse	Salamander
FEATURES	Two - state model Representing the "envelope" of a burst, i.e the calcium conductance. No individual spikes	As described	Four - state model Represents: membrane potential intracellular calcium average spike freq. activation of current	As described
ARCHITECTURE	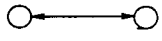 Not commited to a full architecture as yet.	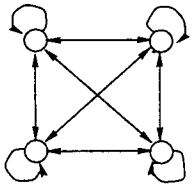	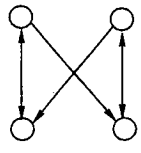	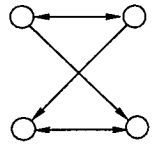
INPUT	Current injection	Tonic - phasic	Tonic - phasic	Current injection
GAIT TRANSITIONS	By alteration of level of current injection i.e tonic component **Semi-intrinsic**	By alteration of phasic component of input **Extrinisic**	By alteration of tonic component of input **Semi-intrinsic**	By alteration of contralateral delay. **Intrinsic**
GAITS ACHIEVABLE	Will depend on chosen architecture	Walk, trot, pace, gallop, pronk	Walk, trot, pace, bound*, gallop	Walk, trot
REPRESENTATION	Neurons simulated and implemented	Architecture simulated	Architecture simulated	Architecture simulated. Machine implemented

Figure 6–4: *A table of relevant CPG models. *Achieving the bound gait is significant because many previous models could not make a transition from a bound gait without extrinsic parameter alteration e.g selective hyperstimulation of neurons*

mentation (synthesis) have been discussed in Chapter 2. The discussion at the end of this chapter raises one issue of relevance to locomotion and locomotor gaits. The Canavier et al. model, whilst unable to produce discrete spikes, does model the average spike frequency as a function of the other three variables. In addition, the rates of change of activation and calcium concentration are dependent on the spike frequency. This creates a *feedback* effect, which enhances the complexity of the neuron's response to changes in input. They provide a quantitative description of this in terms of the phase response curves for the neurons. They have found that *"PRCs that have a complex shape enable a circuit to produce a wider variety of patterns, and since complex neurons tend to have complex PRCs, enriching the repertoire of patterns exhibited by a circuit may be the function of some intrinsic neuronal complexity."*

6.6 Design and Implementation of a Silicon Neuron

A discussion of neurons and the ways in which they can be described and subsequently modelled, was the topic of Chapter 4. The chapter continued with an explanation of the 1991 Mahowald and Douglas silicon neuron; how the design represents the activation, inactivation and kinetic time variables of ion channel conductances according to the Hodgkin-Huxley model. At this stage, no changes are made to the silicon neuron design. These are carried out in the novel silicon neuron design presented in chapter 7. As mentioned in the introduction, all technical details concerning the chip described in this chapter, can be found in Appendix B. Although the Mahowald et al., neuron circuitry has been described in several places [9,76,77], published documentation does not extend much beyond

this. This chapter, in conjunction with Appendix B, represents the only full account of a silicon neuron, including layout and implementation details, currently in existence.

6.7 Results from Simulation: Single Neuron Behaviour

The figures below show graphs of the silicon neuron circuit simulated for figure 6–5 the MOSIS 2μm process and figure 6–6 the Mietec 2.4μm process.

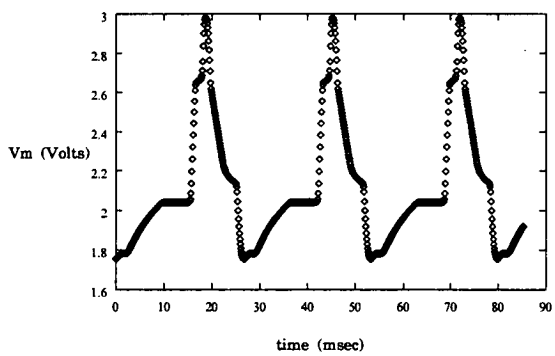

Figure 6–5: *Graph of membrane potential (Vm) output for silicon neuron circuit tuned for MOSIS 2 μm process.*

It can be seen that the Mietec-tuned neuron also produces action potentials of a similar peak amplitude, around 3V, with a similar resting potential, just above 2V, and roughly the same duration, around 10-20msec. Unfortunately, this does not tell us anything definite regarding the circuit's robustness to process variations, or whether the differences in circuit behaviour are occurring as a result of changing the fabrication process and could therefore be compensated for by tuning the appropriate parameters directly on the chip test board. The most

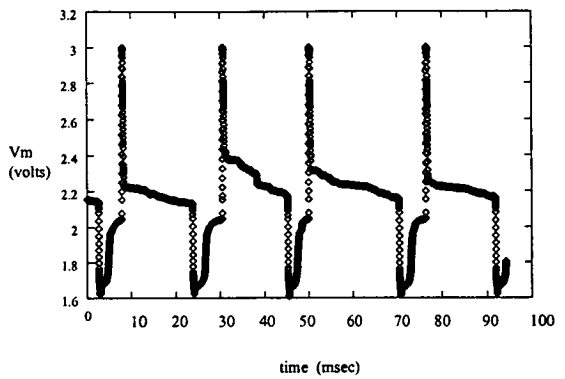

Figure 6–6: *Graph of membrane potential (Vm) output for silicon neuron circuitry tuned for Mietec 2.4 μ process*

significant difference occurs in the hyperpolarisation of the spike. It appears that whilst the repolarisation (falling phase) is very rapid, the Mietec-tuned neuron then enters a slow phase which eventually takes it to hyperpolarisation before it finally returns to rest. However, it was considered that the precise shape of the spike would not affect the performance of the neurons in a central pattern generator.

In order to generate phasic spiking in the simulated neuron, a number of parameters can plausibly be altered. As described previously, it is the hyperpolarisation that is critical in the generation of phasic spiking. Therefore, the sequence of events must be initiated by the K^+ conductance. Secondly, a Ca^{++} conductance is activated and finally, the Ca^{++}–dependent K^+ channels are activated. These correspond with alterable voltage parameters in the silicon neuron circuitry, namely, the K^+ time constant of activation, the Ca^{++} time constant and the K^+AHP conductance, respectively. Increasing the value of the K^+ time constant of activation results in the K^+ conductance occurring later than in normal spiking, so the calcium influx is increased. There is a corresponding increase in

the Ca^{++} time constant, to represent an increased rate of calcium influx. Lastly, the K^+AHP conductance is increased, allowing the neuron to return to its resting potential and subsequently to the spike threshold, the threshold for activation of the Na^+ conductance again. This describes the process underlying a series of spikes. Each spike is generated in the usual way, although it is helpful to lower the value of the spike threshold, the threshold for Na^+ activation, to allow the generation of a spike during the delayed K^+ repolarisation process.

Figure 6–7 shows the effect of decreasing the K^+ time constant for activation and the threshold for Na^+ activation, and increasing the Ca^{++} time constant and the K^+AHP conductance. The result is phasic spiking.

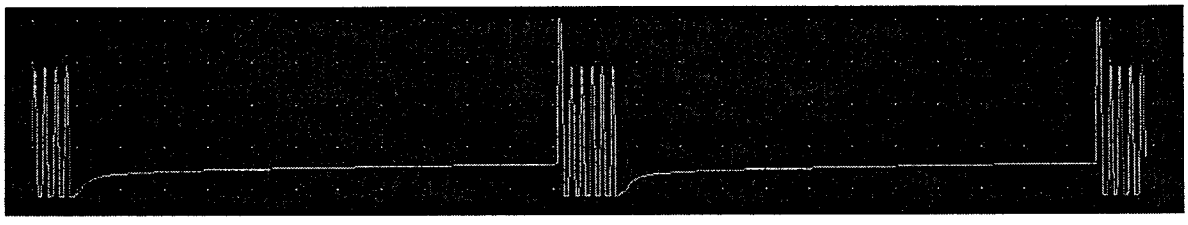

Figure 6–7: *Simulation of a phasically spiking Mietec-tuned silicon neuron*

Currently, the four parameters are altered by toggling the values by hand. It would be possible to incorporate a way by which the toggling of the K^+ time constant for activation would result in an automatic change in the Ca^{++} time constant, the K^+AHP conductance and consequently the threshold for Na^+ activation, with the appropriate timing.

6.8 Results from Simulation: Coupled Neuron Behaviour with Reciprocal Inhibition

The most common method for simulating inhibitory coupling between neurons, is to decrease the magnitude of the inhibit*ed* neuron's input by an amount proportional to the inhibit*ing* neuron's output. For initial ease of simulation, the inhibiting neuron's output to the inhibited neuron has been directly inverted.[1] Inhibition is represented by an inverter connected to each of the neurons, on the "post-synaptic" membrane. Decay is represented by toggling to bypass the inverter circuit completely. Figure 6–8 shows a circuit schematic of one of the coupled neurons with inverter. The other neuron of the coupled pair is identical. The schematic is marked at the point where the inhibitory input occurs. Figure 6–9 shows the results from simulation of reciprocal inhibition of coupled neurons.

6.9 Results from Simulation: CPG Behaviour with Variable Phase Lag

The coupled neurons are connected by excitatory contralateral lines to a further pair of coupled neurons, as shown in figure 6–10.

---

[1]This method more accurately represents an electrical synapse, or gap junction, between the two neurons, rather than a chemical synapse. Representations of chemical synapses usually incorporate a time-dependent, voltage-independent conductive pathway, the expression for which is known as the "alpha function". Details of this can be found in most textbooks of neuronal modelling.[78]

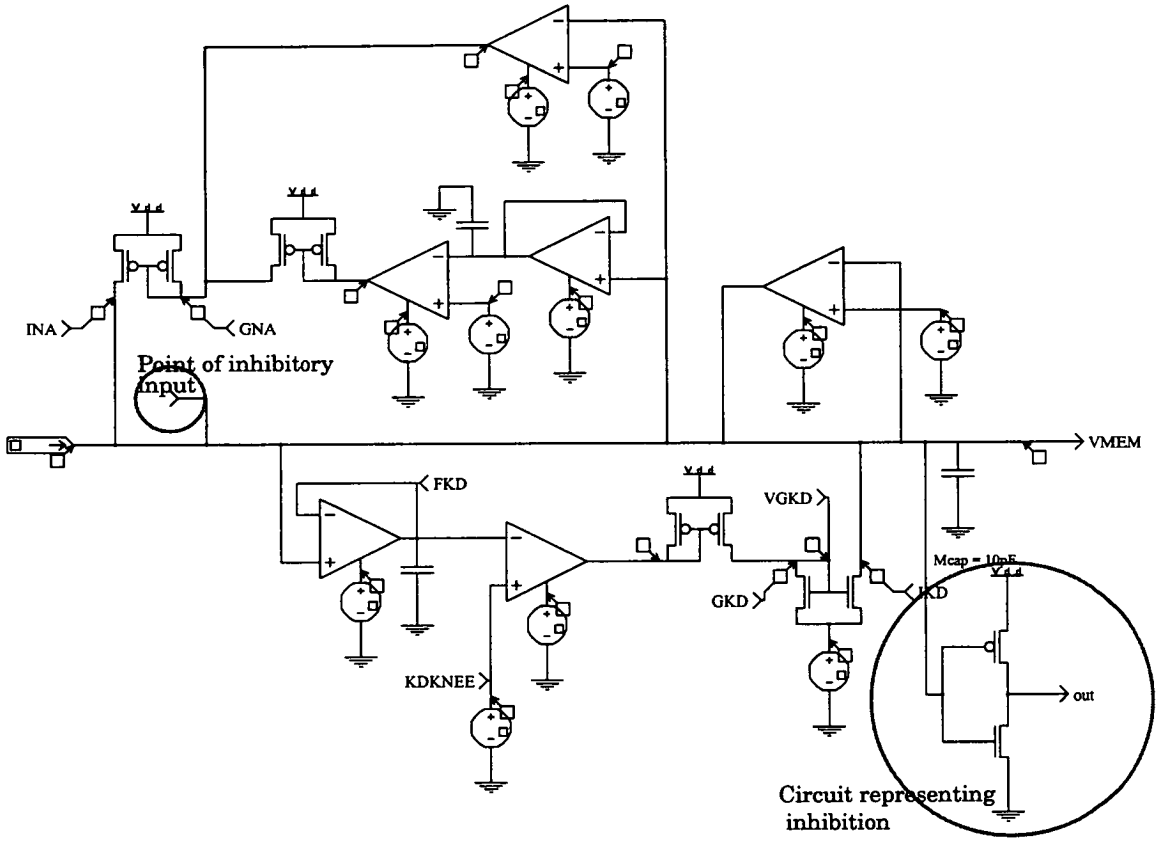

Figure 6–8: *A circuit schematic of one of the coupled neurons with inverter representing inhibition*

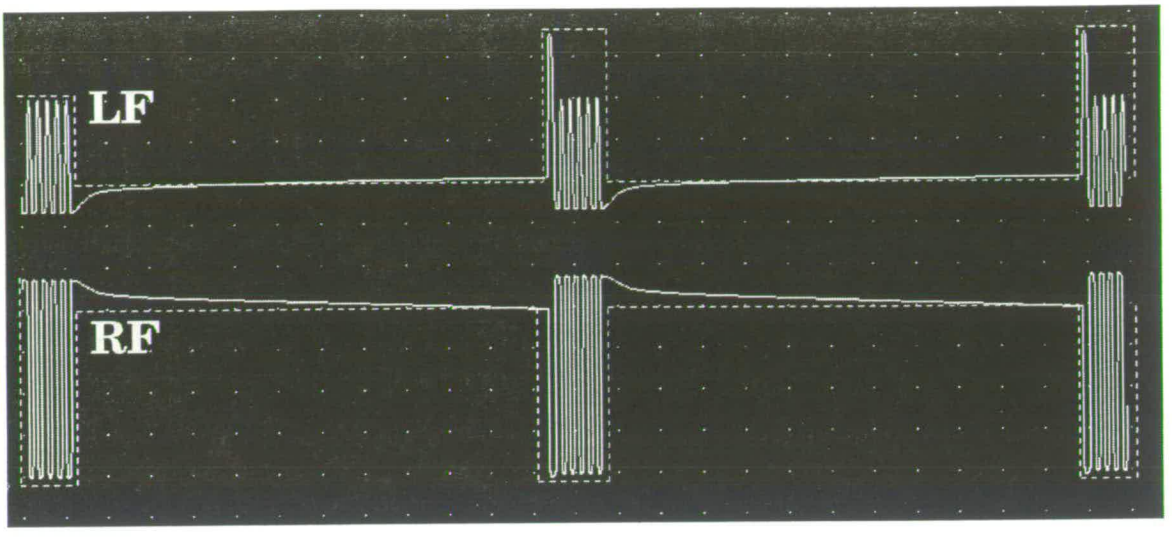

Figure 6–9: *Results from simulation of reciprocal inhibition of coupled neurons.*

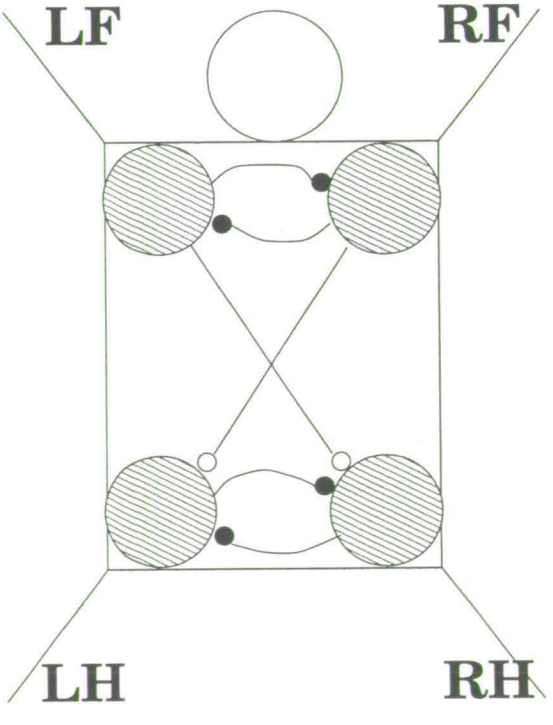

Figure 6–10: *Two pairs of inhibitorily coupled neurons connected by excitatory contralateral delay lines.*

The contralateral lines convert the bursts into square wave pulses. This is necessary to allow a delay to be incorporated. Additional circuitry could be designed either to transmit the individual spikes of each burst, or else to reconvert the square-wave pulses into bursts at the downstream connection. Neurobiological CPGs could be investigated to ascertain the most plausible mechanism. However, the intention here is only to demonstrate the principle of delay in the generation of locomotor gaits. The delay is introduced onto the lines to generate the phase differences required for representing the two quadruped gaits. These delays can be altered to allow transitions between the gaits. The delay lines are implemented by controlling the current through the transistor marked on the circuit schematic in figure 6–11

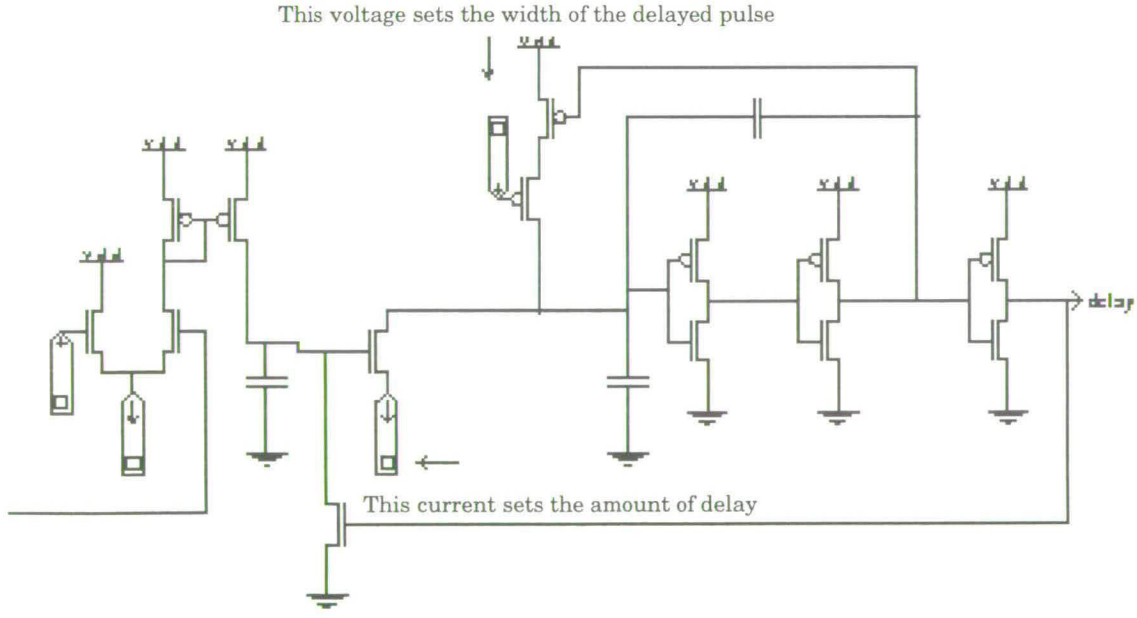

Figure 6–11: *A circuit to implement the excitatory contralateral delay lines.*

In this circuit, initially, the current is mirrored so that regardless of the delaying effect, the membrane potential value remains unaltered. The subcircuit that sets the width of the delayed pulse does so by performing a thresholding operation when the input pulse is decayed enough to produce the falling phase of the output pulse. The subcircuit that sets the amount of delay performs a thresholding operation when the input pulse reaches a value that is high enough to produce the rising phase of the output pulse. Simulations of the entire CPG architecture are shown in figure 6–12

6.10 A Silicon Neuron-Controlled Quadrupedal Walking Machine

This work was carried out in collaboration with Susanne Still of the Institute for Neuroinformatics, ETH, Zurich.[18] In summary, the walking machine consists of a flat, rectangular body, 11cm x 12cm, parallel to the ground, with four DC motors attached parallel to the front axis of the body, and four independently driven legs. A diagram of the robot is shown in figure 6–13.

Transitions between gaits can be made to occur by altering the delay parameters in response to simple sensory input from, for example, tactile and optical sensors that are attached to the legs. The machine's behaviour can be observed by tracking the trajectories of the feet and simultaneously recording the internal states of the neurons.

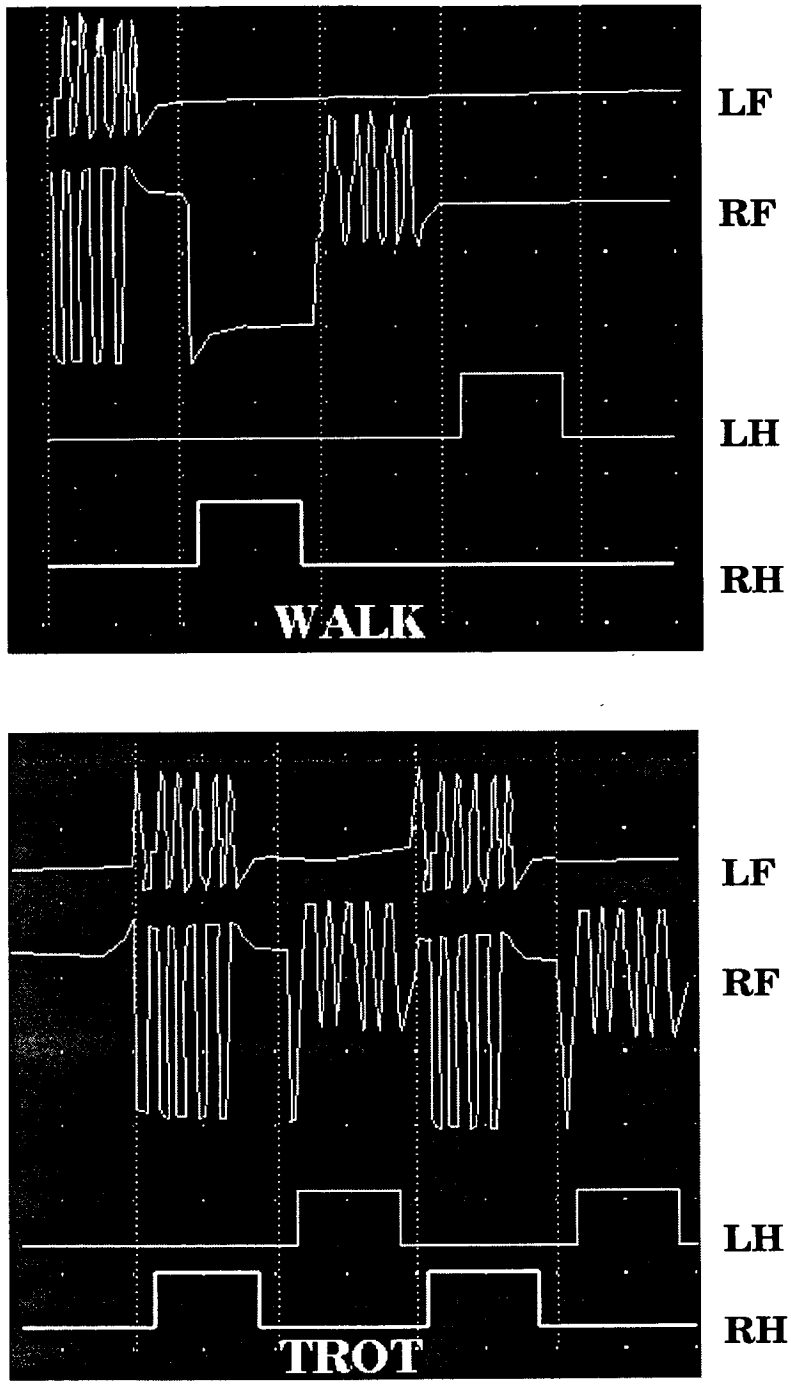

Figure 6–12: *Results of simulation of the entire CPG architecture*

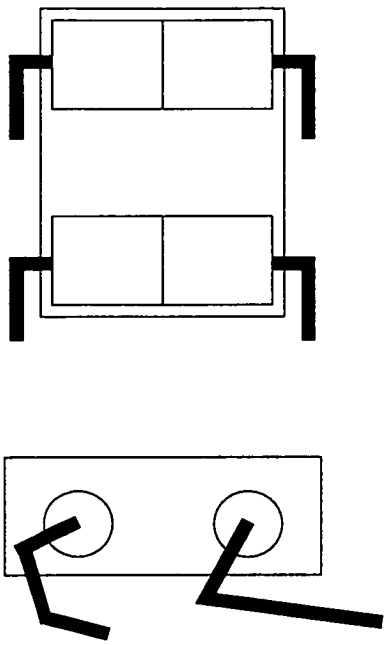

Figure 6–13: *A diagram of the quadrupedal walking machine*

6.11 Results from Implementation: Single Neuron Behaviour

The chip was inserted into the experimental setup detailed in Appendix C and measurements taken with an oscilloscope. The input voltages to the chip were then altered ("tuned") to obtain spiking behaviour. Initially, all parameters were set to zero, apart from Vdd at 5.0V. Then the leakage conductances were activated. This resulted in a membrane potential of 0.714V. If the leak conductance is altered, the resting potential alters accordingly. This demonstrates that the leakage subcell of the chip is correctly functioning. Current injection is increased slowly, at 0.97nA the membrane potential suddenly increases: this is the current injection value at which spiking will be initiated. The sodium parameters are then

set; the maximum conductance of Na^+, or spike amplitude and the threshold for sodium activation. The Na^+ time constant for inactivation sets the rate at which the spike decays to rest. All parameter values are shown in table 6–1. A rough spike then appears, as shown in figure 6–14. Relevant parameter values and how they relate to the form of the spike are included.

GND	0
INJUP	4.3
ELEAK	2.0
NATAUH	0.45
NAOFFKNEE	1.75
NAOFFSAT	0.45
ENA	3.1
NAONSAT	0.5
NAONKNEE	1.75
VDD	5.0

Table 6–1: *Parameter values of the silicon neuron. INJUP denotes current injection, VMEM: the membrane potential output, NA*: Na^+, KD* K^+, CAL*: Ca^{++} and KA*: K^+AHP. Whilst ON denotes activation, OFF: inactivation, KNEE: a threshold, SAT: the maximum conductance and TAU: the time-dependence. (This follows the naming convention used by Mahowald and Douglas)*

This demonstrates that an action potential can be formed with just a sodium conductance activation and inactivation. The potassium parameters are added in the same way. Values are shown in table 6–2, and this produces the spike form shown in figure 6–15. This demonstrates the contribution of potassium to the spike – the maximal K^+ conductance determining the depth of the falling phase, which is set a little higher than the maximum Na^+ conductance, in order to represent hyperpolarisation. The amplitude is 40mV, width 0.5ms and with spikes occurring approximately every 80ms, a frequency of around 12.5 Hz.

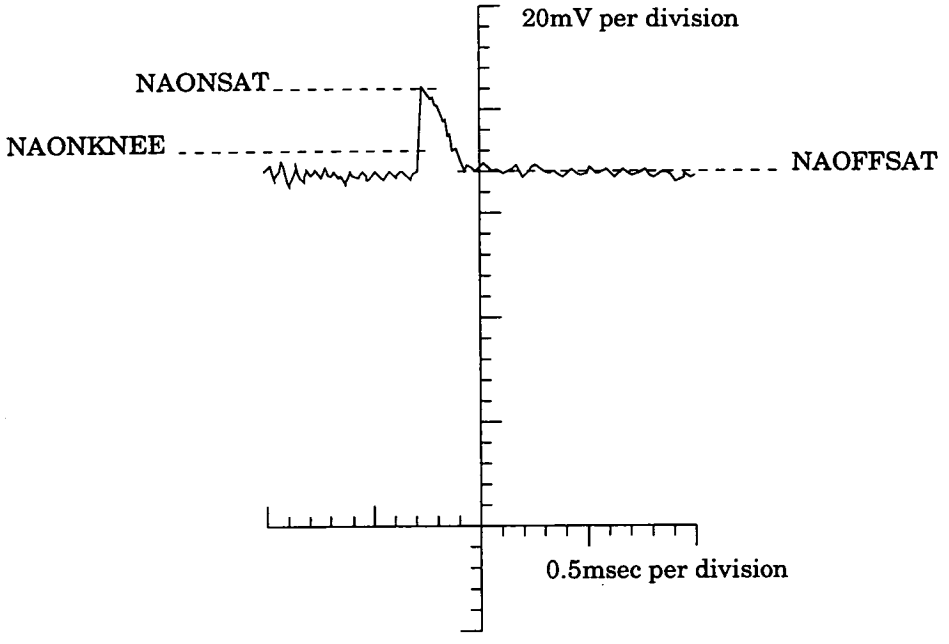

Figure 6–14: *Spiking produced in the presence of a Na^+ conductance only.*

EK	1.5
KDTAUM	0.5
KDKNEE	2.1
KDSAT	1.76

Table 6–2: *Parameter values for the silicon neuron, incorporating Na^+ and K^+ conductances*

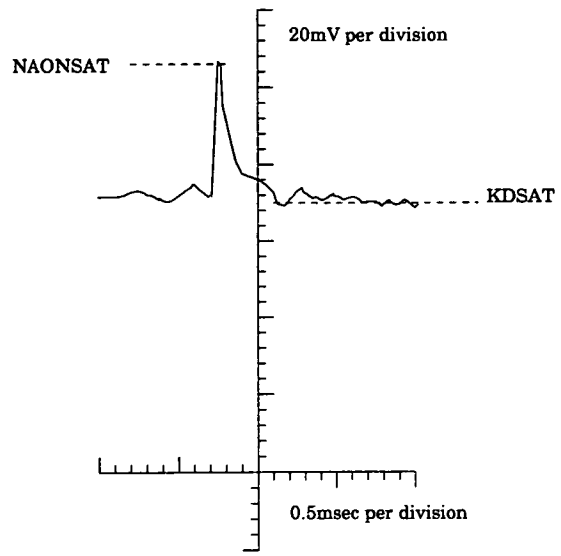

Figure 6–15: *Spiking produced in the presence of Na^+ and K^+ conductances.*

The Mietec-implemented silicon neuron produces spikes that are much smaller and less frequent than those of the MOSIS-implemented silicon neuron. The MOSIS-implemented silicon neuron spikes have a resting potential of approximately 1.8V, and amplitude of 1.6V, width 1-3 ms and a frequency of around 40 Hz. A comparison of Mietec- and MOSIS-implemented silicon neurons is shown in figure 6–16.

When altering the leak conductance, the membrane potential should move between the K^+ conductance and the Na^+ conductance. These were set to 1.3 and 3.0V respectively, but the membrane potential only moves from 0.6V to 0.892V. This might suggest that something is latching the membrane potential at an incorrect level. Shifts in the values of the K^+ conductance and the Na^+ conductance result in corresponding shifts in the range of values for membrane potential, but no overall increase in the absolute range could be obtained. So, the Mietec-implemented silicon neuron has a considerably narrower range than the MOSIS-implemented

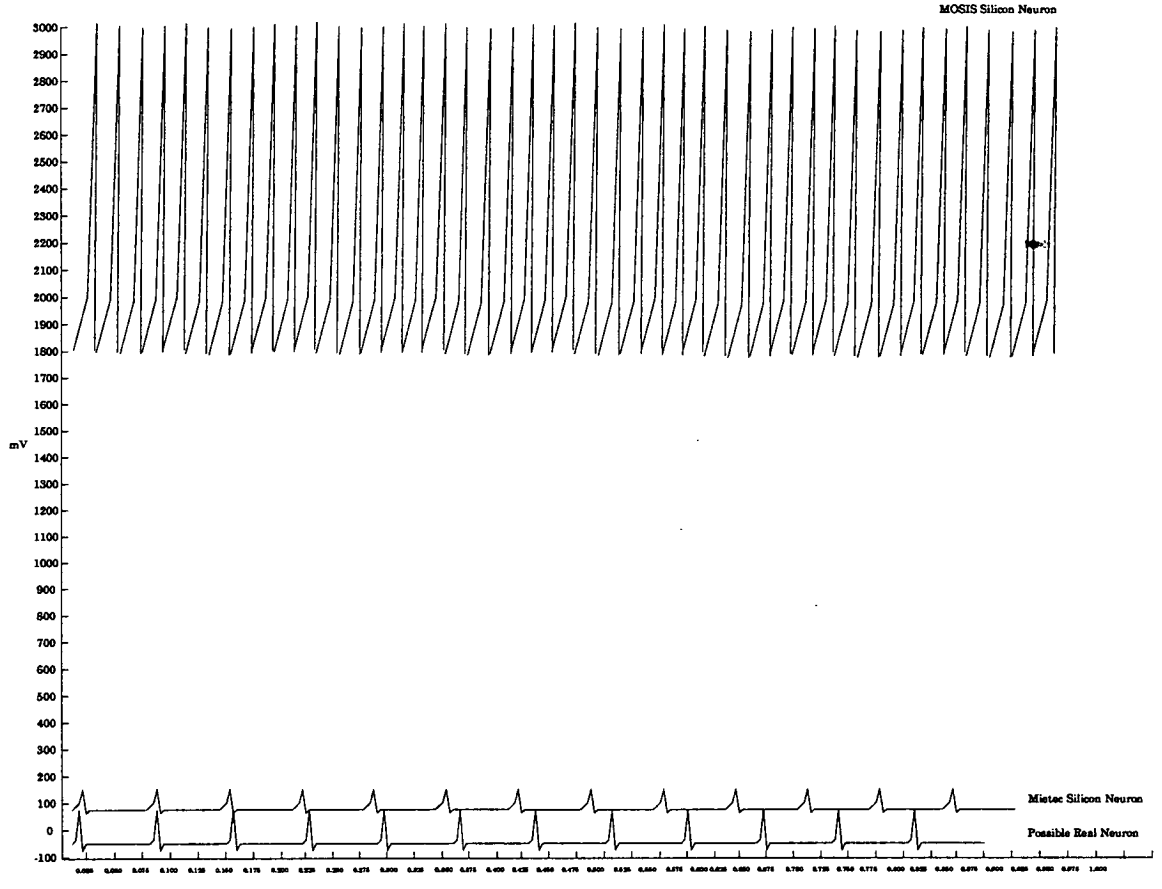

Figure 6–16: *A comparison of spiking in Mietec-, MOSIS-implemented silicon neurons and a real neuron. (Note that spiking in real neurons can have a wide range of values. A trace is included here merely to give an indication of a feasible set of values).*

silicon neuron. This could be a result of imprecision in scaling the subcells for the Mietec process. The result is that its values could be said to be more neurobiologically realistic than the MOSIS ones. Its firing frequency of 12.5Hz is within the neurophysiological range.

6.12 Discussion

This chapter has described the design and implementation of a silicon neuron, based on the Hodgkin-Huxley model, and demonstrated how this implementation could be used to create a central pattern generator for a quadruped machine that can possess several locomotor gaits. It also discussed how this work compared with other relevant models. One thing that emerged was a debate over intraneuronal and interneuronal parameter alteration. As a generalisation, the more neurobiologically plausible a neuron model, the more scope it has for altering its overall output by way of intraneuronal, rather than interneuronal, change, and the less it is necessary to rely on interneuronal parameter change. However, in the case of quadruped locomotion, there are strong arguments for the neurobiological plausibility of interneuronal alteration: such alteration can represent intraspinal neurons being modulated as a result of afferent input from peripheral sensory organs. There is evidence for this from the observation that various pathways from mesencephalic regions to the spinal cord appear to be involved in gait transitions in cats. The decision was taken not to build a machine that used Hodgkin-Huxley neurons for a central pattern generator, until it could be demonstrated that the increase in complexity would provide a quantitative improvement in the machine's behaviour. There are several possible ways to do this. One is to find evidence

for behaviours resulting from intraneuronal adaptation, ideally behaviours that can *only* result from intraneuronal adaptation. If this is found then it would be possible to use the mechanism of intraneuronal adaptation described in Chapter 5, section 5.7. It is suggested that this evidence might be found in less evolved organisms, such as the salamander, since their locomotion is primarily controlled by spinal regions, rather than cortical ones, which is likely to reduce the role of extrinsic input. Earlier in the thesis, it was remarked that no claims were being made to the effect that a neuromorphic engineering method was the *only* way to explore neurobiological phenomena. The phenomenon of locomotion does, however, provide a case for the usefulness of implementation (synthetic neurobiology), over simulation (virtual neurobiology). It could be argued that the only way to ensure that a particular intraneuronal process is required for successful locomotion, is to embed the model in a physical reality which has features of friction, inertia, delay and noise. Furthermore, a species-specific model may be required.

Some preliminary evidence has been obtained for intraneuronal adaptation involving the gating modes of mechanogated channels in *Xenopus* Oocytes[79]. In summary, the gating modes can adapt between a phasic, high-pass mode and a tonic, low-pass mode. A similar process can be observed in audiovestibular hair cells. In addition, flexion neurons in *Tritonia* exhibit spike frequency adaptation to maintained excitation.[80] This takes the form of shaping bursts by preventing an increase in spike rate despite a continued increase in input and also prematurely terminated spiking at high input intensity. Finally, there is theoretical evidence[81] that spikes do perturb the envelope of bursting and that models

which do not take the effect of individual spikes into account, may incorrectly predict tonic and phasic behaviour.

Canavier et al. demonstrated that the ability to vary the spike frequency permitted their CPG to produce gait transitions by altering, almost exclusively, the intrinsic parameters. The delay on the contralateral lines of the Collin-Still model could be made to depend upon spike frequency and this would make the model equivalent to the Canavier et al. one, with the advantage of being tailored for implementation. However, although Canavier et al. assert that their neuron model relies only on intrinsic alteration, it is still dependent on changes in the phasic input. Whilst this certainly shifts the burden of alterability to the neuron itself, extrinsic alteration is present. A possibility for improvement is to design a neuron that is even less dependent upon extrinsic alteration, and from a relatively unchanging extrinsic input, can adapt to produce an alteration of output behaviour. A third possibility would be to move away from locomotion and to apply the model to a neurobiological system which has been found conclusively to depend upon individual spikes. For example, coincidence detection systems, or systems where the temporal nature of the signals is important, for example, in the VIIIth auditory nerve.

Chapter 7

Neuromorphic Ion Channels – Experimental Work

7.1 Introduction

Chapter 6 introduced the first stage of the exploration of intraneuronal adaptation using analogue VLSI circuits. The result was a set of silicon neuron chips, based on the Mahowald and Douglas silicon neuron design with, though for reasons as yet undetermined, a narrower range of behaviour. In simulation, it was demonstrated that the neurons could be used as a central pattern generator for quadrupedal locomotion, but a decision was taken not to implement a host machine, unless the extra complexity – the intraneuronal or intrinsic parameters could be justified. This chapter describes the second stage of the exploration, the design and implementation of neuromorphic ion channels. In order to be able to manipulate parameters representing gating modes and electrokinesis, it is first necessary to deviate a little from the Mahowald and Douglas design. Even so, the designs described here are complementary to the original design and are likewise modular in form, allowing them to be deactivated, if required, and its behaviour returned to the default neuron behaviour. Specifically, it is necessary to alter the

time-dependence, τ_q circuitry, so that different gating modes can be represented with different time constants of activation. The first section describes how the time courses of the different gating modes are translated into the τ_q circuitry, and also how the adaptation task described in Chapter 5 is translated. There are two primary aims for this work. The first is to demonstrate that it is feasible for changes in the gating of ion channels to alter the overall output of a neuron, and the second is to demonstrate that, using this as a mechanism, a simple task is possible, such as adapting to perform conduction. A number of issues arise as a consequence of this work, about the role of gating modes in neuromodulation and the significance of adaptation. The work also has implications for neuromorphic engineering in general. These are presented in the discussion at the end of the chapter. Again, the technical details of the design and implementation of the ion channels chip is described in an appendix, Appendix C. Some sub-circuits were simulated in HSpice, whilst others were simulated in AnaLOG and the chips were fabricated in the Mietec 2.4μm process.

7.2 The Relationship Between Gating Modes and Time-Dependence Circuit Variables

Introducing new parameters into a model has the potential to increase the unconstrainedness of the model, to a point where it loses its predictive power. So far, only the Hodgkin-Huxley formalism has been used. This has the advantage that its variables have been experimentally verified. In introducing a new channel type into the model (N-type Ca^{++}), care has been taken to use all available

experimental evidence to describe its characteristics. The time constant of activation, τ_q, was introduced in Chapter 5. The linear function that best fits the experimental data for τ_q in N-type Ca^{++} channels is shown in equation 7.1. The experimental data was obtained from voltage-clamp and channel blocking studies of rat sensorimotor pyramidal neurons.[82,83]

$$\tau_q = \frac{1.25}{cosh(-0.031(mV - 2.9))} \tag{7.1}$$

This has the form shown in figure 7–1. This is the input-output relation that the τ_q circuit must produce.

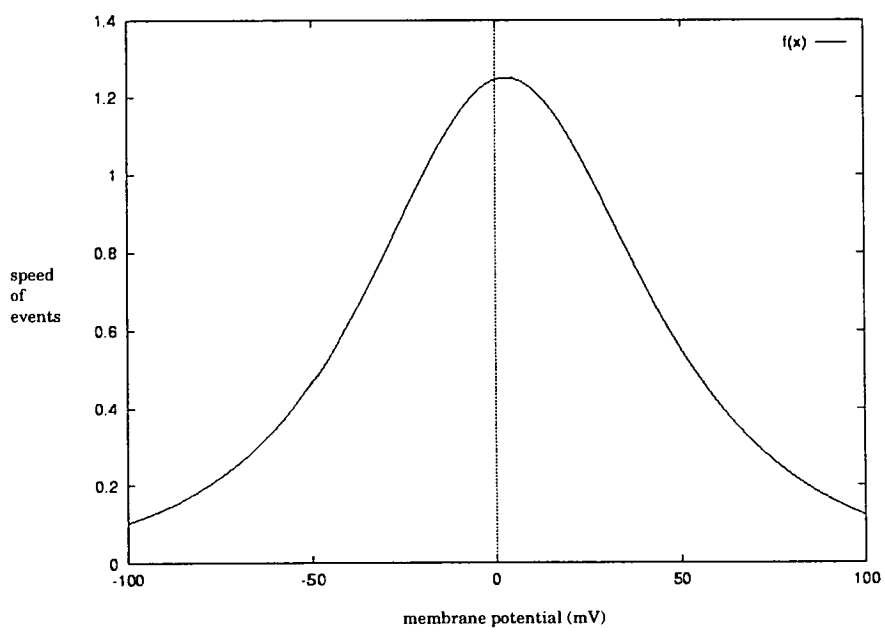

Figure 7–1: *Time-dependency of activation of N-type Ca^{++} channels, taken from characterisation of rat sensorimotor pyramidal neurons.*

The way in which τ_q relates to the variable q that appears in the Hodgkin-Huxley formalism for conductance is shown in equation 7.2

$$\dot{q} = \alpha_q(1 - q) - \beta_q q(q_\infty - q)\tau_q \tag{7.2}$$

where the dot notation is used to denote differentiation with respect to time.

Finally, the Hodgkin-Huxley formalism equation for channel current is shown in equation 7.3.

$$I_{Ntype} = ((G_{Nmax_{Ca++}}.u)q^2)(V - E_{N_{Ca++}}) \tag{7.3}$$

As presented in Chapter 4, the time-dependence, τ_q variable, was implemented using a circuit in which the output voltage "followed" the input voltage, the proximity of the two voltages being determined by a bias voltage that sets the transconductance of the circuit. This represents the neurobiological process of the rate at which ion channels follow alterations in the membrane potential. The membrane potential provides the input to the activation circuit downstream of the time-dependence circuit and determines *where* on the sigmoid the output will be obtained from. This output controls the conductances through the channel. The circuit allows one degree of freedom, namely, the transconductance, steepness or rate of ion channel response. The time-dependence circuit described in this chapter, on the other hand, provides a fixed representation of the time-dependent variable, τ_q. It also ultimately controls the conductance through the channel, but it does so by using the membrane potential itself to determine the rate of events, rather than the rate of change in membrane potential. This rate is represented as

a voltage value which is input to the activation circuit and, as before, determines where on the sigmoid the output will be obtained from. It is clear that the transfer function of the time-dependence circuit is not identical to the transfer function of the time-dependence of activation of N-type Ca^{++} channels. This again demonstrates the concept of algorithmic equivalence. The algorithm that produces the former transfer function is a *representation* of the latter.

τ_q describes the rate of opening of an ion channel, and how this varies with the membrane potential. Altering the *width* of τ_q changes the voltage range that can produce maximal rates of opening. Supposing that the width was increased – this would have the effect of increasing the voltage range at which maximal rates of opening could be achieved. This would, in turn, increase the *probability* of channels being open at any one time. Therefore, an alteration in the width of τ_q will alter an ion channel's open probability. According to experimental evidence on the gating modes observed for N-type Ca^{++} ion channels, the three modes can be distinguished on the basis of open probability. Hence, they are categorised as high-p_o, with an open duration of approximately 3ms, medium-p_o, with an open duration of approximately 1.5ms and low-p_o, with an open duration of approximately 0.3ms. Therefore, high values of width correspond with high-p_o, medium values of width with a medium-p_o and low values of width with a low-p_o.

The next problem was how to determine width values that would be appropriate for representing each of the three gating modes. Given that the neuron will be assigned the task of adapting to perform conduction, the distribution of channels *after* adaptation will be to have diffused as far away from neighbours as possible, and this will be observed as the low-p_o mode. The assumption is that when channels are clustered together, observed as the high-p_o gating mode, this config-

uration effects the membrane in such a way that it is unable to conduct. In the medium-p_o gating mode, there may be partial conduction, whilst in the low-p_o there will be full conduction of spikes. Crucial to the effect of a change in the width of the time-dependent variable on the membrane potential is the summation of the output of the three channels. The summation circuit, described in Appendix C, was configured to produce *sublinear summation.* In neurophysiological terms, this effect occurs because the current through a channel is proportional to the difference between the local membrane potential and the reversal potential. The change in membrane potential due to simultaneous channel opening will be smaller if the membrane potential is already near the reversal potential. Sublinear summation occurs when a set of neighbouring channels of the same type, are activated synchronously.

7.3 Design and Simulation of the Time-Dependence Circuit

The follower-integrator used in the Mahowald and Douglas design is replaced with a circuit that produces the input-output relation shown in figure 7–1, and allows alteration of the width of the curve. The circuit is shown in figure 7–2. This circuit was adapted from a circuit designed by David Mayes[84,85]

The membrane voltage input goes into the node *Vin* in the figure. The voltage *Vcentre* sets the centre of the "bell-shape". The output of this part of the circuit *Idist* feeds into a second, smaller circuit, where *Vwidth* can be altered to vary the width of the bell-shape. The final output, *Vdist*, feeds into the activation

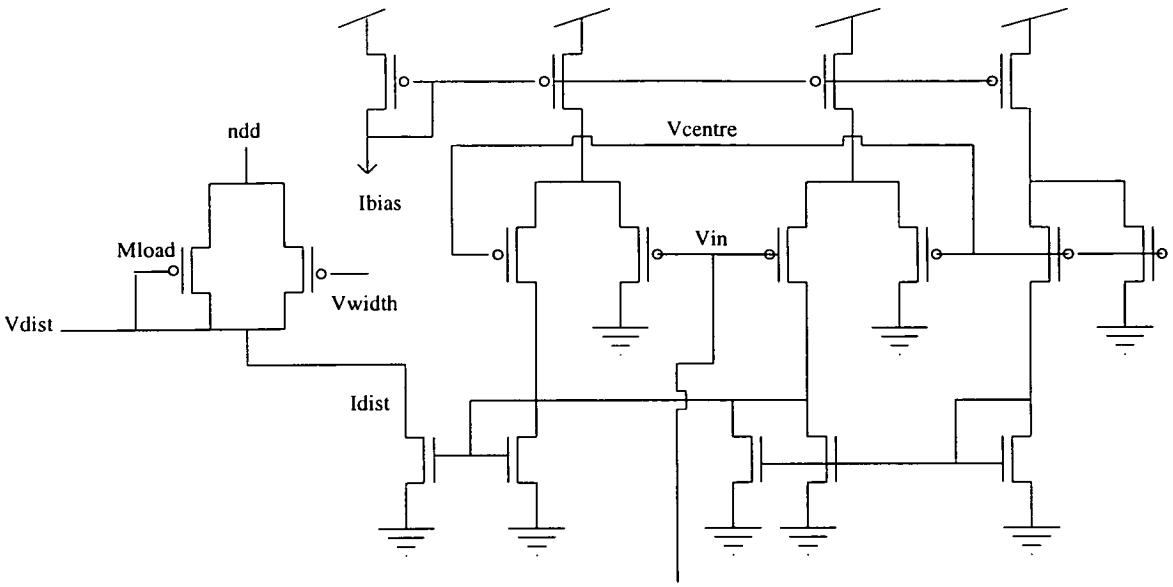

Figure 7–2: *Circuit to produce a bell-shaped curve with alterable width.*

circuitry, as the τ_q circuit did originally. The technical details of this circuit can be found in[84].

7.4 Results from Simulation: The Time-Dependence Circuit

This circuit was simulated in HSpice and produces a series of curves for a range of values of Vwidth. Three distinct time-dependent variable curves for each of the three gating modes were then obtained. These are shown in figure 7–3

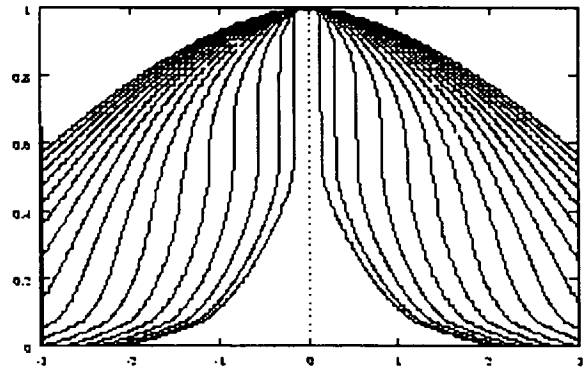

a) Results from simulation

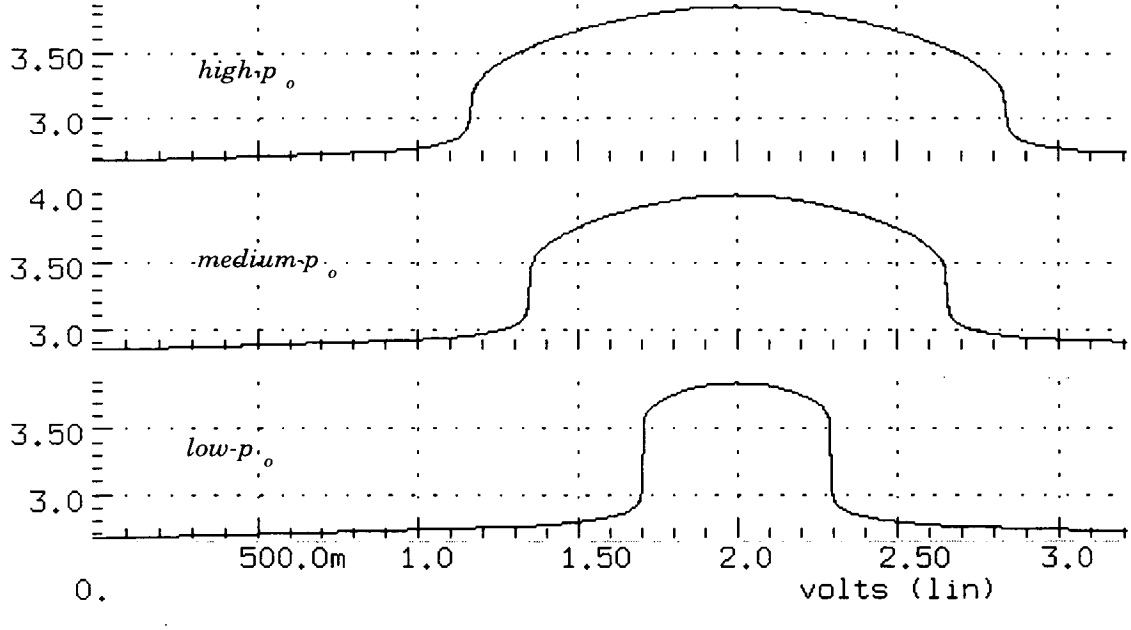

b) Three Vwidth values representing high-, medium- and low-p_o gating modes

Figure 7–3: *Results from the time-dependence circuit*

7.5 Results from Simulation: Testing the Feasibility of Gating Modes Altering the Overall Behaviour of the Neuron

The complete chip contains three alterable channel circuits, the output from each circuit is summed (with sublinear summation, as described previously) and the resulting output becomes the membrane voltage that is supplied to the soma. Figure 7–4 is a circuit schematic of the three alterable channel circuits and figure 7–5 shows spikes produced in simulation at the neuron soma. The decision was taken to use results from simulation to test the feasibility of gating modes altering the overall behaviour of the neuron, rather than the previously obtained results from implementation because the results from implementation were not considered to be an accurate reflection of the proper function of the neuron. Indeed, it will be seen in section 7.8 that the results from the subsequent implementation bear little relationship to the simulations.

7.6 Results from Simulation: The Adaptation Task

The adaptation task was described in Chapter 5. It is presented here again in the context of the τ_q width values. In case A., of figure 5–9 in Chapter 5, all three channels are adjacent. This proximity results in the channel at X possessing ini-

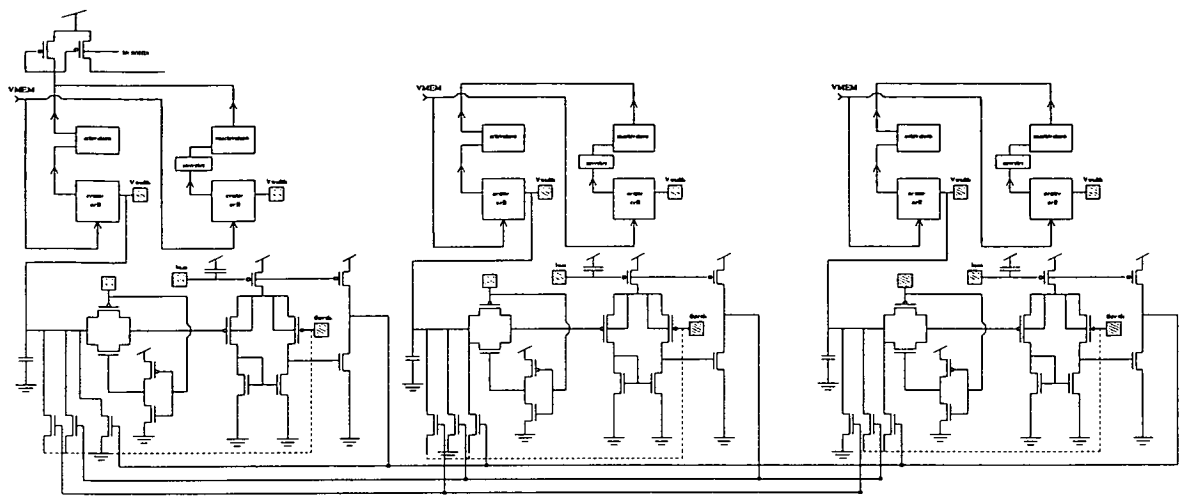

Figure 7–4: *A circuit schematic of the three alterable channel circuits*

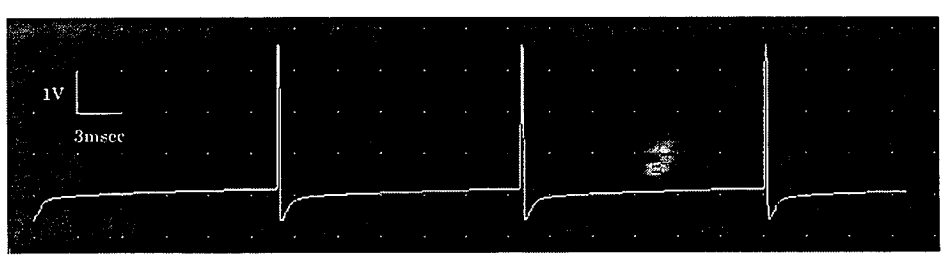

Figure 7–5: *Graph of membrane potential (Vm) output for silicon neuron circuitry tuned for Mietec 2.4 μm process*

tially maximum open probability (a high *Vwidth* value). In B., two of the channels remain adjacent, whilst one has moved away from its neighbour, the open probability of channel X decreases (a reduction to a medium *Vwidth* value). Finally, in C., channels have low *Vwidth* values. With width values having been determined for high-, medium- and low-p_o gating modes, an adaptation circuit was designed to make transitions between the gating modes that were dependent upon the width values. This was carried out using a comparator, which "monitors" the width value, and if it gets above a certain *threshold* (the channel conductance at which, it is assumed, the electrokinetic force on the channel causes it to move) it then lowers the widths until it falls below threshold. This represents the situation whereby channels with a high open probability, move away from their neighbours, thereby reducing the influence of the neighbours on the channel. The threshold value will depend upon the width values selected to represent the modes. All but the low-p_o width will be above threshold. This circuit is shown in figure 7–6

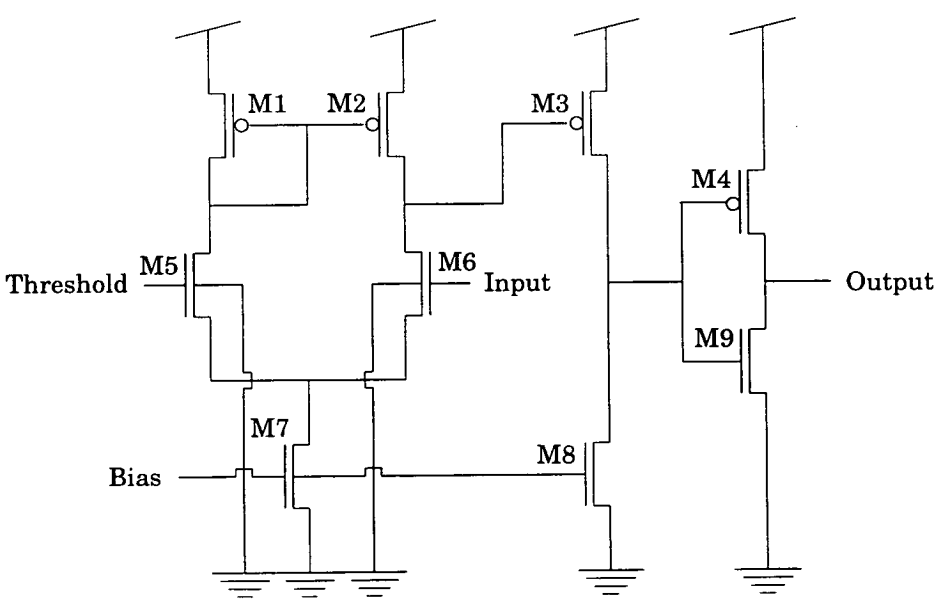

Figure 7–6: *A comparator, used as adaptation circuitry*

Simulations of the complete chip with all three channel circuits represented were carried out and the *Vwidth* values of the circuits were altered to represent cases A., B. and C. of figure 5–9. Transitions between gating modes resulted in an alteration of resting potential of approximately 0.1mV The results in figure 7–7 show how this translates to an effect on spike conduction. Again, this is carried out in simulation, under the assumption that the previous results from implementation do not reflect the proper function of the circuit.

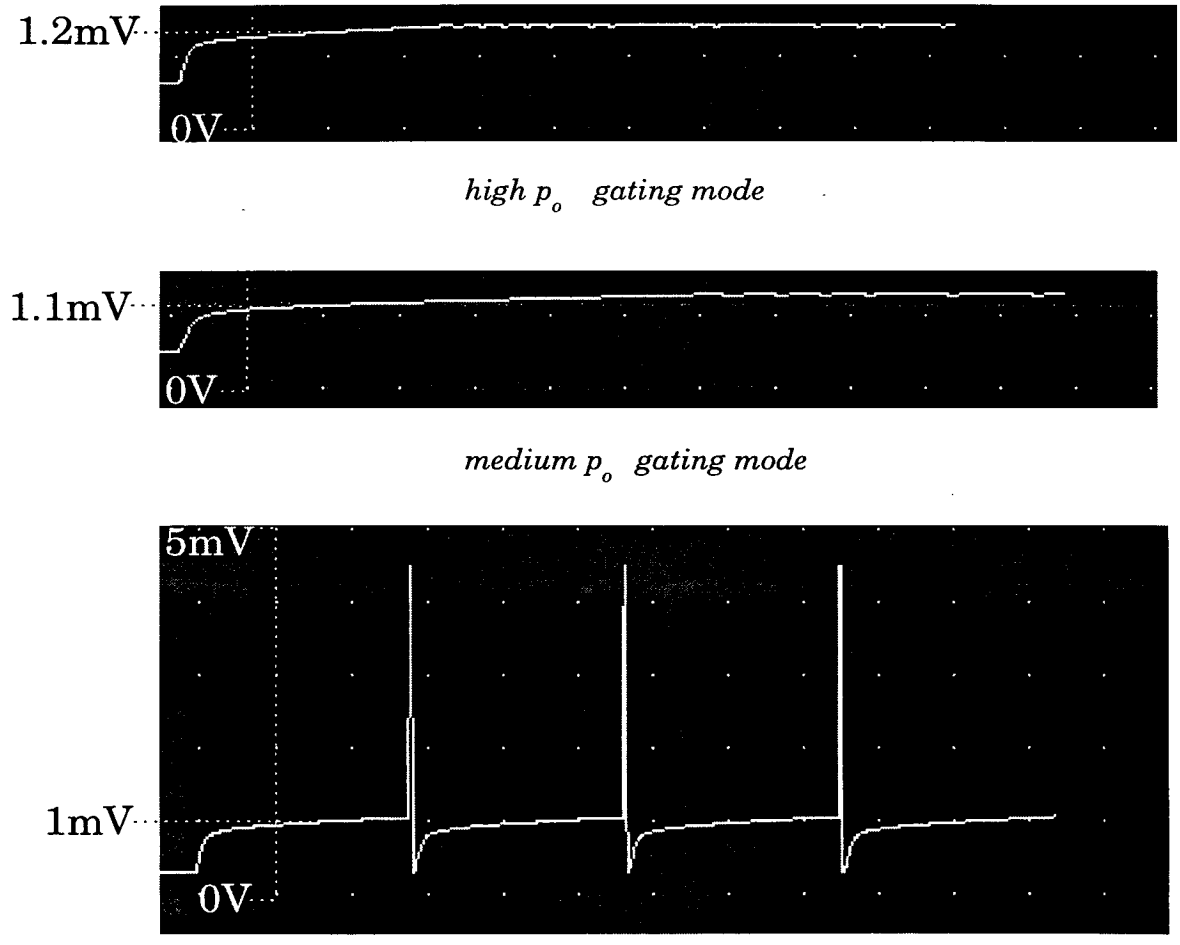

Figure 7–7: *Results from the adaptation task*

In the high- and medium-p_o modes, spikes are not conducted. Spike conduction does not properly occur until transitions to the low-p_o gating mode.

The chip was simulated in both HSpice and AnaLOG software[20], layout for the chip was carried out using CAD software, Cadence 9401/4.3 and fabricated using the Mietec 2.4μm process. The dimensions of the chip are 4635 x 4445μm.

7.7 Results from Implementation: The Soma

It should be noted that all previous results in this chapter are taken from AnaLOG simulation of the circuit, and that given the results from implementation of the circuit presented in Chapter 6, these might not be expected to be a good predictor of the results from implementation. This is considered further in the discussion for this chapter. Four chips in total were tested. Chips no.s one and four were tuned with all initial parameter values (excepting Vdd) at zero. Chips no.s two and three were tuned using the final parameter values of chip no. one as the initial parameter values. Table 7–1 shows the parameter values for the spikes produced at the neuron soma for chip no. one, shown in figure 7–8.

In the implemented soma, the amplitude is 40mV, width 0.5ms and with spikes occurring approximately every 80ms, a frequency of around 12.5 Hz.

INJUP	2.48
NAONKNEE	1.80
NAONSAT	1.32
ENA	2.95
NAOFFSAT	0.75
NAOFFKNEE	1.80
NATAUH	0.55
KDTAUM	0.55
KDSAT	1.32
KDKNEE	1.80
EK	2.95

Table 7–1: *Parameter values for the first chip*

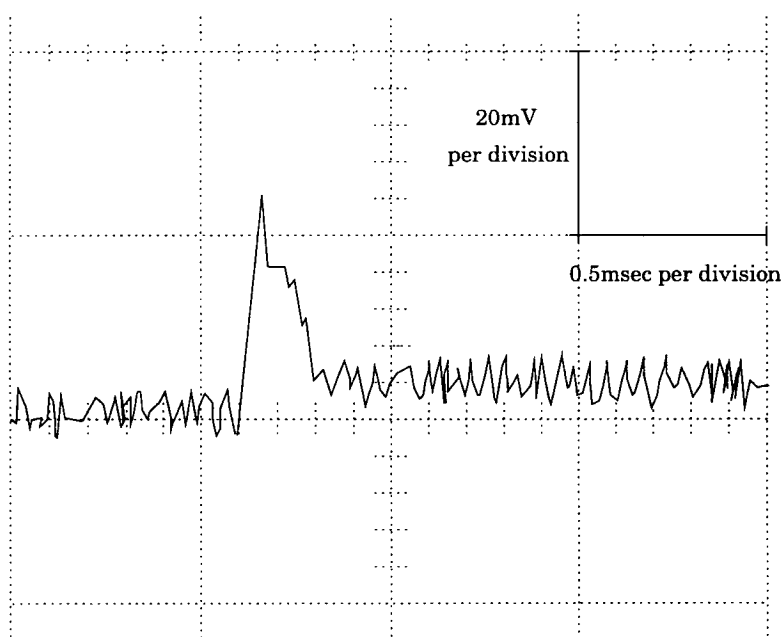

Figure 7–8: *Oscilloscope output from silicon neuron chip*

7.8 Results from Implementation: Demonstrating Alteration of Overall Behaviour by Different Gating Modes

The following results show the effect of a range of τ_q width values on the overall spiking output of the neuron. Parameter values were as given in table 7–1, except for the changes shown in table 7–2.

NDDACT	4.0
CENTRE	2.0
ACT2WIDTH	0.5 – 4.0
CAL	2.3
CALONKNEE	2.4
CALONGMAX	0.6

Table 7–2: *Parameter values for a range of τ_q width values*

The traces show a small increase in the amplitude of the spikes until a τ_q width value of 2.0V. After this point, the amplitude neither increases nor decreases significantly. However, in addition to this initial increase in spike amplitude, there is an increase in the difference between the pre-spike and post-spike levels, primarily as a result of a *decrease* in the pre-spike level, that continues to increase until a τ_q width value of 3.0V. This suggests that an increase in τ_q, or open probability, of ion channels hyperpolarises the membrane. Figure 7–10 shows the traces superimposed. This indicates that the deviation of values is small, a difference of approximately 4mV in amplitude and hyperpolarisation by approximately 12mV.

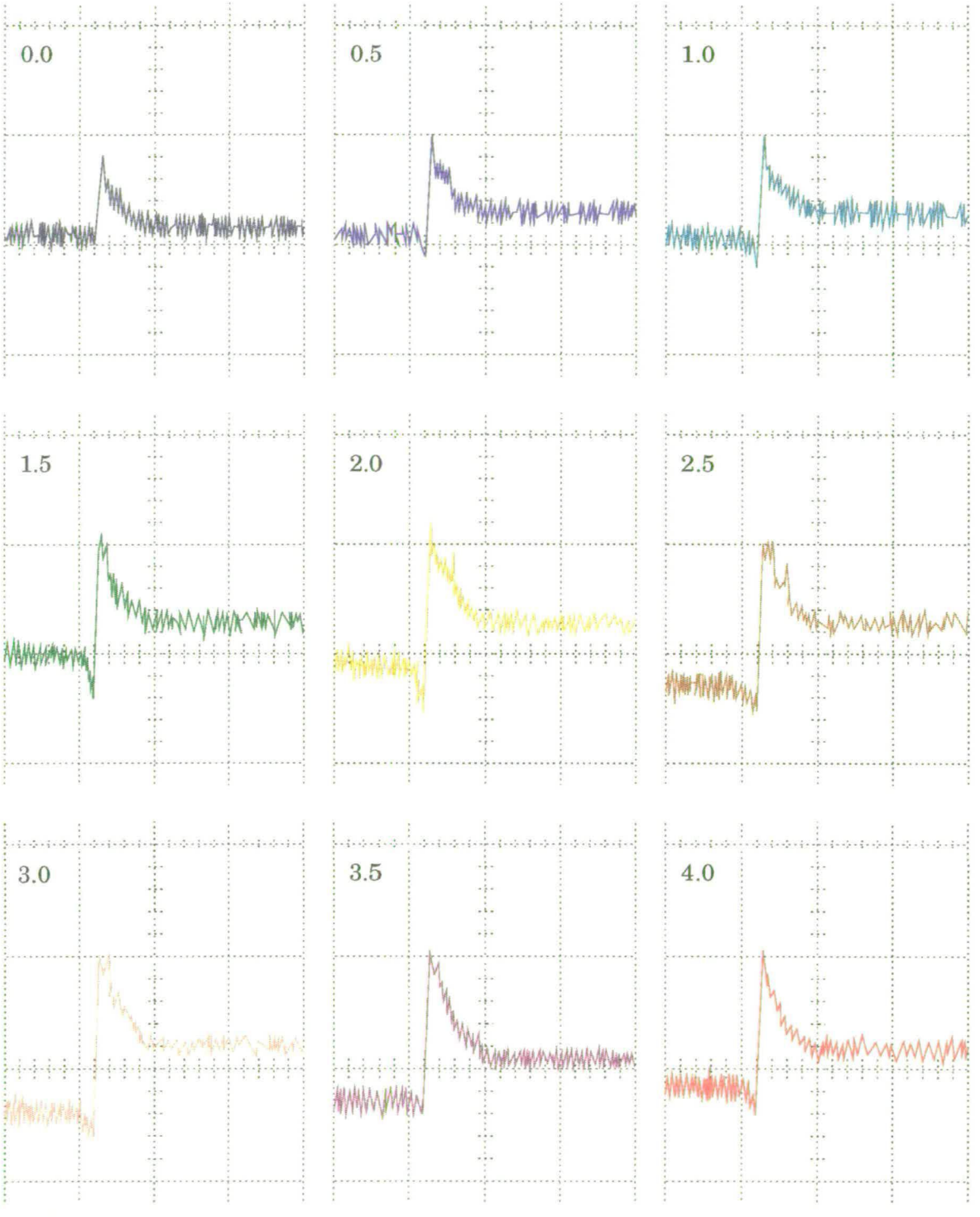

Figure 7–9: *Oscilloscope traces for a range of τ_q width values. Chip no. 1*

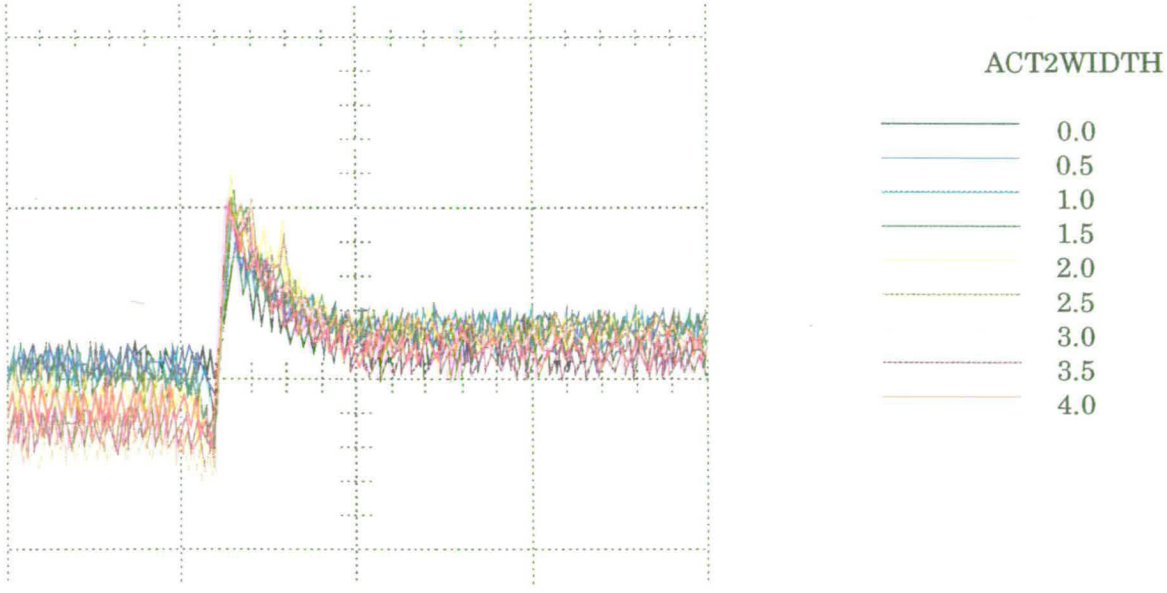

Figure 7–10: *Oscilloscope traces for a range of τ_q width values. Chip no. 1*

The same procedure was carried out for the three other chips. The results for chip no. 2 are shown in figures 7–11 and 7–12.

Chip no. 2 shows some variations in response from that of chip no. 1. Again the amplitude of the spike increases until a τ_q value of 2.0V is reached. However, pre-spike hyperpolarisation also increases until this value is reached, and then shows a decrease in hyperpolarisation.

The results from chip no. 3 are shown in figures 7–13 and 7–14.

Chip no. 3 shows no significant increase in amplitude as the τ_q width value increases. The amplitude remains constant until a τ_q width value of 2.0V, where the amplitude decreases significantly, and continues an erratic decrease for still higher values of τ_q width. For chip no. 3, there is no significant increase in the hyperpolarisation of the membrane prespike.

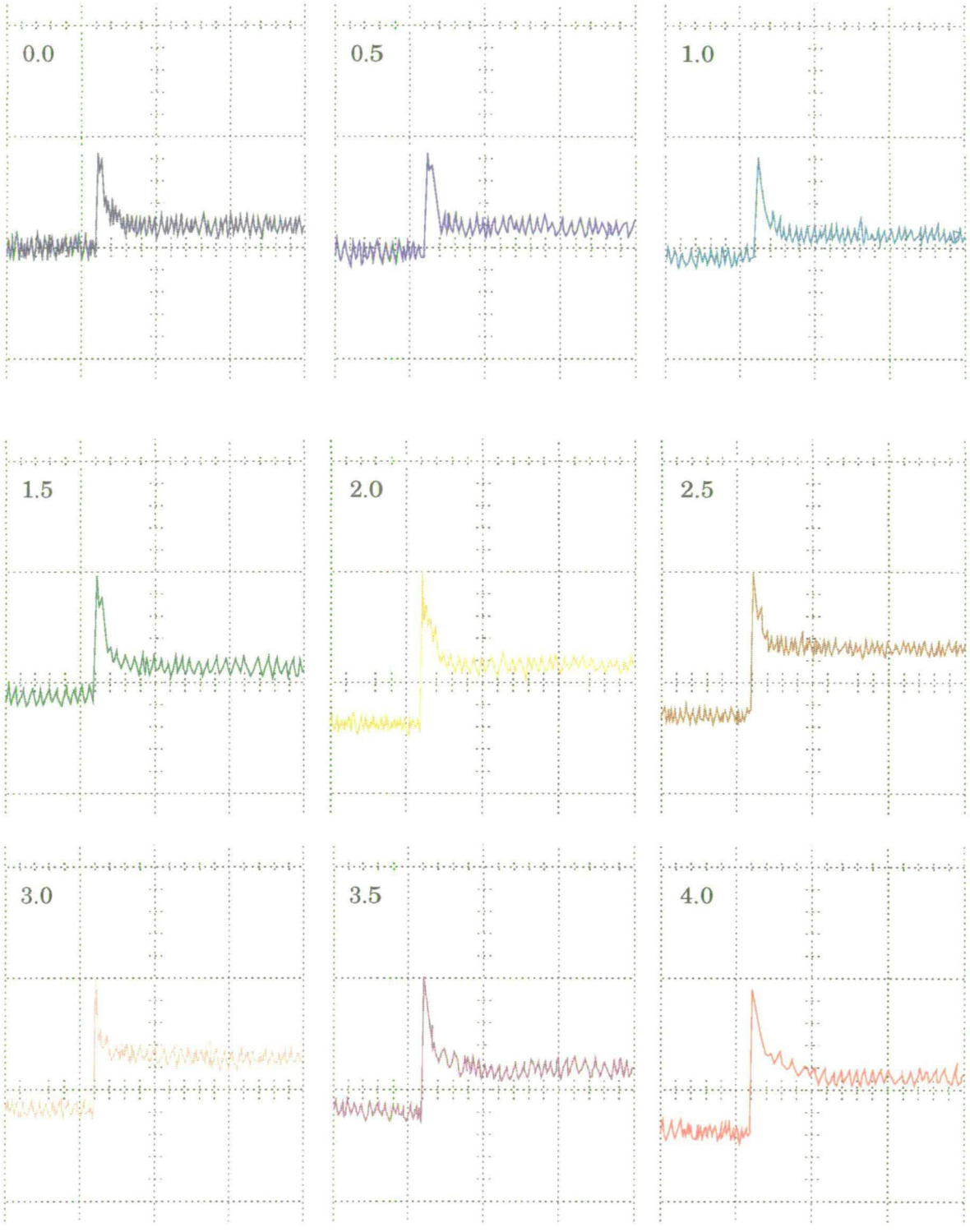

Figure 7–11: *Oscilloscope traces for a range of τ_q width values. Chip no. 2*

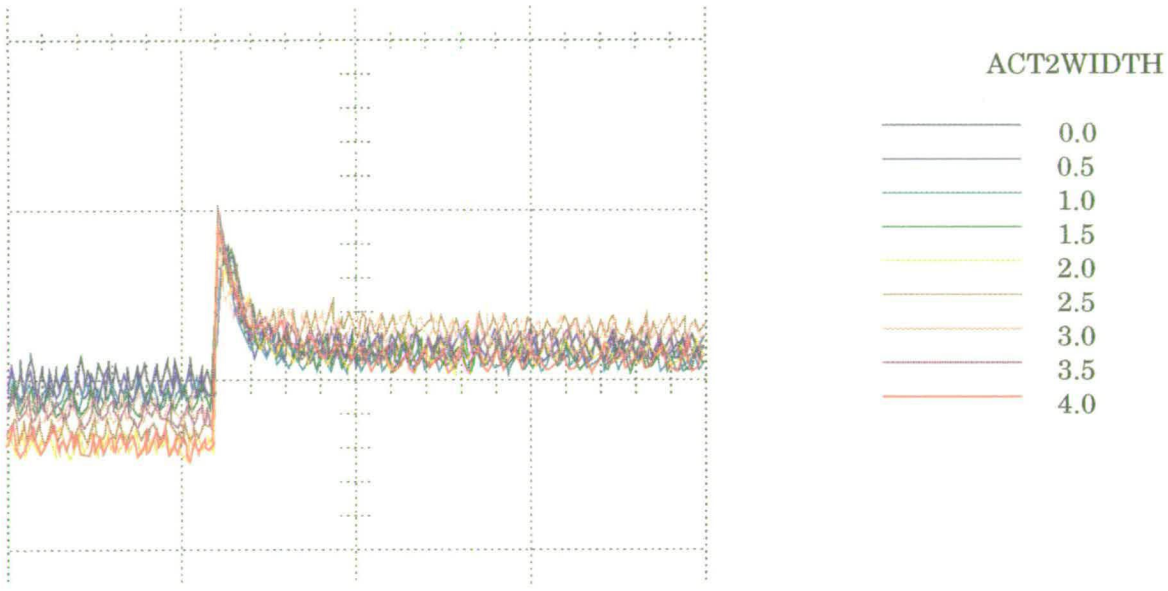

Figure 7–12: *Oscilloscope traces for a range of τ_q width values. Chip no. 2*

Finally, chip no. 4, which was retuned from all initial parameter values at zero. The final parameter values are shown in table 7–3

The results for chip no. 4 are shown in figures 7–15 and 7–16

Chip no. 4 shows no perceptible increase in spike amplitude as the τ_q width value increases. After a τ_q width value of 2.0V it shows a general decrease in spike amplitude. The difference between pre- and post-spike levels remains relatively constant throughout.

From these traces, three τ_q width values were selected, on the basis of them displaying some degree of separability. These are shown, for all four chips, in figures 7–17, 7–18, 7–19 and 7–20

It can be seen that only chip no. 1 could be successfully separated into high, medium and low τ_q width values, for all three regions – prespike, spike and post-spike, and for both the amplitude and the width of the spike. With chip no. 2,

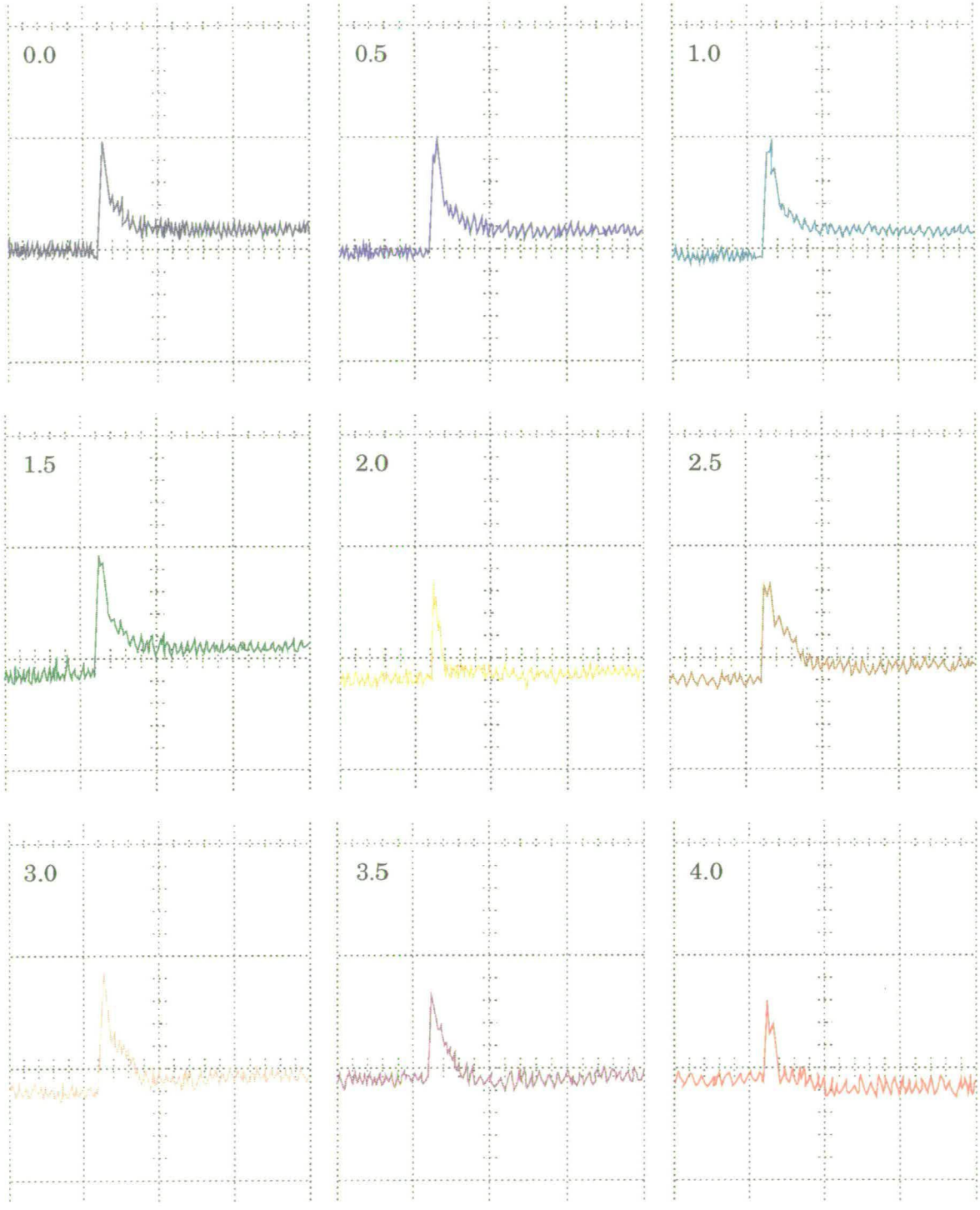

Figure 7–13: *Oscilloscope traces for a range of τ_q width values. Chip no. 3*

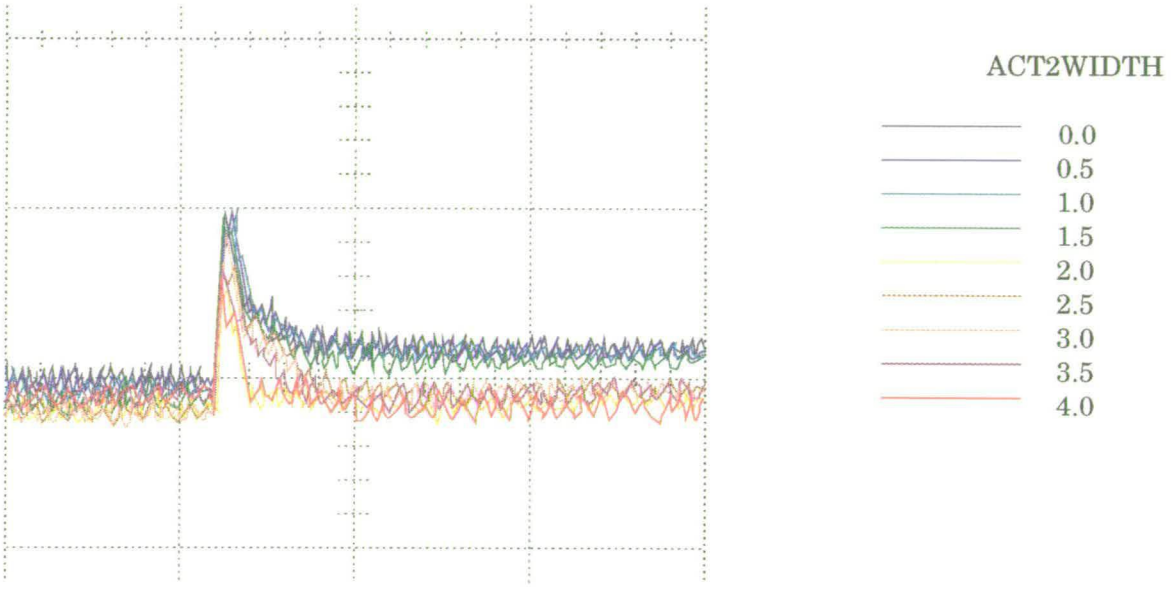

Figure 7–14: *Oscilloscope traces for a range of τ_q width values. Chip no. 3*

GND	0
INJUP	2.001
ELEAK	2.02
GLEAK	1.813
VDD	4.0
NAONKNEE	1.798
NAONSAT	1.618
ENA	2.971
NAOFFSAT	0.749
NAOFFKNEE	1.798
NATAUH	0.555
KDTAUM	0.555
KDSAT	1.618
KDKNEE	1.80
EK	2.971

Table 7–3: *Parameter values for chip no. 4*

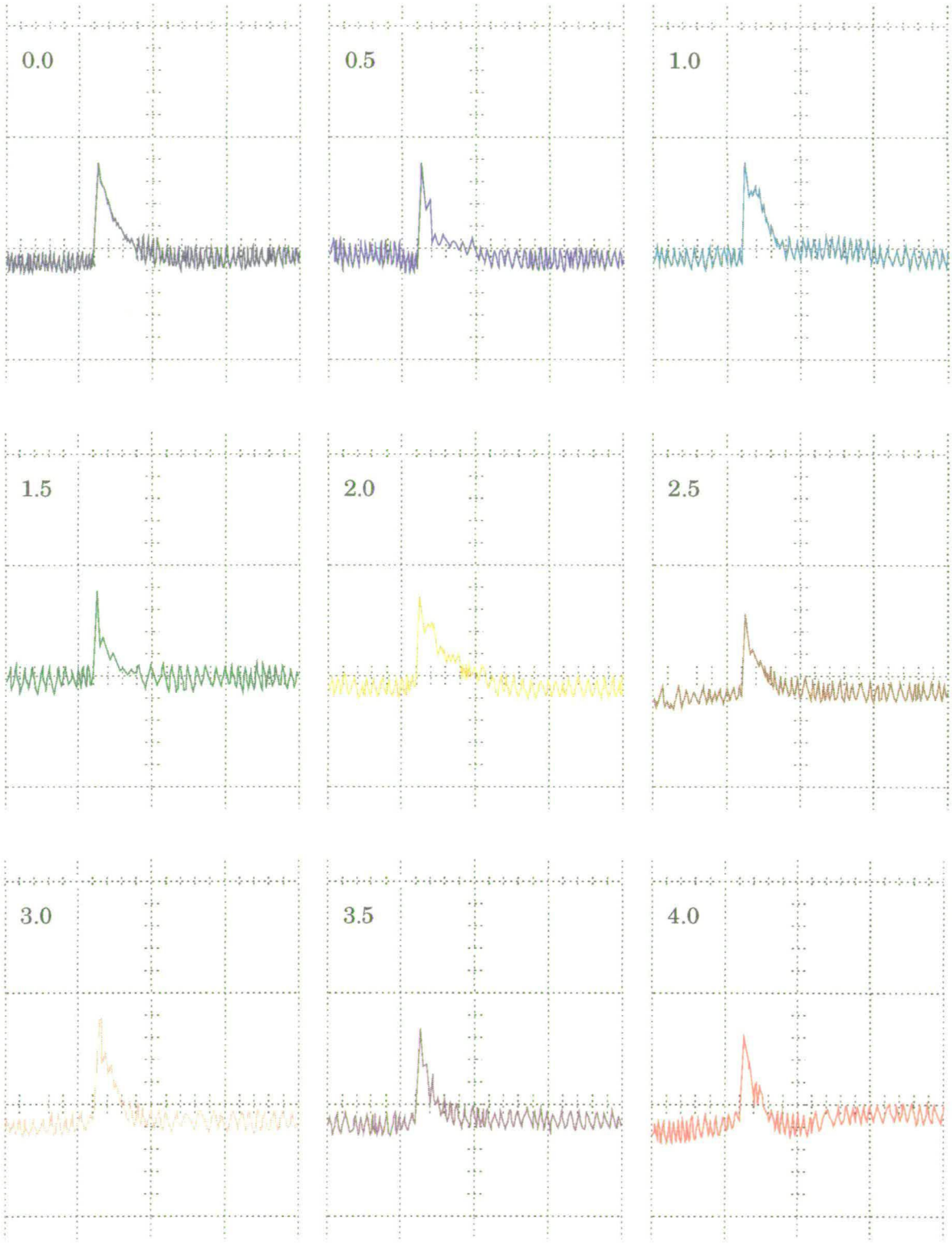

Figure 7–15: *Oscilloscope traces for a range of τ_q width values. Chip no. 4*

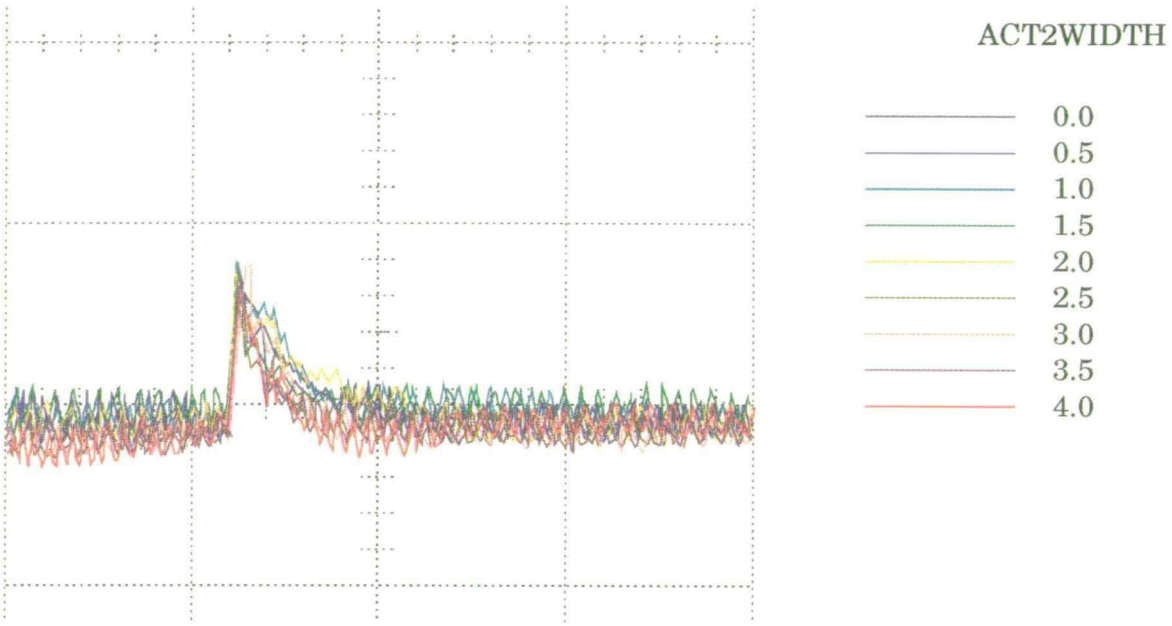

Figure 7–16: *Oscilloscope traces for a range of τ_q width values. Chip no. 4*

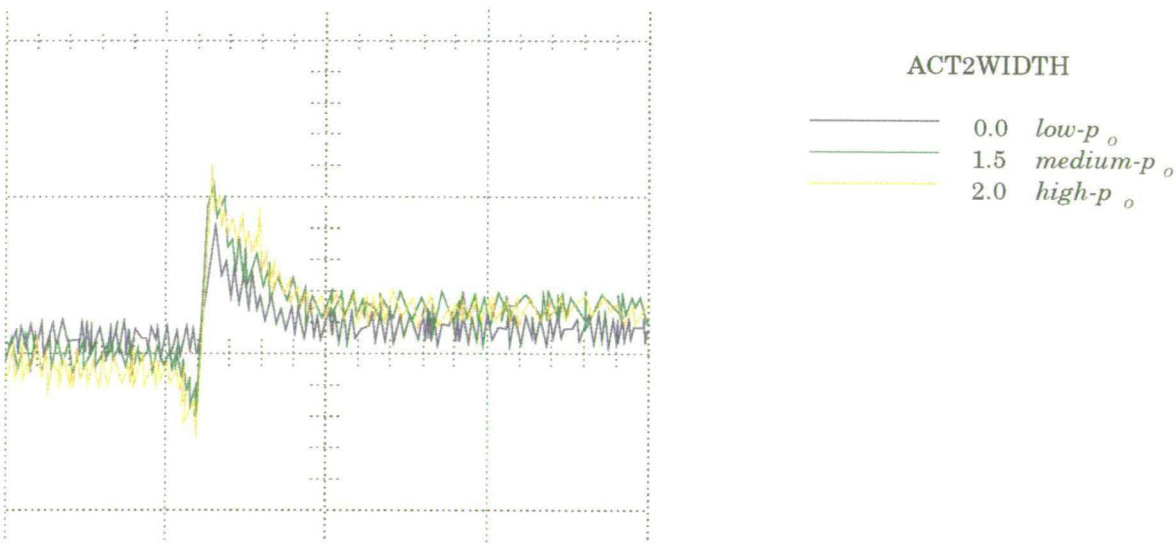

Figure 7–17: *Oscilloscope traces for high, medium and low τ_q width values. Chip no. 1*

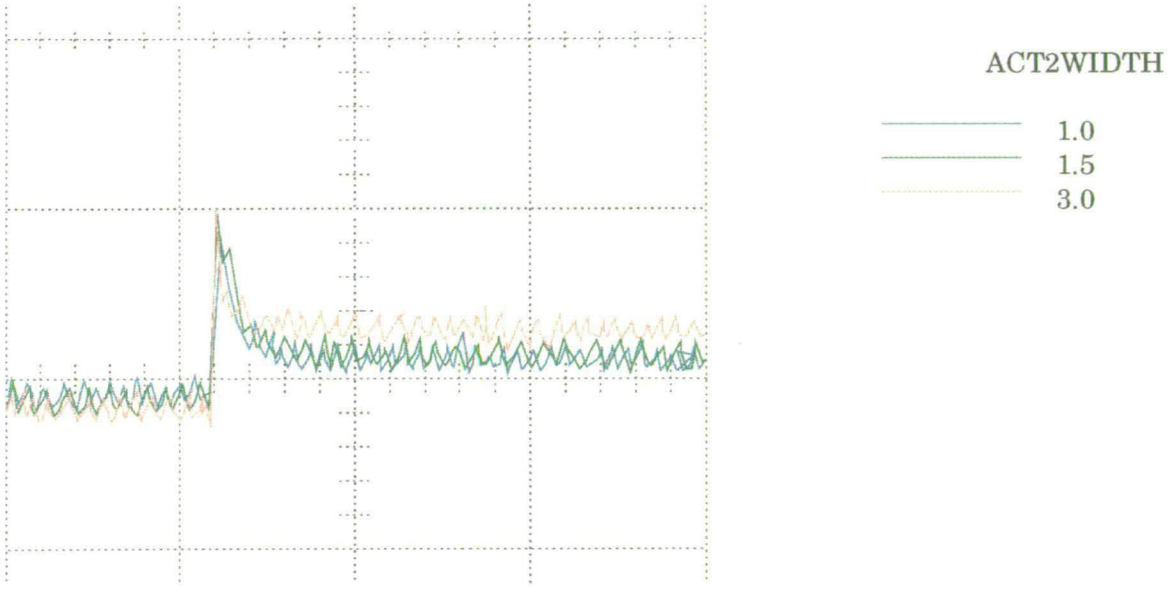

Figure 7–18: *Oscilloscope traces for high, medium and low τ_q width values. Chip no. 2*

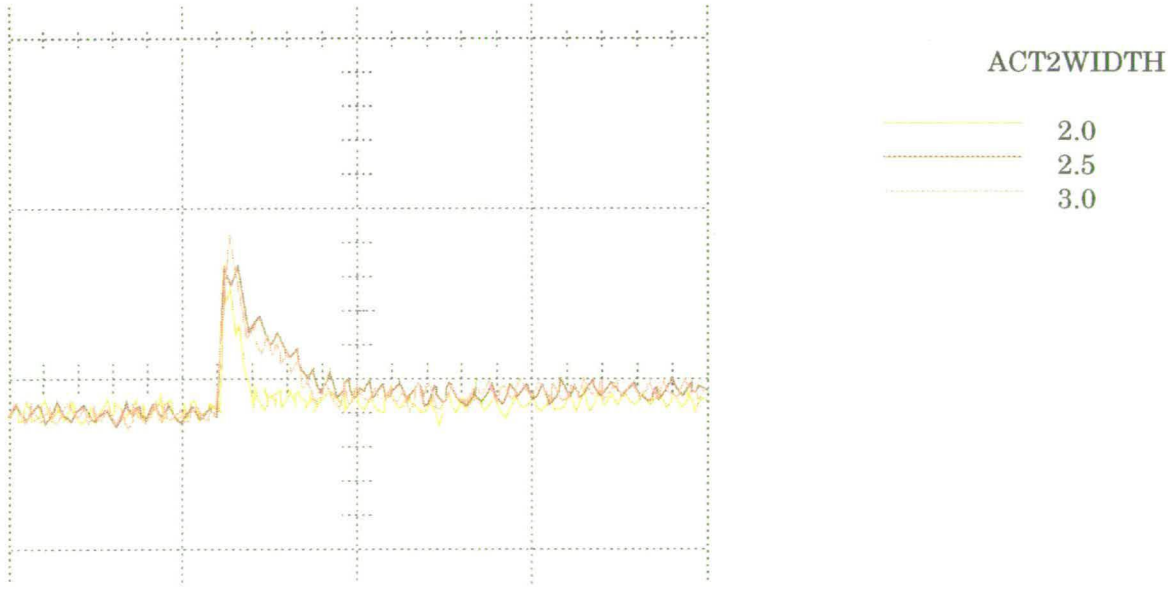

Figure 7–19: *Oscilloscope traces for high, medium and low τ_q width values. Chip no. 3*

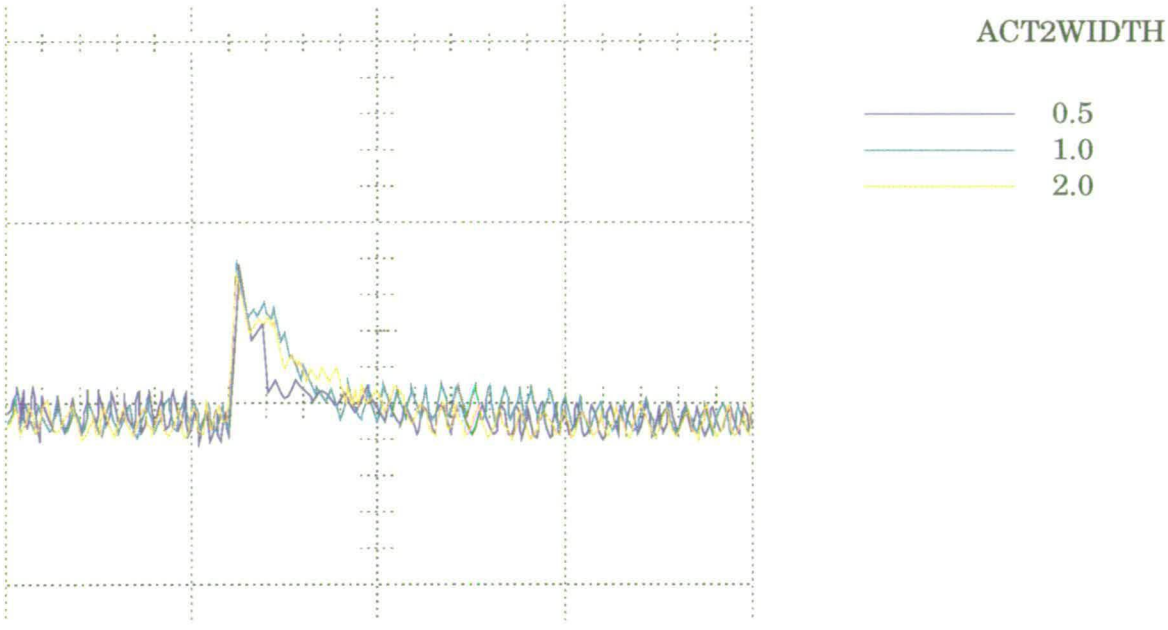

Figure 7–20: *Oscilloscope traces for high, medium and low τ_q width values. Chip no. 4*

only the postspike region was partially separable. For chip no. 3, the spike region was separable, but only for amplitude and not for width and the postspike region partially separable and for chip no. 4, only the spike region was separable, not for amplitude, but possibly for width.

7.9 Results from Implementation: The Adaptation Task

The τ_q width values obtained for each of the gating modes, with just one channel active, were then applied to all three ion channels, and altered by hand, to represent cases A, B and C of the adaptation task. The values are shown in the tables 7–4 and 7–5. The results of applying the τ_q width values to all three of the channels, for each chip, are shown in figures 7–21, 7–22, 7–23 and 7–24.

chip1	A	B	C	chip2	A	B	C
ACT1WIDTH	1.5	0.0	0.0	ACT1WIDTH	1.5	1.0	1.0
ACT2WIDTH^X	2.0	1.5	0.0	ACT2WIDTH^X	3.0	1.5	1.0
ACT3WIDTH	1.5	1.5	0.0	ACT3WIDTH	1.5	1.5	1.0

Table 7–4: *Parameter values for high-, medium- and low τ_q width values for cases A, B and C of the adaptation task, for chips no.s 1 and 2*

chip3	A	B	C	chip4	A	B	C
ACT1WIDTH	2.5	2.0	2.0	ACT1WIDTH	1.0	0.5	0.5
ACT2WIDTH^X	3.0	2.5	2.0	ACT2WIDTH^X	2.0	1.0	0.5
ACT3WIDTH	2.5	2.5	2.0	ACT3WIDTH	1.0	1.0	0.5

Table 7–5: *Parameter values for high-, medium- and low τ_q width values for cases A, B and C of the adaptation task, for chips no.s 3 and 4*

All four chips show some degree of separation between the trace for post-adaptation, case C, and the traces for pre-adaptation, cases A and B. Whether this is significant enough to classify output C, but not that of A or B, as proper conduction is unclear, though chips no.s 1 and 4 are the best candidates. C of chip no. 1 has a greater amplitude and width, whilst C of chip no. 4 has a greater width

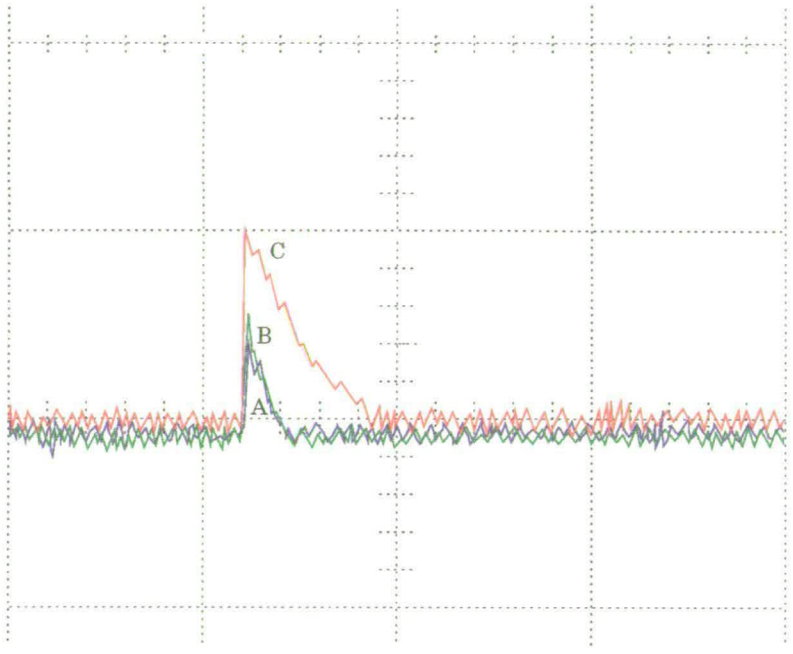

Figure 7–21: *Results of the adaptation task. Chip no. 1*

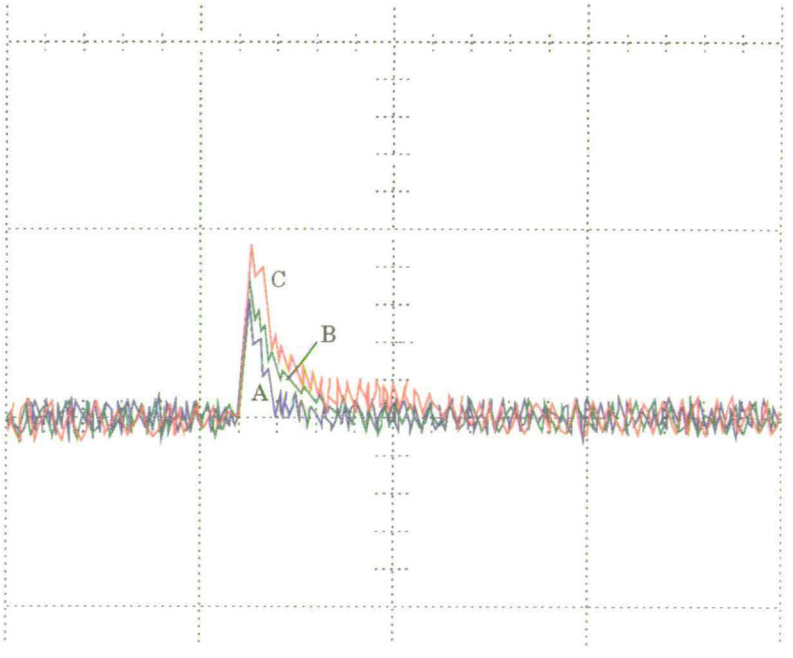

Figure 7–22: *Results of the adaptation task. Chip no. 2*

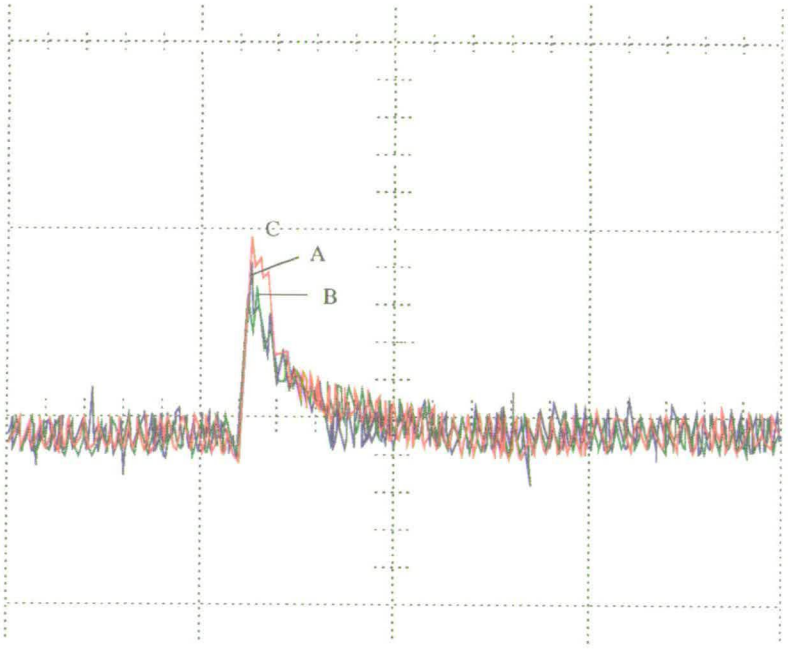

Figure 7–23: *Results of the adaptation task. Chip no. 3*

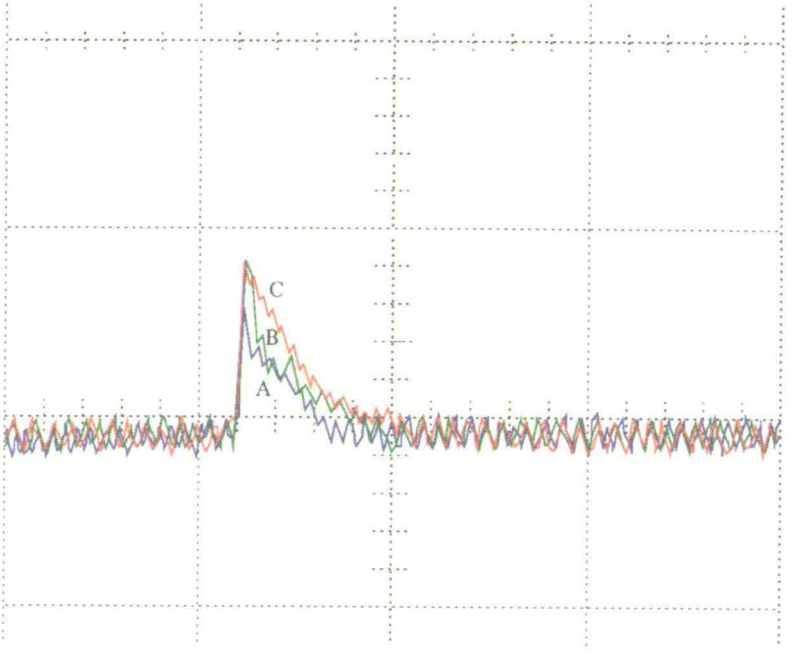

Figure 7–24: *Results of the adaptation task. Chip no. 4*

only. This corresponds with the success of separating the spike region of a single channel into high-, medium- and low-p_o gating modes. Chips no.s 1 and 4 were tuned with all initial parameter values at zero, whereas chips no.s 2 and 3 were tuned using the parameter values of chip no. 1 as a benchmark. The former method is more time-intensive and likely leads to more appropriate parameters, so it is unsurprising that the results are improved.

7.10 Results from Implementation: Self-Regulation of the Adaptation Task

The next experiment was to allow the ion channels to self-regulate their adaptation by using the comparator circuit. The result of this for chip no. 1 is shown in figure 7–25, where the blue line indicates the membrane potential before the comparator circuit is activated, and the red line indicates the membrane potential after the comparator circuit has been activated.

Whilst the pre- and post-adaptation membrane potentials do separate, and could be categorised into non-conduction and proper conduction using some thresholding mechanism, the results are even less conclusive than those where τ_q width values are set manually, as shown in figure 7–21. This could be the result of a general masking effect caused by the addition of the comparator circuitry, and specifically, the off-chip switching mechanism. For this reason, the experiment was not repeated for the remaining chips. Additionally, a thresholding mechanism would introduce an element to the model that had no neurophysiological correlate.

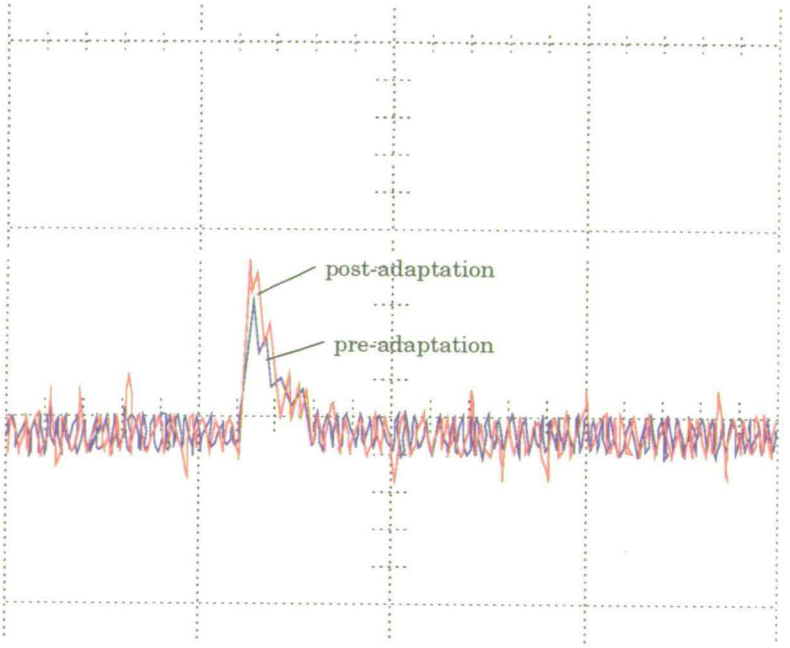

Figure 7–25: *Results of the self-regulating adaptation task. The blue line indicates the membrane potential before the comparator circuit is activated, the red line indicates the membrane potential after the comparator circuit has been activated. Chip no. 1*

7.11 Discussion

The results show some degree of intraneuronal adaptation for the task specified. However, there are some issues to consider. One is that it is possible to construct a model in such a way that it will inevitably complete its given task successfully. This relates to the point made in Chapter 3 concerning the determination of appropriate constraints for a model. The ultimate aim of the work is to construct a model that can be used to make predictions about ion channel behaviour with respect to intraneuronal adaptation. In order to retain neurobiological plausibility, at least at the level of algorithmic equivalence, it is necessary to represent ion channels and some mechanism of adaptation. It is then possible to make choices about what degree of information to incorporate into the model. For example, data from voltage-clamp studies of rat sensorimotor pyramidal neurons and observations of N-type Ca^{++} channel gating modes was incorporated. This data provides constraints on the model. An input-output relation for τ_q circuitry is specified, thereby constraining the choice of circuits for representing τ_q. An alternative would be to use a circuit that provided an abstract, only computationally equivalent, representation of τ_q. The disadvantage of this method is that it involves making assumptions which may not be bourne out by experimental evidence. This was apparent in the discussion of Chapter 6, in which theoretical evidence was mentioned, which demonstrated that the assumption that an abstract representation of phasic spiking could correctly predict neuronal behaviour was misplaced. However, in order to have predictive ability, a model is necessarily involved with uncertainties, and therefore some assumptions are required. For

this model of ion channel behaviour and intraneuronal adaptation, it has been suggested that gating modes occur as a result of adaptation. The degree to which this is an assumption is lessened somewhat by the fact that there is evidence for gating modes and for intraneuronal adaptation and only the interdependency of them is assumed. It is also assumed that conditions might arise whereby a nonadapted patch of membrane is unable to conduct spikes, whereas an adapted patch has this ability. If these assumptions and conditions are reasonable, a tentative prediction can be made – that dendritic N-type Ca^{++} channels will be observed in a low-p_o gating mode when actively conducting spikes. Generally, however, it would be inappropriate to draw too many neurobiological implications from these results, as some of the parameters are only indirectly and qualitatively linked with neurobiological processes. A quantitative investigation has not been carried out to characterise any electrokinetic force, to determine numerical values for it, or to determine how it might vary with distance and how this would quantitatively affect gating modes.

Another point relates to the viability of implementing in analogue VLSI a mechanism which has not been satisfactorily simulated. In simulation, the transition between gating modes resulted in an alteration of resting potential of approximately 0.1mV. The implemented circuit described in Chapter 6, had a range of only 200mV. Both these values are small with respect to the range of the functioning of integrated circuits and so greater consideration might have been given to whether to implement the simulated circuits at all. One might wonder, therefore, exactly what contribution an analogue integrated circuit representation of gating modes and adaptation can make. This issue concerns both the choice of system to model, as well as the methodology. It is possible that a better choice of sys-

tem to model could have been made, using higher, and therefore more detectable and measurable voltage values. Given the time it takes to design and fabricate analogue integrated circuits, these issues need to be well thought through before embarking on a full neuromorphic process. Chapter 8 discusses the potential contribution, future contributions and issues concerning neuromorphic engineering in general.

Chapter 8

Explorations of Neurobiology with Analogue ICs – Conclusions

This thesis has described the use of analogue integrated circuits to investigate neurobiological phenomena and to make predictions about these phenomena that can be verified by physiological experimentation. This places the work within the field of computational neuroscience and, like computational neuroscience, it is concerned with determining the degree of information it is necessary to incorporate in a model, the degree to which it is reasonable to incorporate information in an abstracted form, and when it is reasonable to omit information altogether. All models, regardless of the method used to construct them, depend on the fact that the medium the model is composed of is more fully characterised than the medium that the system being modelled is composed of. When an unnecessary amount of information is incorporated, the model is in danger of becoming less well characterised, to the point where it can be as opaque as the system being modelled. Neuromorphic engineering has thus far depended on the fact that analogue integrated circuits are more fully characterised than neuronal circuits. Neuromorphic engineering has been described as both a methodology for system

synthesis and as an explanatory activity. If it is to be used as a methodology for system synthesis, then a successful outcome is usually only dependent upon the creation of a useful application. If, however, it is to be used as an explanatory activity, it becomes necessary to demonstrate that the outcome has, or can have, predictive ability. Computational models are thought to possess this property because there is considered to be an *equivalence* between the brain and computational systems. The issue of determining the degree of information to incorporate in a model relates to this concept of equivalence. If equivalence is being considered at the level of the computation performed by a neuronal circuit, then it might be less necessary to incorporate information about the behaviour of individual neurons, than if the equivalence being considered is at the level of the *physical* nature of the computation performed by a neuronal circuit, say, or at the level of the computation performed by an individual neuron. There are therefore two issues arising for any project using neuromorphic engineering as an explanatory activity. One is the choice of level at which to model: computational, algorithmic or physical, and the other is the choice of system to model.

The thesis began with a discussion of Carver Mead's notion of a physical equivalence between field-effect transistors and ion channels in the neuronal membrane. The unique feature of neuromorphic engineering is its capacity to model a system at the physical level. Digital computer simulations (virtual neurobiology) do not model at this level, but use abstracted representations of the physical, or algorithms. However, subsequent work in neuromorphic engineering does not exploit this physical equivalence and as such, the only advantage that the algorithms used possess over algorithms used in simulation is computational speed. If the

system modelled has a significant temporal component, the use of implementation may be justified by speed alone.

It is also the case that the work presented in this thesis of representing the electrokinesis of ion channels, uses only an algorithmic equivalence, and as there is no significant fast temporal component to this mechanism, it is perhaps an unwise choice of system to model. Particularly when there is insufficient quantitative information available to ensure the validity of the algorithmic equivalence. Perhaps the most obvious suggestion for further work, therefore, is to obtain more quantitative information. For example, experiments could be carried out, using the experimental setup of Delcour[2,1], in conjunction with the measurement of ion channel movement, to determine whether there is any correlation between the gating modes observed and ion channel movement. If this was demonstrated, it would suggest an alternative to the state diagrammatic description of ion channel behaviour and provide a fresh perspective on intraneuronal processes occurring outside development. A second experiment would be to observe the gating modes present during conduction of spikes in dendrites. Other possibilities include devising an experiment to measure any electrokinetic forces present with ion channels in the membrane, extending the model and subsequent implementations to include clusters of ion channels or synapses, and exploring intraneuronal phenomena in sensorimotor systems, where they can perhaps be most easily observed and for which more quantitative information might exist. Incorporating more quantitative information increases the chance of algorithmic equivalence being present.

As described previously, the Mahowald and Douglas silicon neuron is capable of producing a membrane potential spike in response to current injection. The circuit uses differential stages and low-pass filters to represent activation, inac-

tivation and time-dependent variables. In order to properly exploit the physical equivalence between transistors and neuronal membranes, these variables would have to be properties of the single transistor itself. For example, the activation variable is the dependence of the opening of the channel upon the membrane potential. In a field-effect transistor, this is equivalent to the dependence of the formation of the channel depletion region upon the gate voltage. In a neuron, this relationship is a result of the movement of gating particles from the intracellular to the extracellular face of the membrane. In a transistor, it is the result of the repulsion of free electrons from the region under the gate. In neurons, this is described by the m variable of the Hodgkin–Huxley model. In transistors, by equations for the change in surface potential, which is dependent upon the oxide capacitance, charge density and the permittivity of silicon. m differs from one channel type to another, whilst the surface potential differs with the degree of doping of the silicon. However, transistors do not undergo a process equivalent to inactivation, unlike many ion channel types. Finally, the time-dependent variables – for ion channels this varies from hundreds of microseconds to many seconds. In transistors, it is instantaneous. It remains to determine the implications of a transistor's inability to inactivate, and its instantaneous time-dependence.

To improve the physical equivalence, it is necessary to examine more closely the device physics of field-effect transistors. This might force a shift in perspective from asking the question, for example, about adaptation: "How can silicon be used to model neurobiological adaptation?" to asking: "How might a silicon entity adapt?" This may also cause a shift from using analogue integrated circuits as a tool to make predictions about neurobiological phenomena, to making

analogue integrated circuits that exhibit some of the characteristics that define life. However, the two approaches are not mutually exclusive. It may also involve the use of silicon technologies other than analogue integrated circuit design. The latter approach may be particularly relevant when considering phenomena that do not as yet, have any silicon equivalent, such as mobility of substances larger than charge particles. Work in this area includes using genetic algorithms and field-programmable gate arrays to evolve hardware[86,87,88]. Circuits are demonstrated to be capable of evolving to form functional digital logic units using less transistors than human designers. The reason is that the circuits are using properties of the circuits that designers ignore, such as parasitic capacitances and conductances between circuit elements. The significance is that the circuits use the silicon's inherent properties to solve the task. The danger, for a modelling approach is that, as mentioned previously, modelling is possible by virtue of the fact that the technology used to model the system has properties that are better understood than the system being modelled. This is often not the case for the inter-device (parasitic) properties of integrated circuits.

Exploiting the physical equivalence implies that integrated circuits will be of systems composed primarily of ion channels. However, this spreads over a spectrum of evolutionary sophistication of organisms and biological components. At one end, there are unicellular, eukaryotic organisms such as *Paramecium*, next, carnivorous plants, then Coelenterates (including jellyfish), through to mammalian neurons, such as pyramidal cells of the cerebral cortex and of Purkinje cells of the cerebellum. Degree of sophistication could be a measure of the variety of ion channel types present and of structural complexity. For example, Na^+ channels are a relatively late evolutionary occurrence, as is the transition from generating

graded potentials to generating action potentials. This thesis suggests that it may be beneficial to study organisms with less sophisticated ion channel configurations and cellular structural complexity. This has the additional advantage that the link between ion channels and observable behaviour is relatively direct. *Paramecium*, for example, are unicellular, eukaryote organisms that are found free-swimming in freshwater pools. Behaviour in these organisms is accomplished by ion channel processes. An example of this is its behaviour upon encountering an obstacle: mechano–sensitive calcium channels are opened. The resulting depolarising potential activates calcium channels in the ciliary membrane, turning the orientation of the ciliary power stroke, so that the *Paramecium* swims backwards, until potassium channels are activated, repolarising the cell. In addition, *Paramecium* have been used in many interdisciplinary studies of the biophysics and cell biology of membrane polarisation and of sensory–motor behaviour in a unicellular organism. They are almost entirely characterised and since they have no recourse to mechanisms other than ion channels, provide an excellent medium for studying them. An additional advantage is that it would not be necessary to represent phenomena such as the action potential – a complex form of electrical signalling that took millenia to evolve. An exploration of *Paramecium* with analogue integrated circuitry would use the physical equivalence of field-effect transistors and ion channels and result in an autonomous silicon organism with a complete behavioural repertoire capable of allowing predictions to be made, not just about ion channels, but about behaviour. This would represent a very successful outcome for neuromorphic engineering.

In general, it is profitable for neuromorphic engineers to retain close ties with experimentalists such as neurophysiologists. At the same time, neuromorphic

engineers profit from having a wider perspective on the neuroscience field than is perhaps possible from within one subdiscipline. Ideally, this allows them to perform a successful synthesis of apparently disparate phenomena. However, the conclusion of this thesis is that there are two ways to ensure the fruitfulness of neuromorphic engineering. That explorations of neurobiology with analogue integrated circuits should either exploit the physical equivalence between field-effect transistors and neuronal membranes or else model, with algorithmic equivalence, a system for which real-time modelling is useful or necessary.

Appendix A

Modification of AnaLOG for the Mietec 2.4μm Process

A.1 Introduction

This appendix to Chapters 6 and 7 describes some aspects of AnaLOG and the technical details required to adapt the AnaLOG simulation environment for use with a Mietec 2.4μm CMOS fabrication process. A complete account can be found in[20]. This appendix provides an outline of how the simulation environment was adapted. The first section describes the Enz, Krummenacher, Vittoz (EKV) model for CMOS devices in the weak-inversion region. The second section describes the parameters and how they can be adapted and the third section describes improvements that could be made to the accuracy of the parameters.

A.2 AnaLOG

The screen is divided into three sections, the upper section contains a clock, which displays the current time and current timestep during simulation, the middle section is the drawing area, and the lower section contains the circuit symbols for use in drawing a schematic, and all the AnaLOG commands. All the circuit symbols can be configured to the values required, for example, a transistor has configurable parameters for length, width, kT/q and parasitic capacitance etc. Circuits can be saved to, and loaded from, files. AnaLOG simulates circuits constantly, even during editing, although circuit parameters can always be reset to their initial values. Any number of voltmeters and ammeters can be used to monitor the circuit during simulation. Transistors are equivalent to SPICE level 2 in complexity. They were initially tuned for a 2 micron process and to be most accurate in the weak-inversion region. Voltage and current sources can generate a number of different waveforms. It is possible to gain an intuitive feel for the voltages in the circuit by selecting a mode which displays the circuit in varying colours, according to the voltage being carried. AnaLOG has a Scope mode, which displays plots of output waveforms and can be written to a file. It is also possible to obtain a SPICE file from a circuit drawn in AnaLOG. The AnaLOG workspace, with a silicon neuron schematic, can be seen in figure A–1.

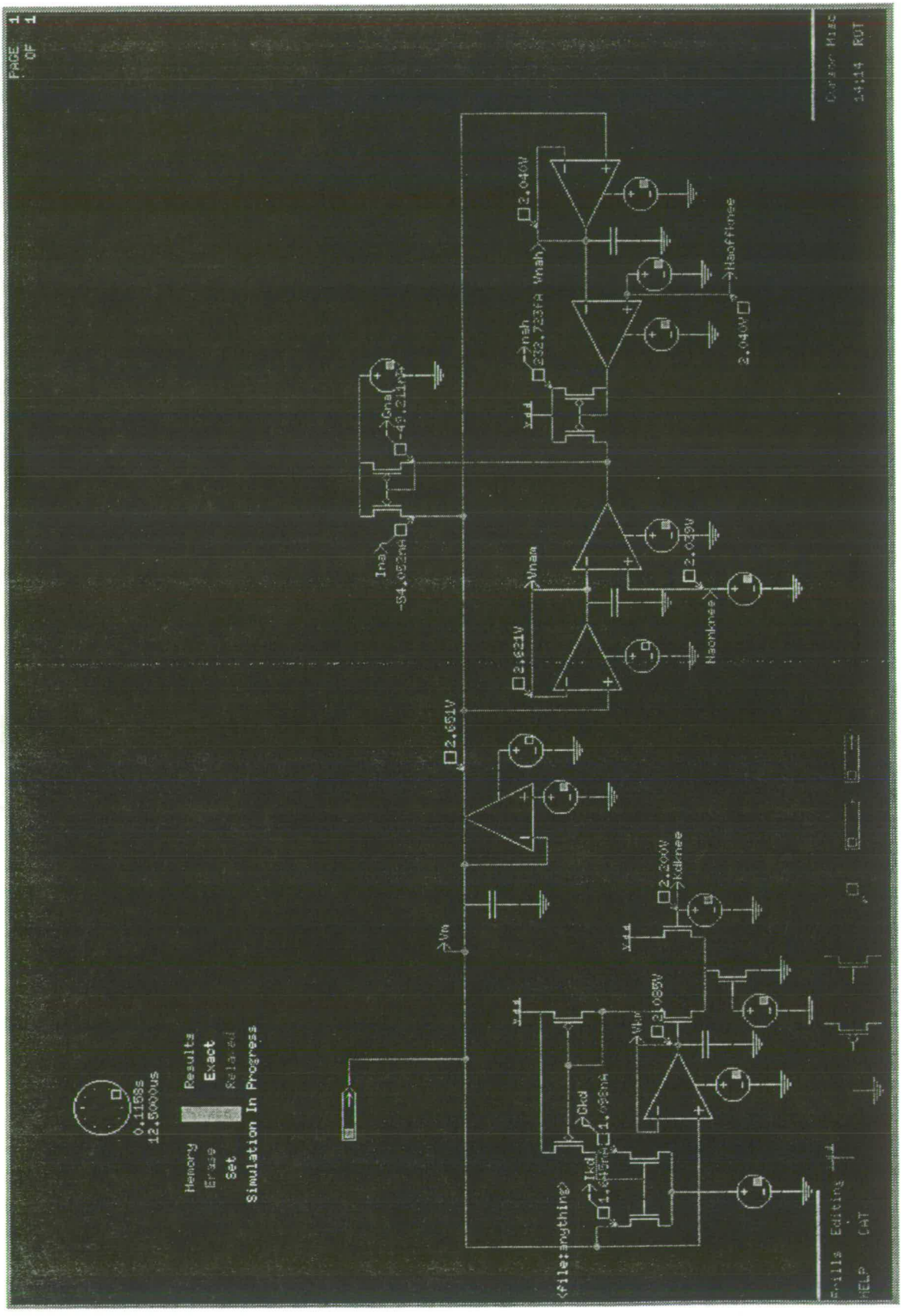

Figure A–1: *The AnaLOG Workspace*

A.3 The EKV Model

The significant property of the EKV model is that it provides square-law behaviour for large values of its argument and exponential behaviour for small values. Therefore, if the argument is an appropriate function of gate voltage, the result is source-drain current. The transition from exponential to square-law behaviour is continuous. The problem with the usual parameterisation of device models is that it is not physically realistic to alter any one parameters without making corresponding adjustments in all the other parameters. For AnaLOG, the EKV model has been adapted to allow the use of three parameters which are independent from the physical process and can therefore be adjusted to allow modelling of different fabrication processes. The adapted model is used by the devices NFET7F and PFET7F – Four terminal N- and P- channel transistors, respectively.

A.4 Parameters for Transistor Models in AnaLOG

- Physical parameters — these provide the quantitative information about the materials used in semiconductor device construction.

- Independent parameters — these parameters are independent in process terms and are of significance in the AnaLOG model, as they are used to

"adjust" the model for specific technologies and specific fabrication runs, they are:

- Q_{ss} - charge due to surface states in the channel. Charges in the channel surface states arise from several sources. Fabricators often use a channel implant step which creates a fixed charge in the channel in order to lower V_t. This is most commonly done for well devices in an N-well process. This parameter is not normally extracted or published for SPICE purposes. Q_{ss} shifts the threshold voltage and subthreshold current. This is why it is used as a fabrication "tuning" parameter.
- N_a - substrate doping concentration. The value for this parameter is usually depth dependent and the doping profile affects device behaviour.
- μ_O - carrier mobility. This value simply scales the value of the threshold current

- Fabrication parameters — these are the properties of devices which are determined by the processing steps used in fabrication. Most of these parameters are routinely measured for each fabrication process and reported as SPICE parameter values, but there are several which require the user to obtain her own values from experimental data. This is explained in the section below.

	AnaLOG default (MOSIS 1.2 micron)		Altered parameters (Mietec 2.4 micron)	
	nmos	**pmos**	**nmos**	**pmos**
Physical parameters				
Temperature (K)	*298*			
Boltzmann's constant (joule/K)	*1.380658e-23*			
Charge on an electron (coulomb)	*1.60217733e-19*			
Permittivity of a vacuum (f/m)	*8.854187817e-12*			
Permittivity of Si (f/m)	*1.035939974589e-10*			
Permittivity of SiO_2 (f/m)	*3.453133248630e-11*			
Silicon-oxide interface charge	*-0.3*			
Independent parameters				
Na multiplicative delta (Na_0)	*1*	*1*	*1* [2]	*1* [2]
Fixed oxide charge (Q_{SS})	*0.00061*	*0.000126*	*0* [2]	*0* [2]
mu multiplicative delta (mu_0)	*1*	*1*	*1* [2]	*1* [2]
Fabrication parameters				
lambda (LAMBDA * e-6)	*0.6e-6*	*0.6e-6*	*1e-6*	*1e-6*
oxide thickness (TOX)	*200e-10*	*200e-10*	*400e-10*	*422e-10*
potential at neutral edge of depletion region (PSI)	*0.6*	*0.6*	*0.61*	*0.68*
bulk doping concentration (NSUB)	*3.106e+16*	*2.692e+16*	*0.141e+16*	*0.911e+16*
carrier mobility (UO)	*686.6*	*205.0*	*610.7*	*233.42*
Ldrawn - Leff (LD)	*0.33e-6*	*0.41e-6*	*0.22e-6*	*0.35e-6*
Wdrawn - Weff (WD)	*0.49e-6*	*0.04e-6*	*0.028e-6*	*0.06e-6*
Drain-dependence Na factor	*0*	*0*	*0*	*0*
Early effect slope parameter	*0.16*	*0.16*	*0.16* [3]	*0.16* [3]
Early effect intercept parameter	*0.1e-6*	*0.1e-6*	*0.1e-6* [3]	*0.1e-6* [3]
active area capacitance (CJ * e-13)	*262e-18*	*470e-18*	*689e-18*	*312e-18*
well-to-bulk capacitance	*1e-18* [1]	*272e-18*	*1e-18*	*100e-18*
overlap capacitance (CGSO * e-6)	*3.9687e-16*	*4.7888e-17*	*1.8e-16*	*2.8e-16*
gate capacitance (CGBO * e-6)	*3.8241e-16*	*3.5683e-16*	*5.57e-16*	*5.57e-16*

Figure A–2: *Parameters required in the AnaLOG model for simulation of circuits in the weak-inversion region for both MOSIS 2μm and Mietec 2.4μm processes. The equivalent level 3 HSPICE parameter is shown in uppercase.* [1] *Since the n-channel transistor is in the substrate, this parameter is meaningless. An insignificantly small non-zero value is used to prevent numerical problems in simulation.* [2,3] *Set to these values for initialisation.*

A.5 Improving the Accuracy of the Parameters

There is some minor additional work to be carried out in order to provide a thoroughly Mietec-tuned simulator. The simulator contains some predefined devices, such as transconductance amplifiers, which, as yet, still use the original MOSIS-tuned parameters. The solution to this is to redraw these devices from their Mietec-tuned component parts, simulate their behaviour and incorporate the values obtained into the equations used by the simulator for its predefined devices.

Also, the values used for the Early effect slope and intercept parameters were for initialisation. More accurate values can be obtained by creating I_{ds} vs. V_{ds} curves for Mietec-tuned transistors of different lengths and gate voltages and fitting the following equation:

$$I_{out} = I_{norm} * (1 + \lambda_c * V_{ds}) \tag{A.1}$$

where I_{norm} is the output of the transistor model with all effects except for the Early effect modelled,
where,

$$\lambda_c = Early_s/(V_g + L - L_O) \tag{A.2}$$

where L is the length of the transistor and V_g is the gate voltage.

Finally, the Independent parameter values were for initialisation only. Obtaining more accurate values is a fairly detailed process and is not described here. It

Appendix B

Technical Details: Silicon Neurons

B.1 Introduction

This Appendix to Chapter 6 describes the technical details required to implement a silicon neuron in a Mietec 2.4μm fabrication process. The first section uses the example of capacitors to describe how alterations were made to ensure compliance with the design rules. The second section includes circuit diagrams and layout plans of each of the subcells, and of the complete chip plus pads, alongside layout plans for the original MOSIS fabrication. The final section provides details of the test circuitry and experimental setup. Layout for the chip was done using CAD software, "Cadence 9401/4.3", and fabricated by Europractice. The dimensions of the chip were 4411 x 3886 microns. A legend for the layers in the layout plans is shown in figure B–1

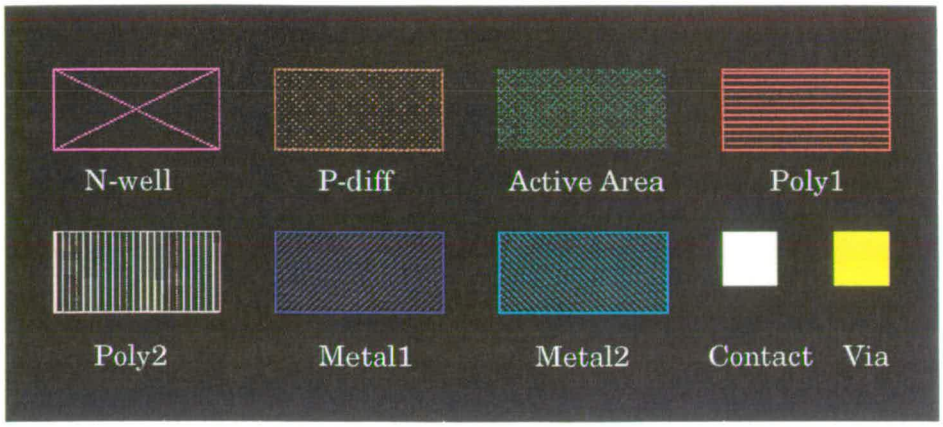

Figure B–1: *A legend for the layers seen in the layout plans.*

B.2 Subcells of the Silicon Neuron

B.2.1 Capacitor Redesign

Capacitors can be formed by placing two conducting layers, in this case, polysilicon – "poly1" and "poly2", separated by a dielectric, in this case, an oxide layer. This is shown in figure B–2. The top plate defines the area of the capacitor.

There are a number of design rules relating to the use of poly2 layers. Exact specifications cannot be divulged, as the rules are confidential, however it is possible to outline a few constraints:

- There are some layers which cannot be placed on top of a poly2 layer.

- When placing legitimate layers on top of a poly2 layer, there are minimum distances of overlap to observe.

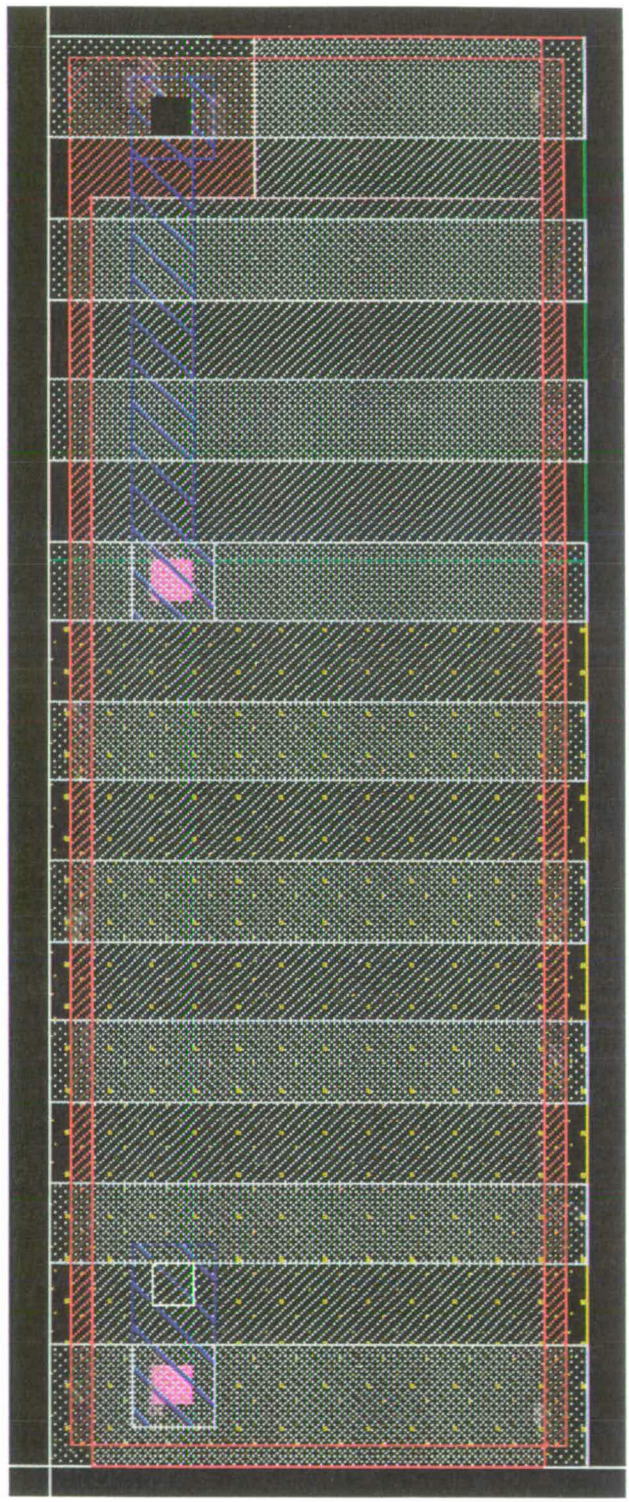

Figure B–2: *Polysilicon-oxide-polysilicon capacitor.*

- A poly1 layer placed on top of a poly2 layer must be placed entirely *within* the poly2 layer.

According to these rules, the capacitors laid-out for MOSIS fabrication are not legal. In order to comply with the design rules, capacitors were "pulled-out" from the core of each subcell. Metal2 lines have also been pulled out, although this is not strictly necessary. The design rules, to some extent therefore, dictate how a capacitor can be laid-out. In addition, there are principles of analogue design that suggest good techniques for the layout of certain components.

The capacitance of integrated circuit capacitors is given by:

$$C = \frac{\sum_{ox} A}{t_{ox}} \tag{B.1}$$

where $\sum_{ox}$ is the dielectric constant of the oxide, t_{ox} is the thickness of the oxide, and A is the area of the capacitor. It is possible for errors in capacitance values to be introduced by variations in the oxide thickness. These can be reduced by designing capacitors to have a common centroid geometry.[89] Plates can be square, in order to minimise the relative error in the length and width definition.

Figure B–4 shows these principles applied to a subcell of the silicon neuron, laid-out for a Mietec process.

One of the subcells of the silicon neuron consists of an array of capacitors. This subcell occurs 10 times across the layout. In two of the occurrences, it represents the membrane capacitance, in the other 8 occurrences, it represents a dendritic capacitance. In addition to complying with the design rules, and following good techniques of analogue design, capacitance had to be recalculated to take into

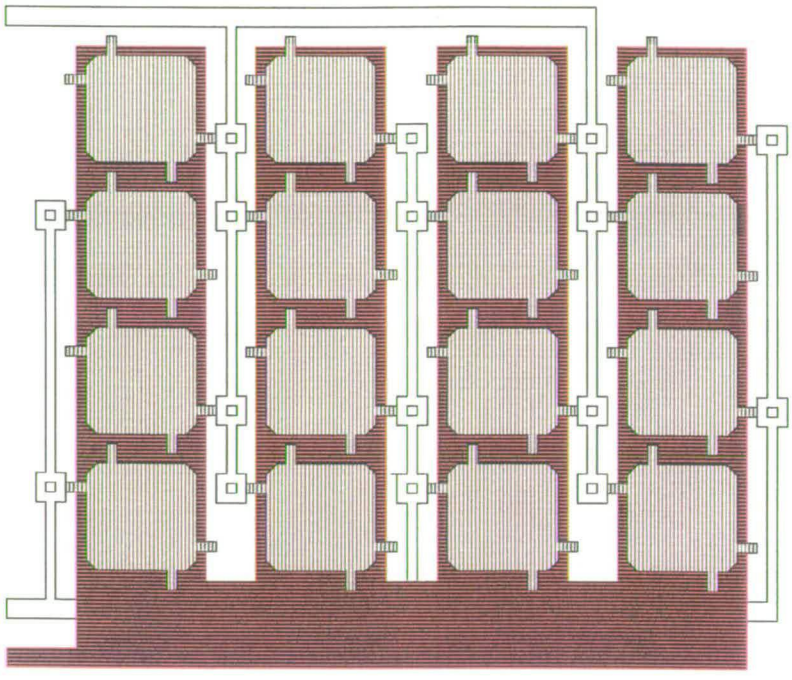

Figure B–3: *A Theoretical Example of Capacitor Layout with Common Centroid Geometry. (From Allen, P. and Holberg D., 1987, CMOS Analog Circuit Design).*

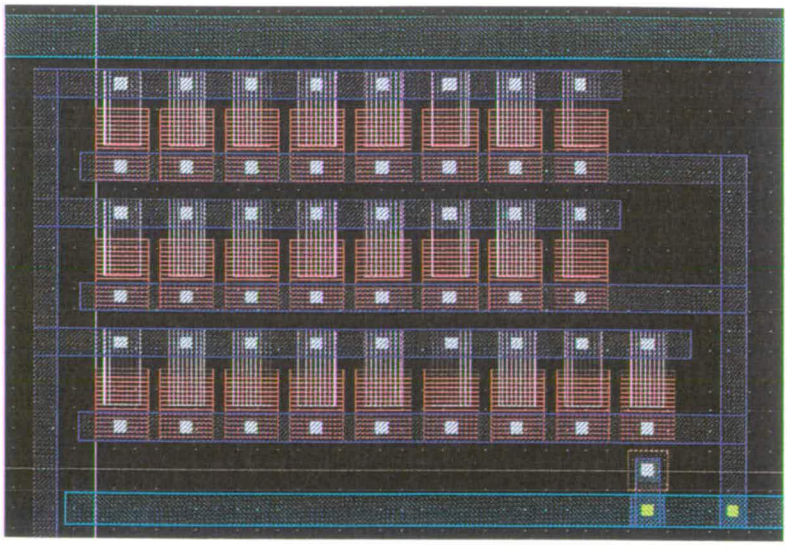

Figure B–4: *An Actual Example of Capacitor Layout with Common Centroid Geometry*

account the scaling difference between the two fabrication processes, and the different sheet capacitance (CP) values for the polysilicon layers.

B.2.2 Leakage (NODE)

The leakage circuit contains a wide-range transconductance amplifier that represents the leakage conductance, as described in Chapter 4.

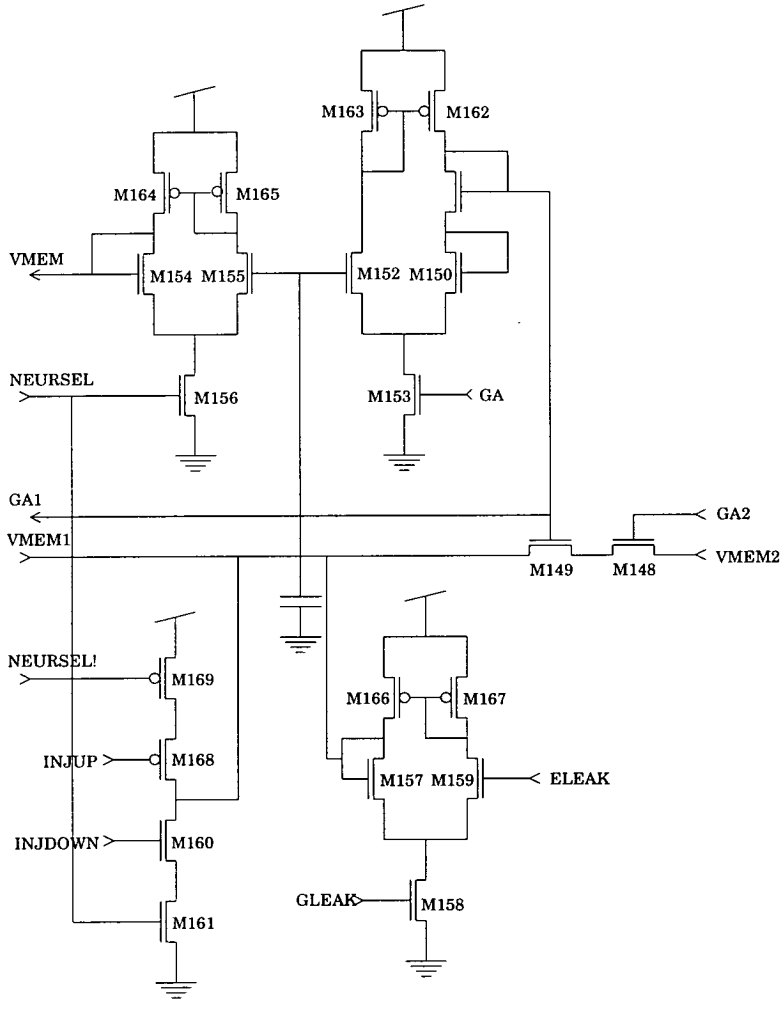

Figure B–5: *Leakage (NODE) Circuit Schematic*

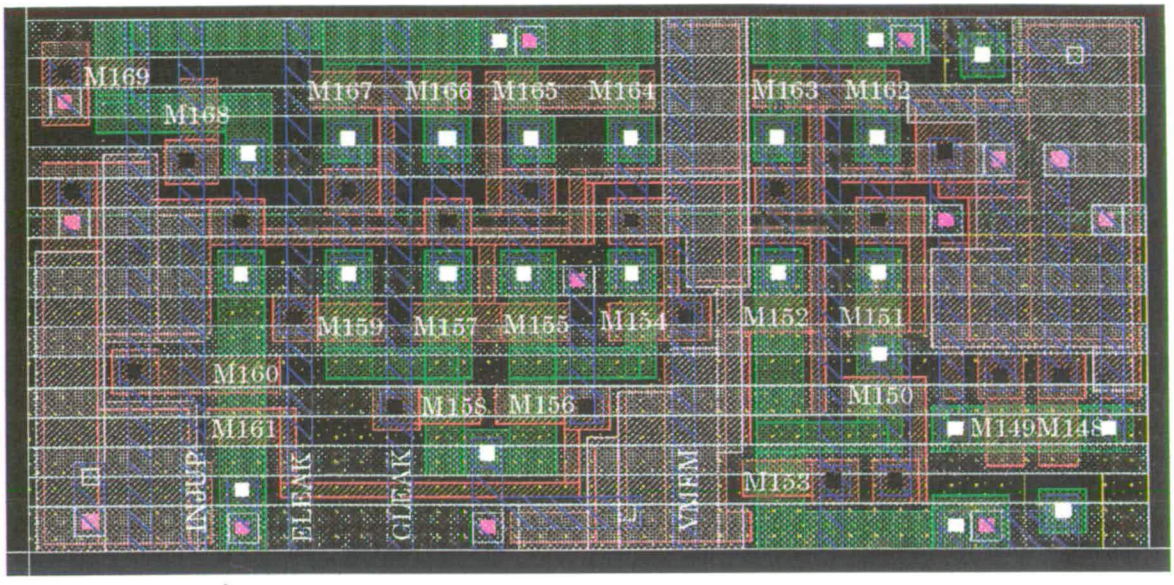

Figure B–6: *Layout for MOSIS–Fabricated NODE*

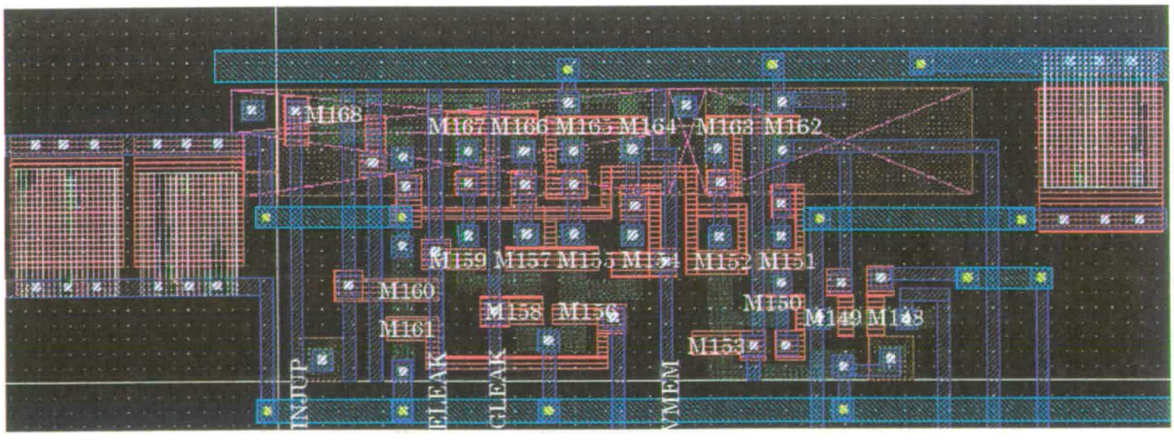

Figure B–7: *Layout for Mietec–Fabricated NODE*

B.2.3 Sodium (NA)

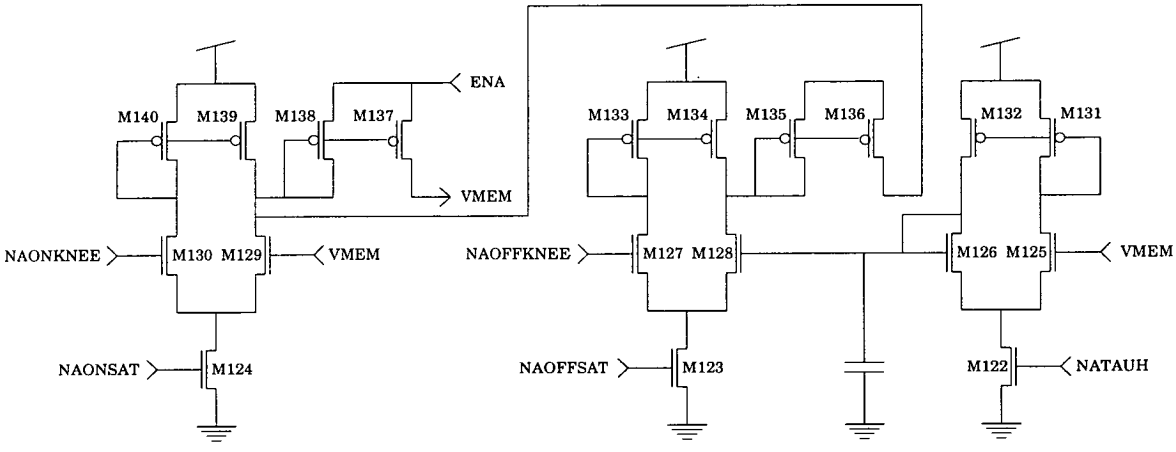

Figure B–8: *Sodium (NA) Circuit Schematic*

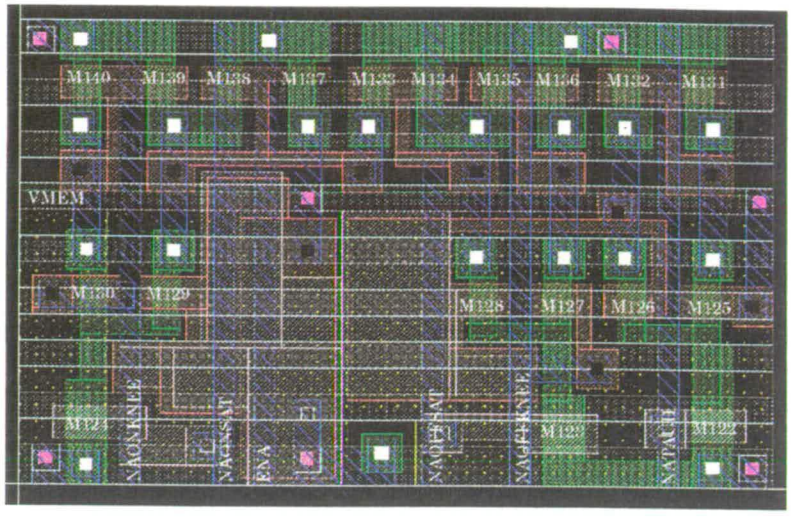

Figure B–9: *Layout for MOSIS–Fabricated NA*

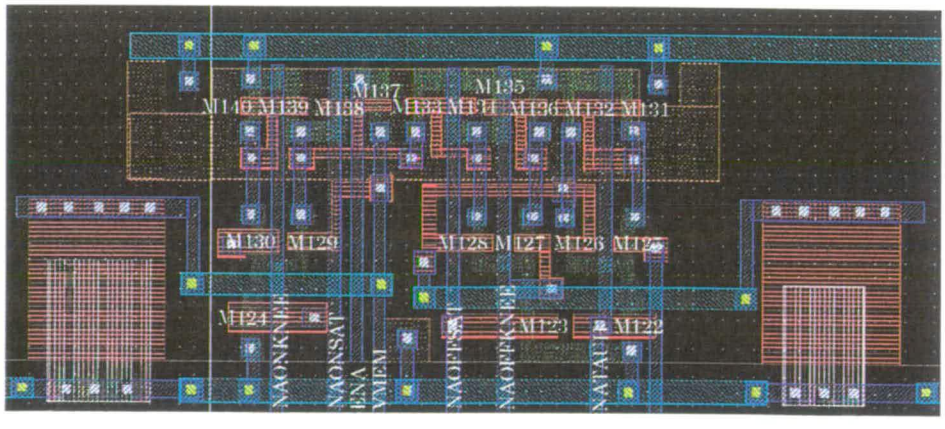

Figure B–10: *Layout for Mietec–Fabricated NA*

B.2.4 Potassium (KD)

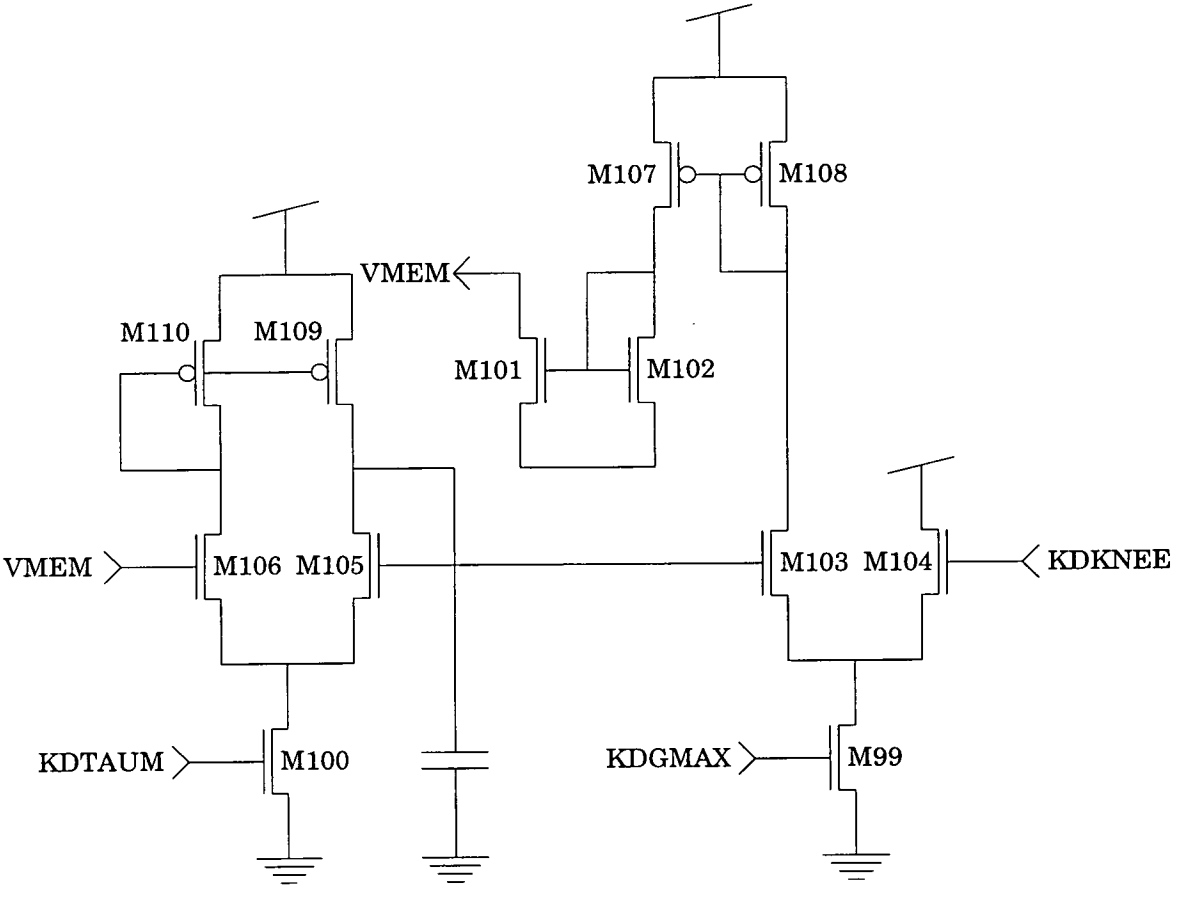

Figure B–11: *Potassium (KD) Circuit Schematic*

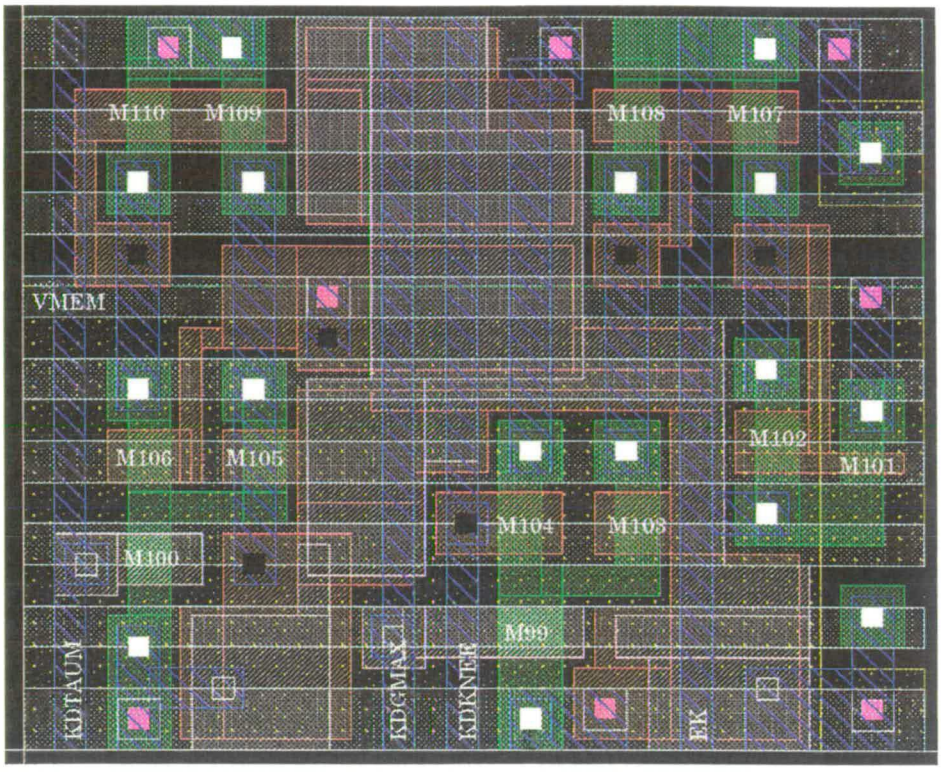

Figure B–12: *Layout for MOSIS–Fabricated KD*

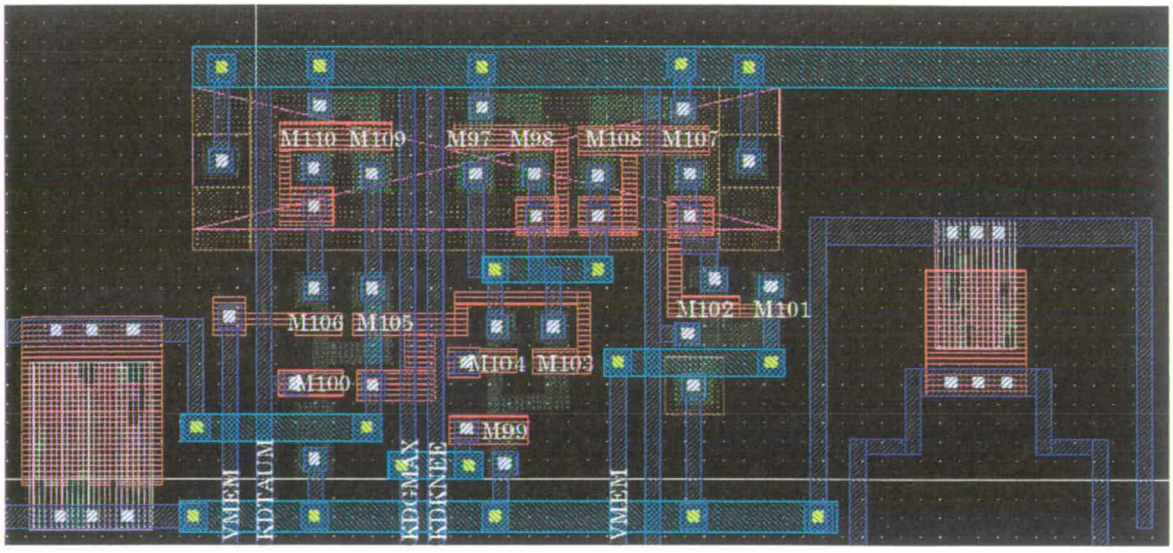

Figure B–13: *Layout for Mietec–Fabricated KD*

B.2.5 Potassium (KA)

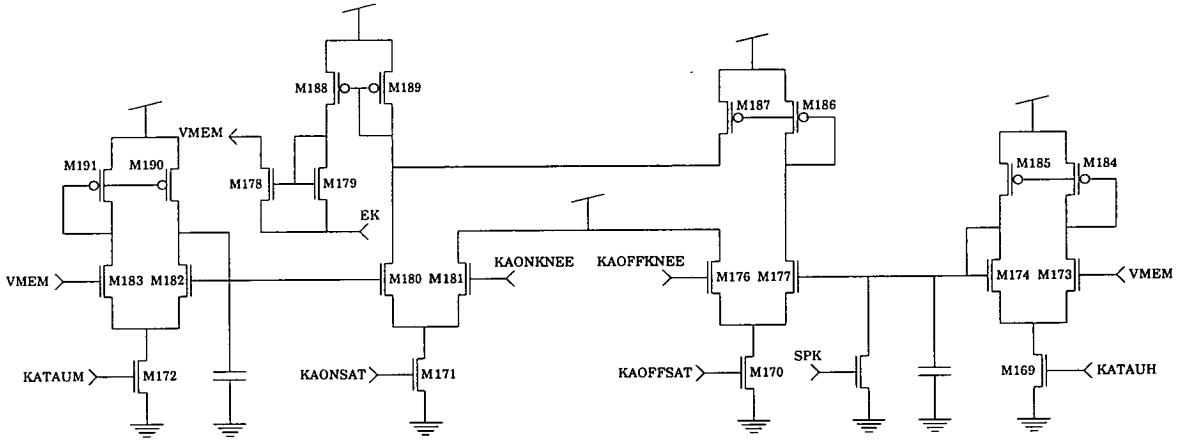

Figure B–14: *Potassium (KA) Circuit Schematic*

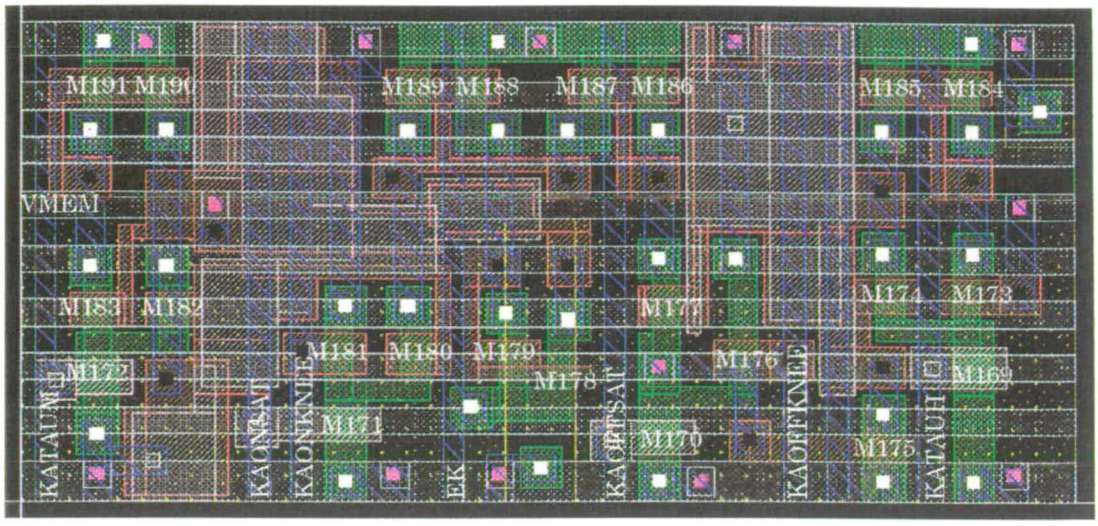

Figure B–15: *Layout for MOSIS–Fabricated KA*

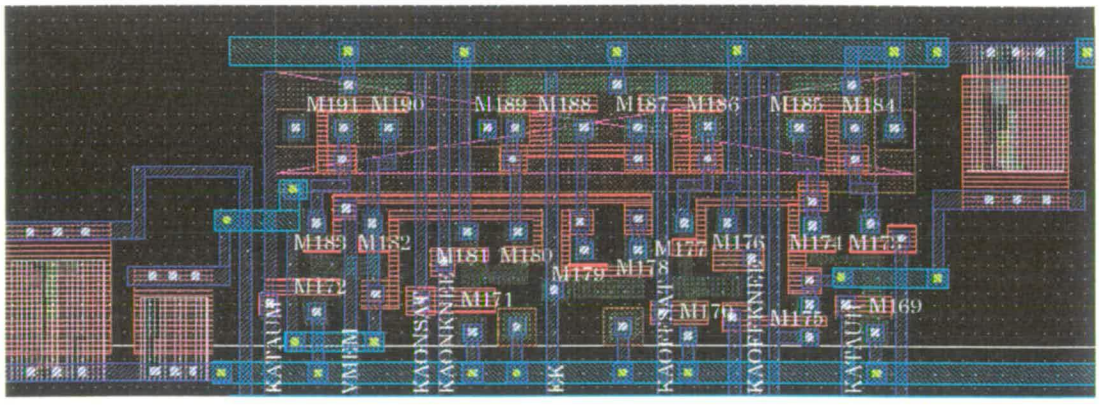

Figure B–16: *Layout for Mietec–Fabricated KA*

B.2.6 Calcium (CAL)

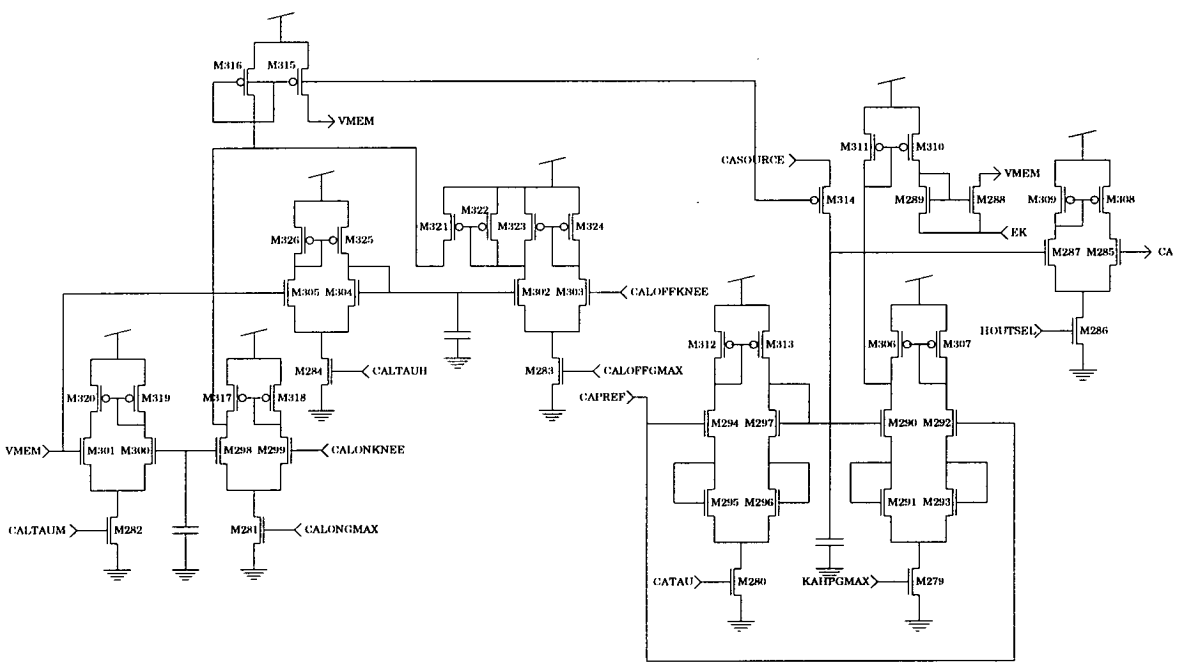

Figure B–17: *Calcium (CAL) Circuit Schematic*

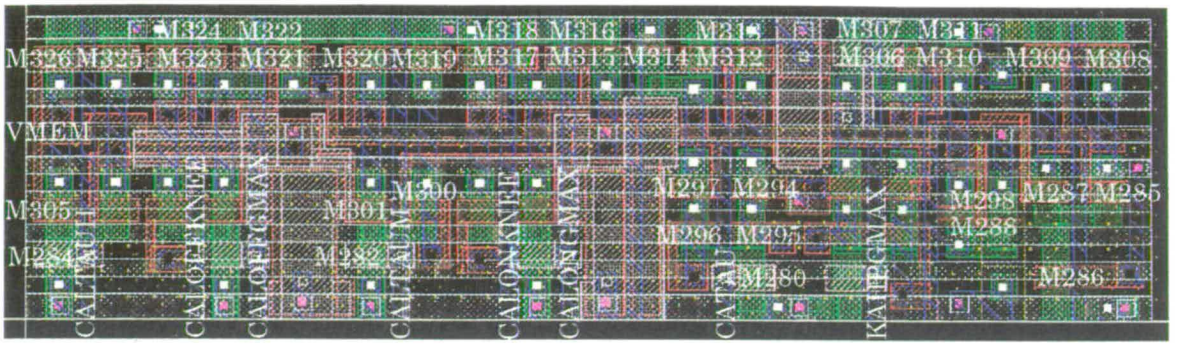

Figure B–18: *Layout for MOSIS–Fabricated CAL*

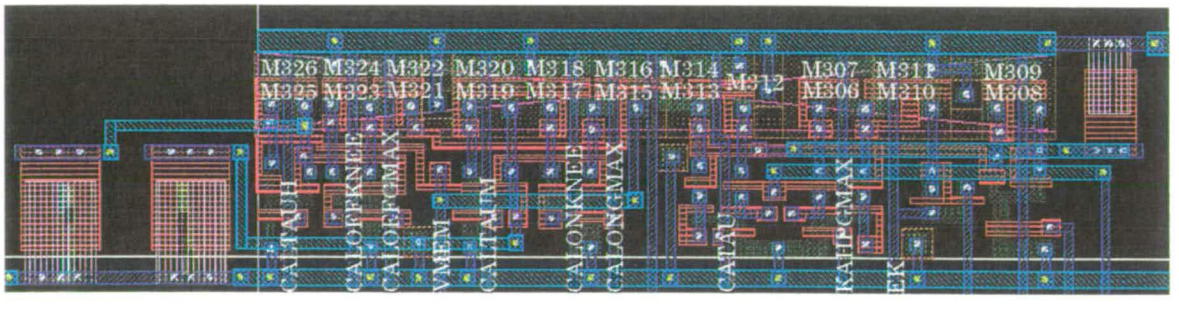

Figure B–19: *Layout for Mietec–Fabricated CAL*

B.2.7 Complete Core (TESS)

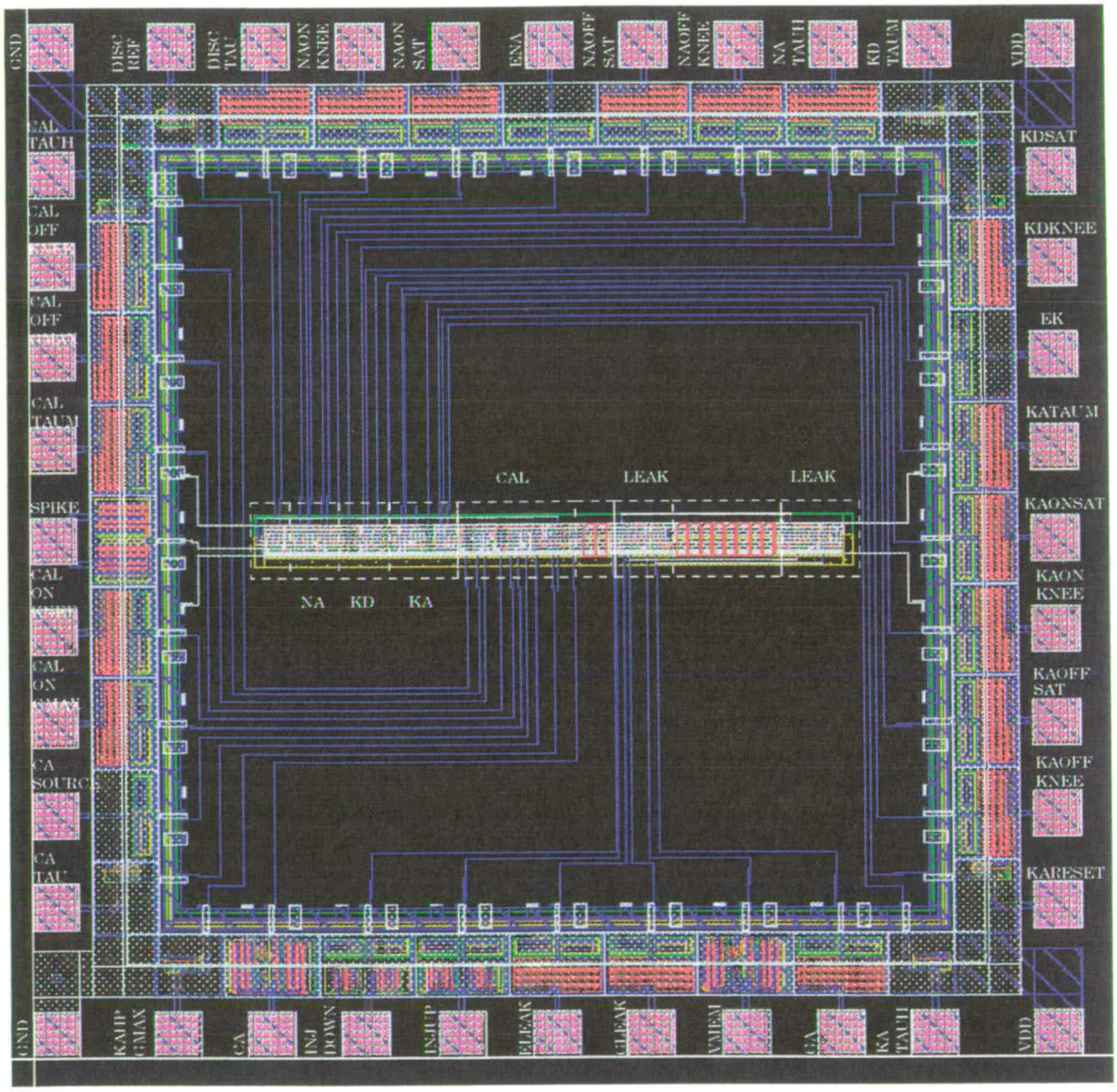

Figure B–20: *Layout for MOSIS–Fabricated Complete Core*

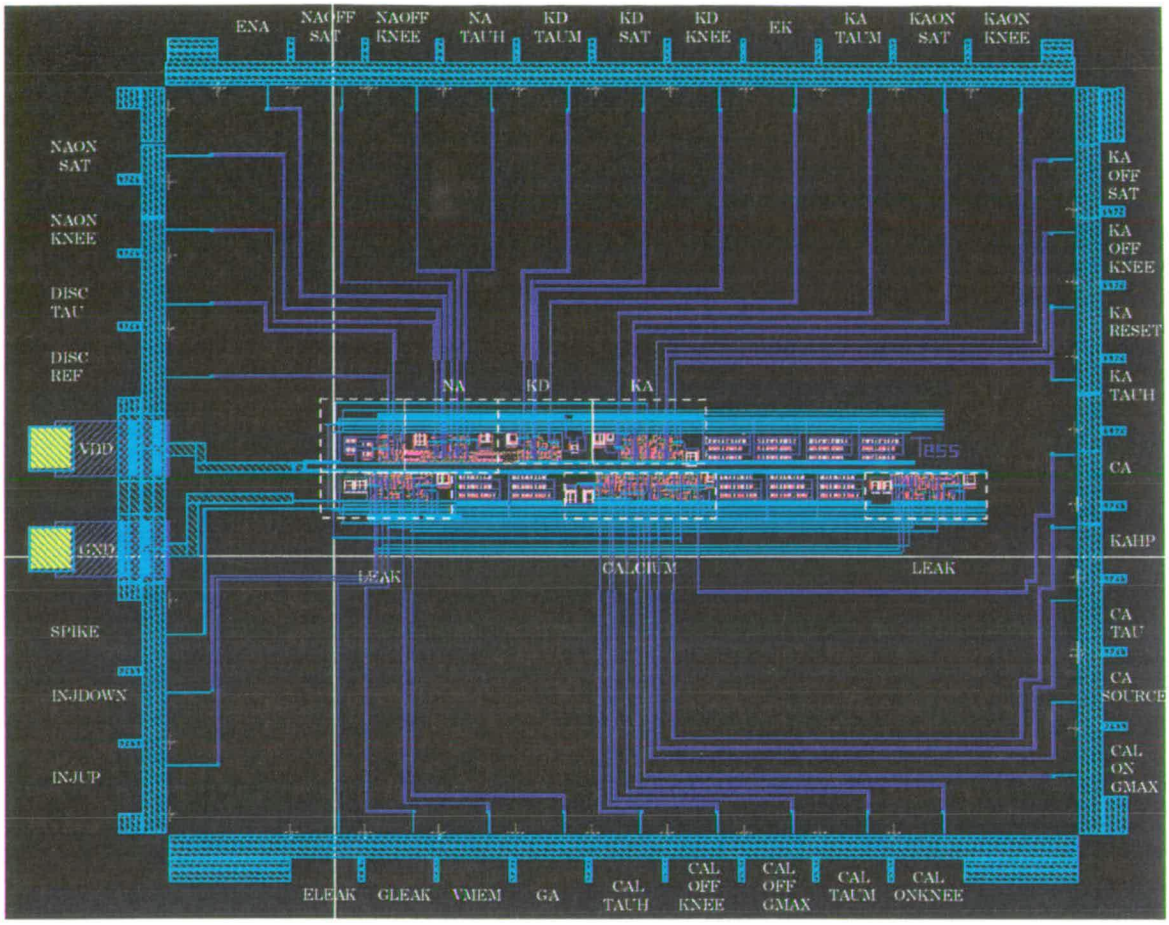

Figure B–21: *Layout for Mietec–Fabricated Complete Core*

B.3 Test Circuitry and Experimental Set-up

The test board was constructed using the original schematics for the Mahowald and Douglas silicon neuron. It was originally constructed by Brian Baker (Department of Psychology, University of Oxford). A plan of the test board is included below:

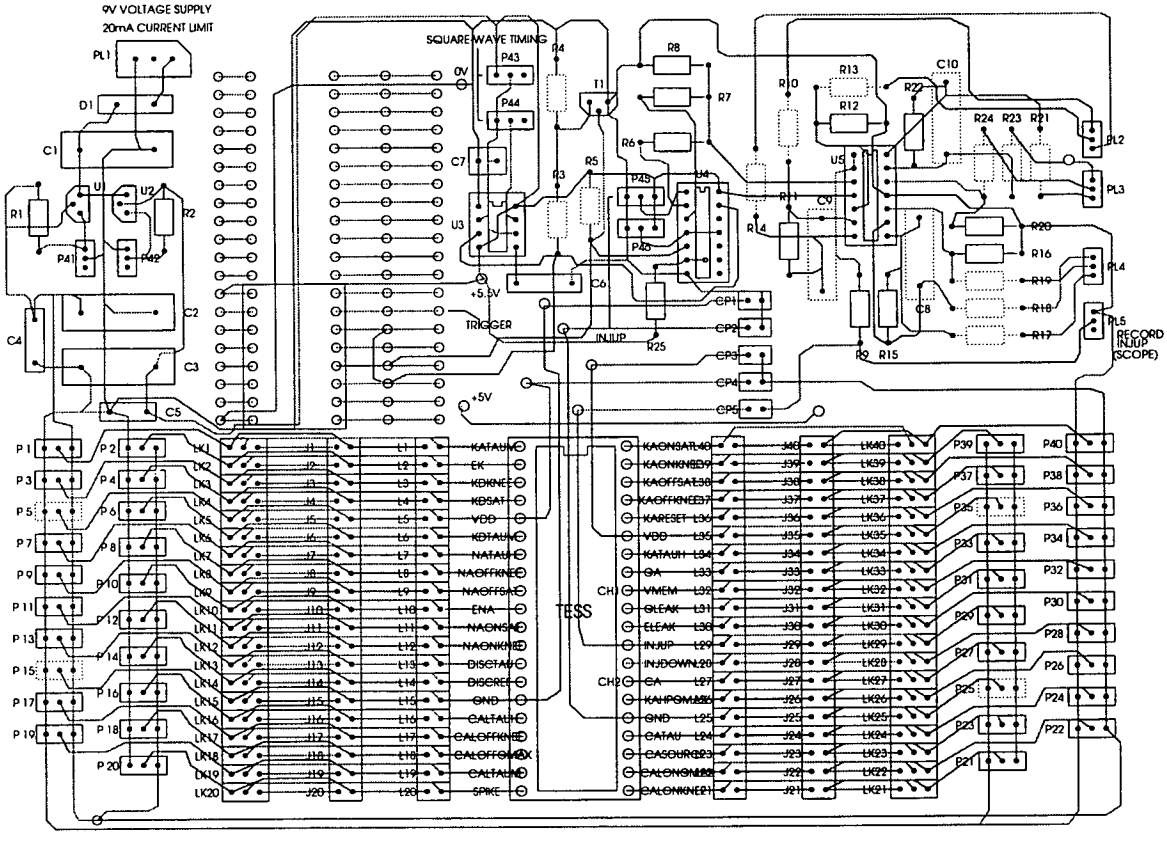

U1: A power supply chip that converts the battery voltage to 5V and 5.5V. (The capacitors and resistors surrounding are necessary for the proper function of U1 and U2).
U2: As U1.
U3: An astable oscillator.
U4: An analogue switch.
$U5_B$: A buffer amplifier for the injection signal (INJUP). U3, U4 and U5 ensure that the signal going to pin 29 is a square wave of adjustable frequency and with accurate known amplitudes.
U6: A buffer for the scope trigger, and to invert the signal going to the analogue switch (U4).

P1 - P40: 100K Potentiometers for setting the parameters of the chip.
P41, P42: 1K Potentiometers
P43 - P46: 100K Potentiometers
J1 - J40: Jumpers
PL1: 9V supply, 30mA current limit
pin 32: Membrane voltage output
pin PL5:2: Injection current.
pin 27: Calcium concentration
P43, P44: Timing of square wave input.

Figure B–22: *A Wiring Diagram for the Silicon Neuron Test Board*

Appendix C

Technical Details: Neuromorphic Ion Channels

C.1 Introduction

This Appendix to Chapter 7 describes the technical details required to implement and test the function of N-type Ca^{++} ion channels in a Mietec 2.4μm fabrication process. The Appendix contains circuit schematics, equations and layout for:

- The Activation Time-Dependence Circuit
- The Summation Circuit
- The Adaptation Circuit

As before, layout for the chip was done using CAD software, "Cadence 9401/4.3", and fabricated by Europractice. The dimensions of the chip were 4635μm by 4445μm. The circuits were designed to be modular, so that they could be included or excluded from the circuit as required and also so that they were compatible with the original neuron design, and could be used to complement its function if the opportunity arose.

C.2 Subcells of Neuromorphic Ion Channels

C.2.1 The Activation Time-Dependence Circuit (τ_q)

The subcircuit outlined by a dashed line in figure C–1 is removed and replaced by the activation time-dependence circuit shown in figure C–2

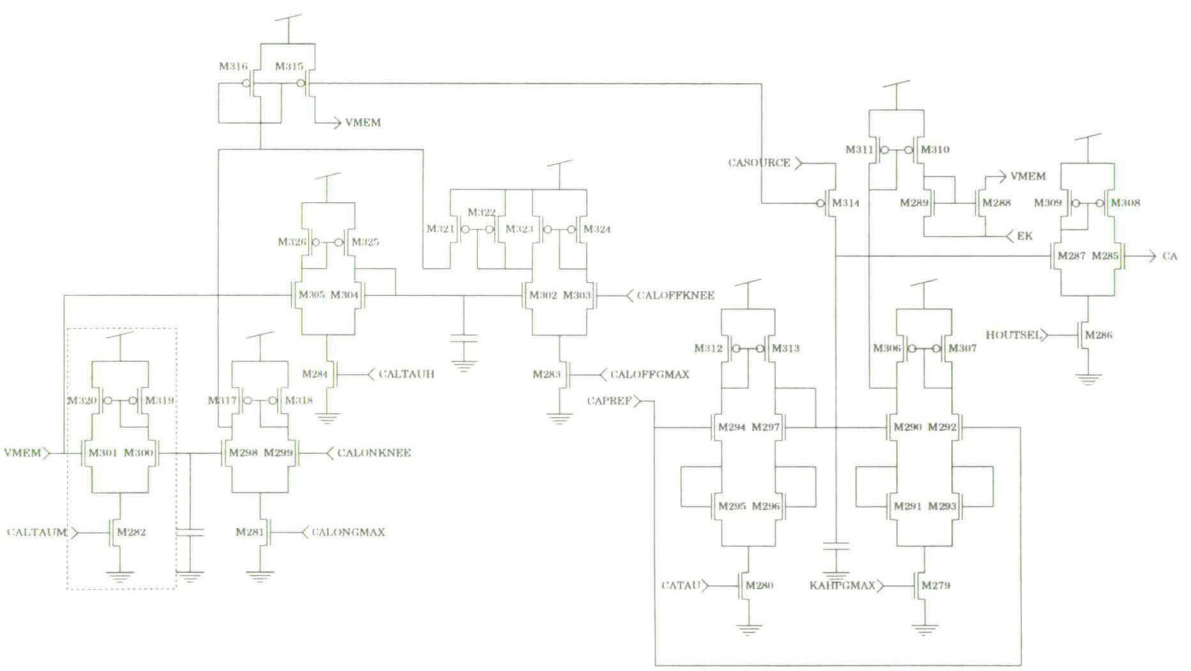

Figure C–1: *The Location for the Time-Dependence Circuit*

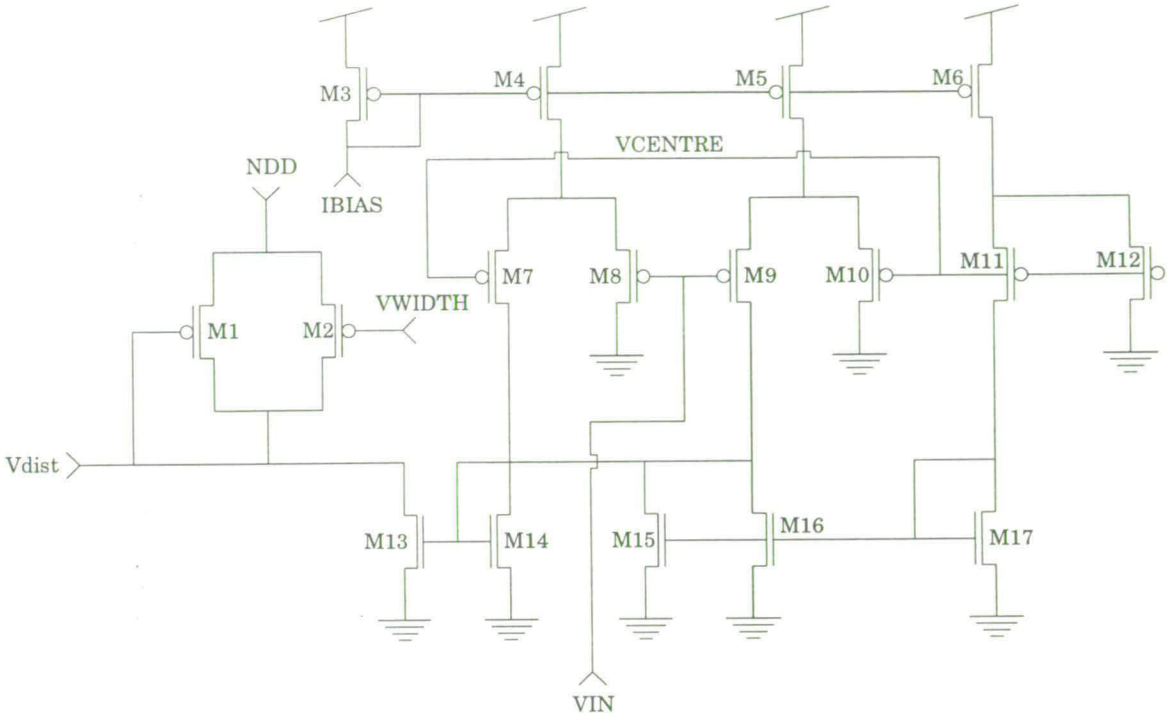

Figure C–2: *The Activation Time-Dependence Circuit*

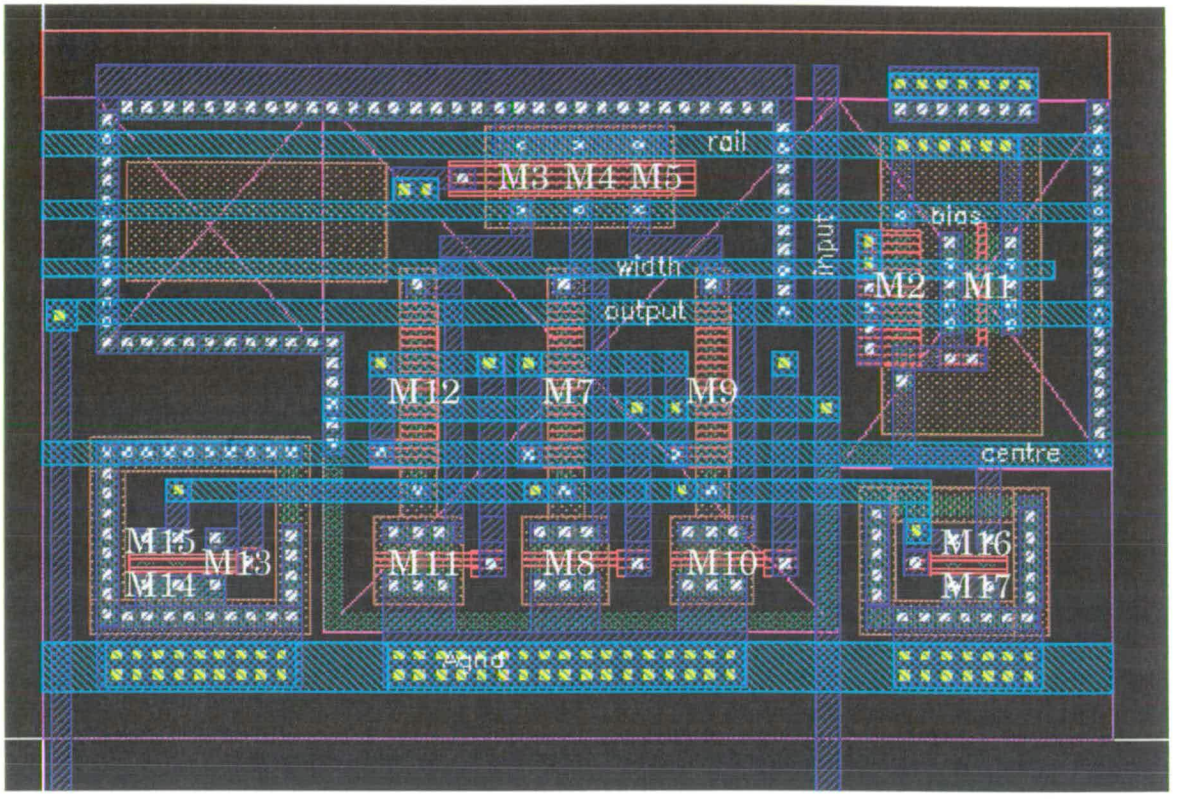

Figure C–3: *The Activation Time-Dependence Layout*

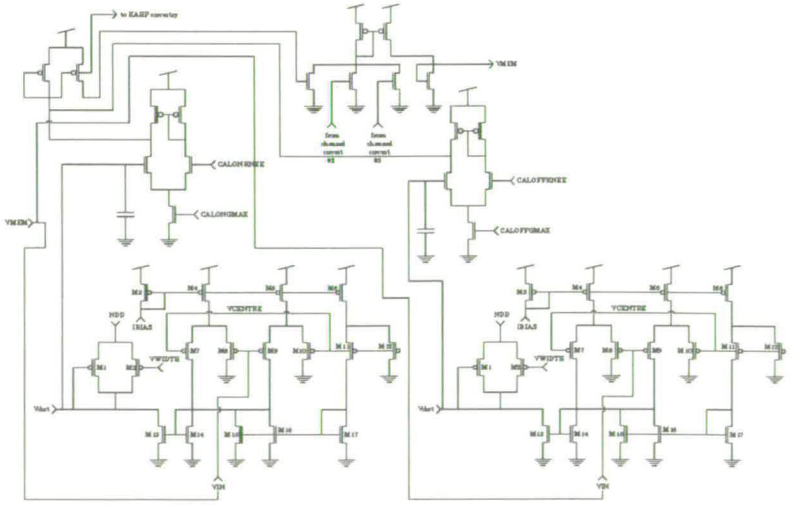

Figure C–4: *The Time-Dependence circuit after inclusion in the Ca^{++} activation circuit*

C.2.2 The Summation Circuit (ϵ)

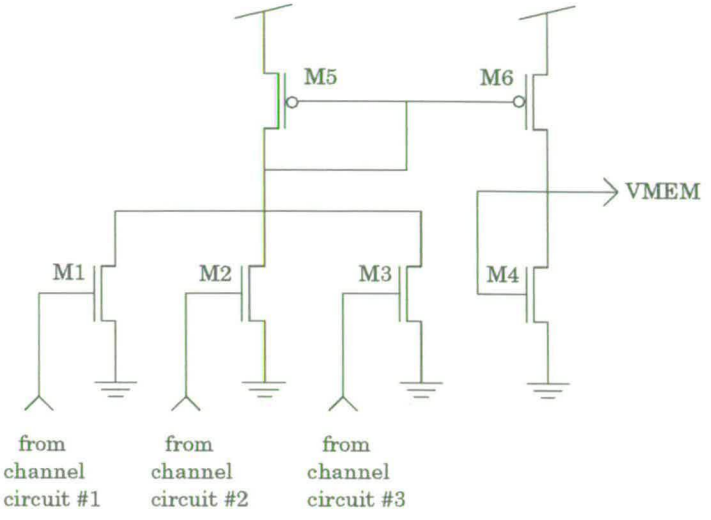

Figure C–5: *The Summation Circuit*

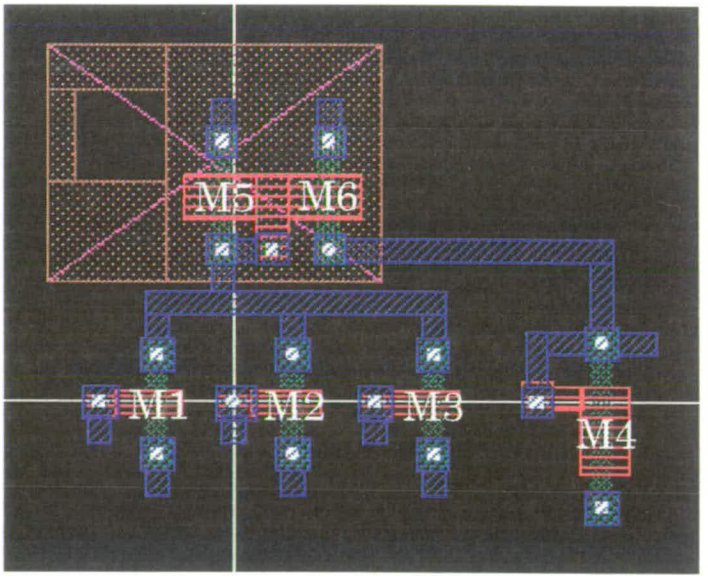

Figure C–6: *The Summation Layout*

C.2.3 The Adaptation Circuit (α)

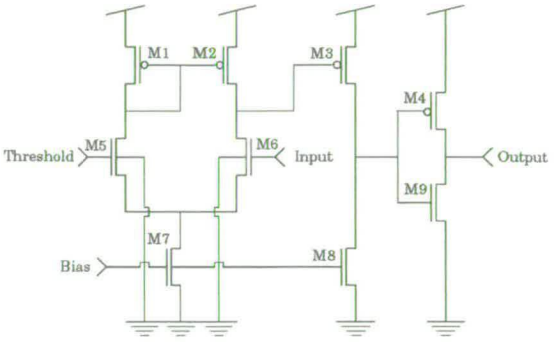

Figure C–7: *The Adaptation Circuit*

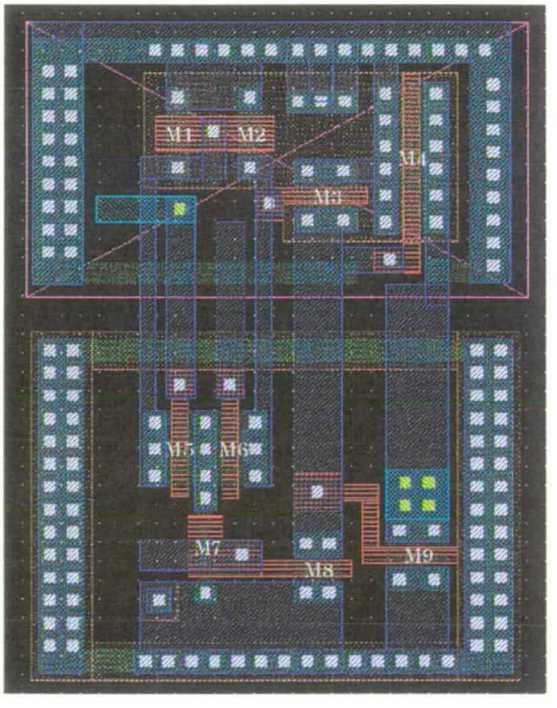

Figure C–8: *The Adaptation Layout*

Figures C–9 and C–10 show the circuitry and layout that connect the three adaptation modules.

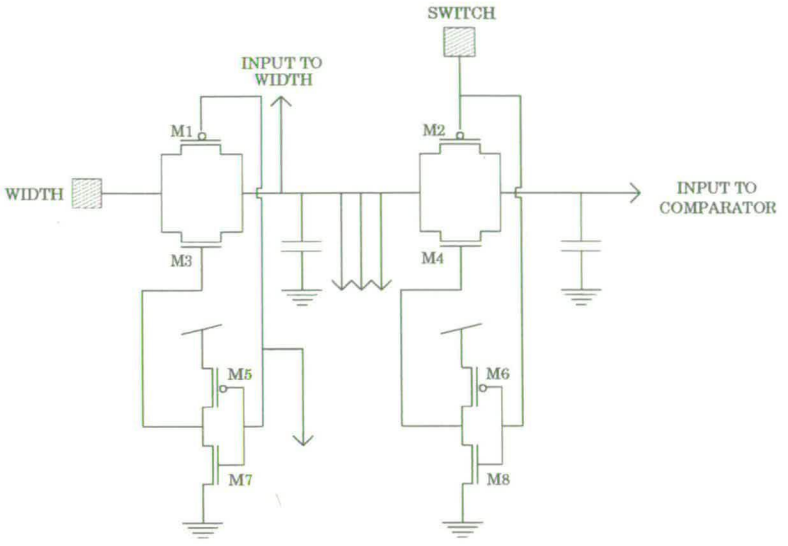

Figure C–9: *Circuitry connecting the three adaptation modules*

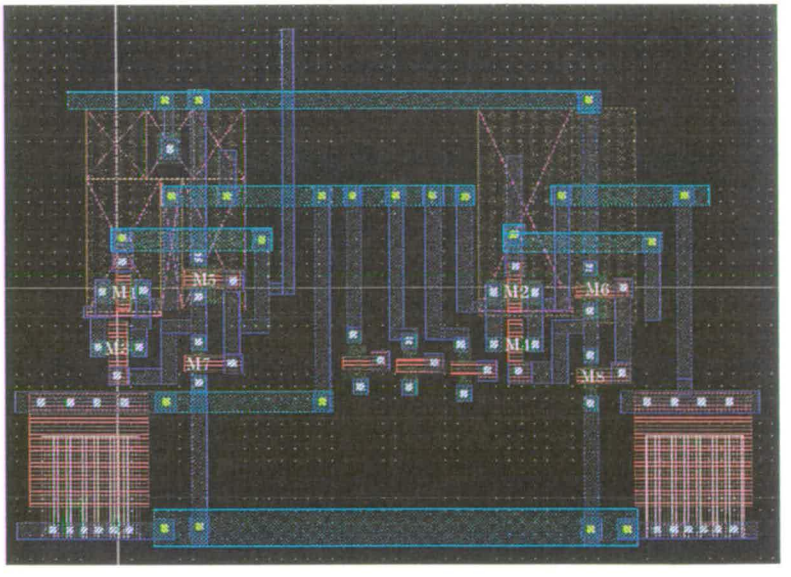

Figure C–10: *Layout for the connections between the three adapation modules*

C.2.4 Complete Core (WEE HENRIK)

Figure C–11 shows how all three ion channel circuits are connected into the Ca^{++} activation circuitry, with the adaptation circuitry also shown.

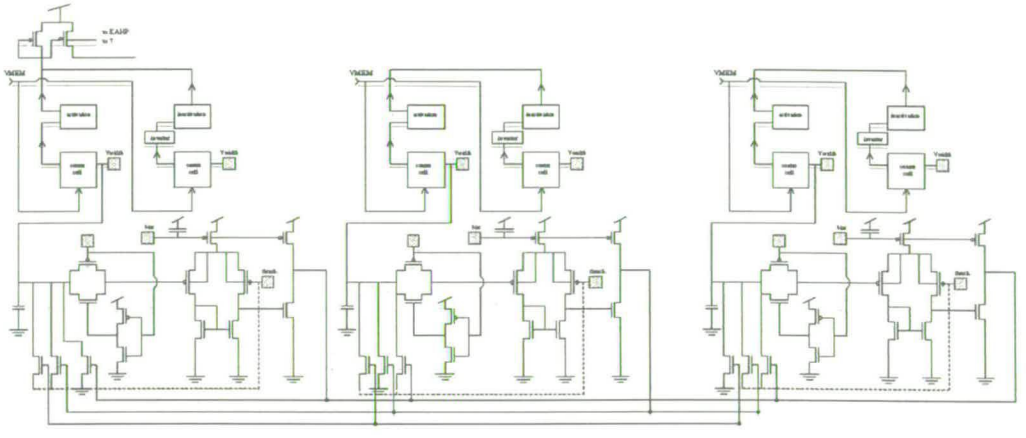

Figure C–11: *A Schematic of all three ion channel circuits and adaptation circuitry*

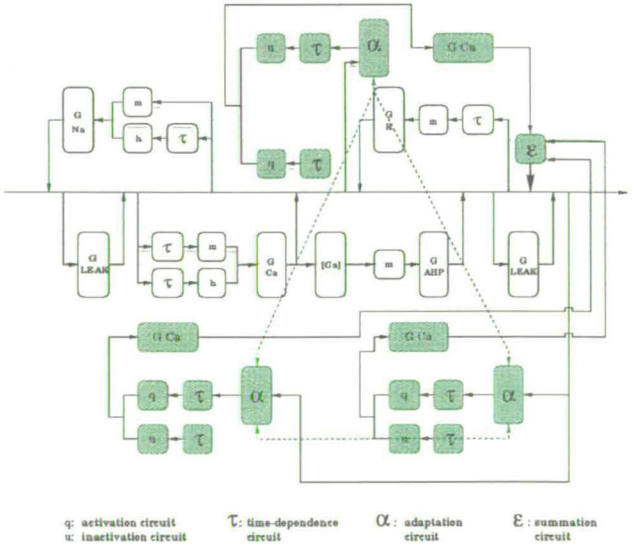

Figure C–12: *A Diagram of the Location of the Ion Channel Modules Within the Silicon Neuron*

Figure C–13 shows the pads and layout of the complete chip.

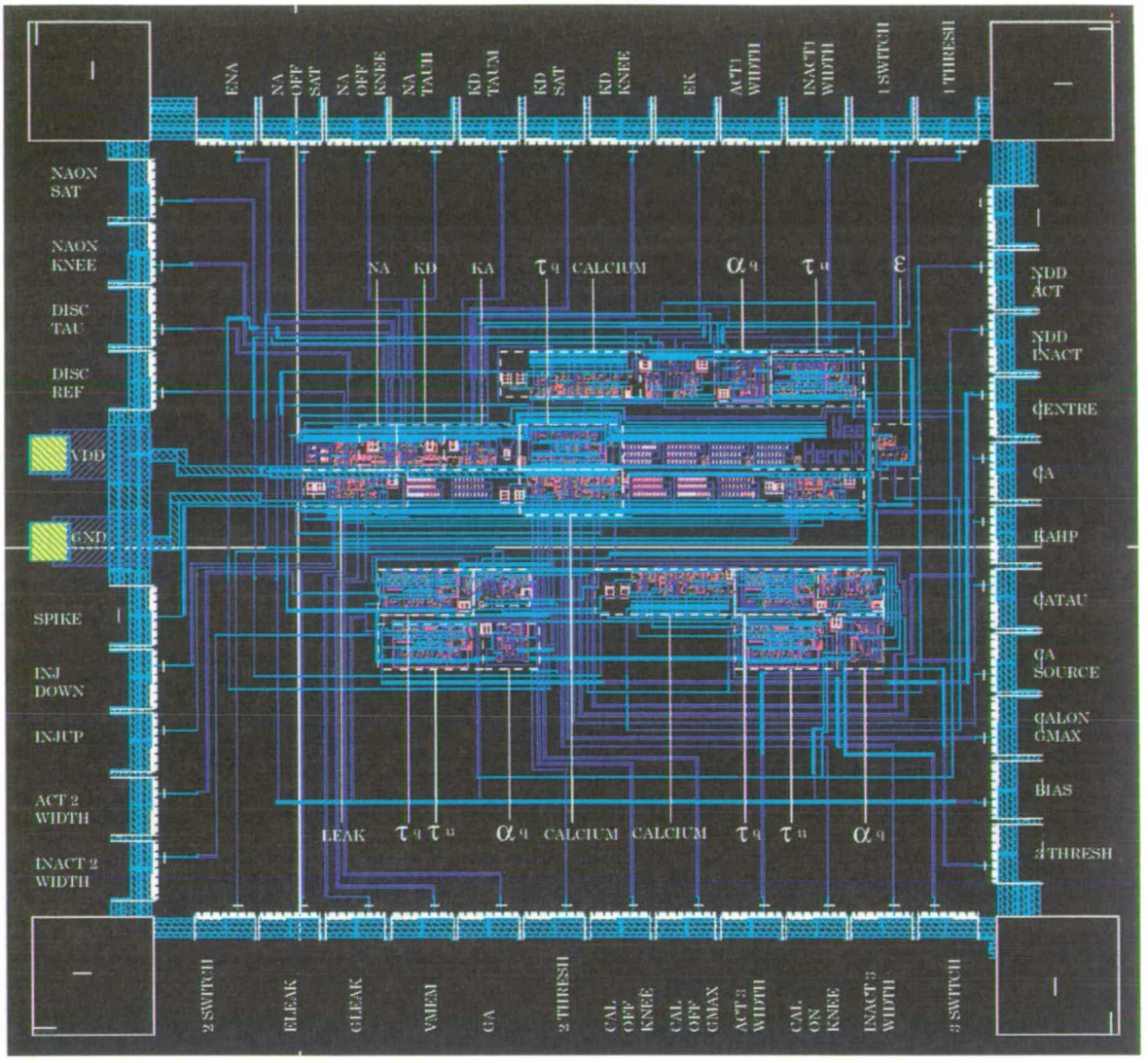

Figure C–13: *The Complete Chip Layout*

Bibliography

[1] A. Delcour, D. Lipscombe, and R. Tsien, "Multiple modes of n-type calcium channel activity distinguished by differences in gating kinetics", *The Journal of Neuroscience*, vol. 13, pp. 181 – 194, 1993.

[2] A. Delcour and R. Tsien, "Altered prevalence of gating modes in neurotransmitter inhibition of n-type calcium channels", *Science*, vol. 259, pp. 980 – 983, 1993.

[3] B. Hille, *Ionic Channels of Excitable Membranes*, Sinauer Associates Inc., Sunderland, Massachesetts, 1984.

[4] A. Andreou, "On physical models of neural computation and their analogue VLSI implementation", *IEE Computer Society Reprint from Workshop on Physics and Computation Phys-Comp '94 Conference*, vol. , 1994.

[5] G. Shepherd, *The Synaptic Organisation of the Brain*, Oxford University Press, Oxford, 1990.

[6] J. Kelso, *Dynamic Patterns: The Self-Organization of Brain and Behaviour*, MIT Press, Cambridge, Massachusetts, 1995.

[7] A. Bell, *A Channel Space Theory of Dendritic Self-Organisation*, Technical report VUB AI-lab memo no. 91-4, Vrije Universtiteit Brussel, 1991.

[8] A. Bell, *Self-Organisation of Neural Dynamics*, Phd thesis, Vrije Universtiteit Brussel, 1993.

[9] M. Mahowald and R. Douglas, "A silicon neuron", *Nature*, vol. 354, pp. 515 – 518, 1991.

[10] A. Hodgkin and A. Huxley, "A quantitative description of membrane current and its application to conduction and excitation in nerve", *The Journal of Physiology*, vol. 117, pp. 500 – 544, 1952.

[11] C. Mead, *Analog VLSI and neural systems*, Addison-Wesley, 1989.

[12] L. Smith and A. (Eds.) Hamilton, *Neuromorphic systems: engineering silicon from neurobiology*, World Scientific, Singapore, 1998.

[13] D. Marr, *Vision : A Computational Investigation into the Human Represenation and Processing of Visual Information*, W H Freeman: New York, 1982.

[14] A. Newell, "Physical symbol systems", *Cognitive Science*, vol. 4, pp. 135 – 183 , 1980.

[15] A. Newell, "The knowledge level", *Artificial Intelligence*, vol. 18, pp. 87 – 127, 1982.

[16] C. Collin and R. Woodburn, "Neuromorphism or pragmatism?: A formal approach", in S Smith, L and A Hamilton, editors, *Neuromorphic systems: engineering silicon from neurobiology.* World Scientific, Singapore, 1998.

[17] L. Liebovitch and A. Todorov, "Using fractals and nonlinear dynamics to determine the physical properties of ion channel proteins", *Critical Reviews in Neurobiology*, vol. 10, pp. 169 - 187, 1996.

[18] C. Collin and S. Still, "Towards a neuronally-controlled walking machine", *in Abstract In Proceedings. Second International Conference on Cognitive and Neural Systems.* Boston University, 1998.

[19] C. Collin, "Neuromorphic ion channels: Gating and adaptation", *in Paper In Proceedings. International ICSC Symposium on Neural Computation.* Technical University of Vienna, 1998.

[20] J. Lazzaro, *anaLOG: A Functional Simulator for VLSI Neural Systems*, Technical report number 5229:tr:86, California Institute of Technology, 1986.

[21] S. Harnad, "Levels of functional equivalence in reverse bioengineering: The darwinian turing test for artificial life", *Artificial Life*, vol. 1, pp. - , 1994.

[22] P. Churchland and T. Sejnowski, *The Computational Brain*, MIT Press, Cambridge, Ma, 1992.

[23] R. Douglas, M. Mahowald, and C. Mead, "Neuromorphic analogue VLSI", *Annual Review of Neuroscience*, vol. 18, pp. 255 - 281, 1995.

[24] S. Sze, *Physics of Semiconductor Devices*, Wiley, New York, 1981.

[25] R. Eckhert and P. Brehm, "Ionic mechanisms of excitation in paramecium", *Annual Review of Biophysics and Bioengineering*, vol. 8, pp. 353 - 383, 1993.

[26] W. Westerman, D. Northmore, and J. Elias, "Neuromorphic synapses for artificial dendrites", *Analog Integrated Circuits and Signal Processing*, vol. 13, pp. 167 - 184, 1997.

[27] R. Douglas, M. Mahowald, and K Martin, "Neuroinformatics as explanatory neuroscience", *Neuroimage*, vol. 4, pp. S25 - S28, 1996.

[28] A. Kenny, *Frege*, Penguin, London, 1995.

[29] T. Sejnowski, C. Koch, and P. Churchland, "Computational neuroscience", *Science*, vol. 241, pp. 1299 - 1306, 1988.

[30] C. Foster, *Algorithms, Abstraction and Implementation: Levels of Detail in Cognitive Science*, Cognitive Science Series, London, 1990.

[31] J. Elias, "Artificial dendritic trees", *Neural Computation*, vol. 5, pp. 648 - 664, 1993.

[32] B. Mel, "Information processing in dendritic trees", *Neural Computation*, vol. 6, pp. 1031 - 1085 , 1994.

[33] J. Collins and S. Richmond, "Hard-wired central pattern generators for quadrupedal locomotion", *Biological Cybernetics*, vol. 71, pp. 375 - 385, 1994.

[34] M. Glover, A. Hamilton, and L. Smith, "Analogue VLSI integrate and fire neural network for clustering onset and offset signals in a sound segmentation

system", in L. Smith and A. Hamilton, editors, *Neuromorphic systems: engineering silicon from neurobiology.* World Scientific, Singapore, 1998.

[35] S. Wolpert and E. Micheli-Tzanakou, "A neuromime in VLSI", *IEEE Transactions on Neural Networks*, vol. 7, pp. 300 – 306, 1996.

[36] A. Destexhe, "Conductance-based integrate-and-fire models", *Neural Computation*, vol. 9, pp. 503 – 514, 1997.

[37] G. Patel and S. DeWeerth, "An analog VLSI morris-lecar neuron", *Electronics Letters*, vol. , in preparation.

[38] C. Canavier, R. Butera, R. Dror, D. Baxter, J. Clark, and J. Byrne, "Phase response characteristics of model neurons determine which patterns are expressed in a ring circuit model of gait generation", *Biological Cybernetics*, vol. 77, pp. 367 – 380, 1997.

[39] W. Rall, "Theory of physiological properties of dendrites", *Annals of the New York Academy*, vol. 96, pp. 1071 – 1092, 1962.

[40] W. Rall, "Theoretical significance of dendritic trees for neuronal input-output relations", in R. Reiss, editor, *Neural Theory and Modelling: Proceedings of the 1962 Ojai Symposium.* Stanford University Press, Stanford, California, 1962.

[41] W. Rall, "Distinguishing theoretical synaptic potentials computed for different soma-dendritic distributions of synaptic input", *Journal of Neurophysiology*, vol. 6, pp. 111 – 120, 1967.

[42] J. Elias, "Silicon dendritic trees", in J. Meador, editor, *Silicon Implementation of Pulse-Coded Neural Networks.* Kluwer Academic Press, 1994.

[43] J. Elias and D. Northmore, "Switched-capacitor neuromorphs with wide-range variable dynamics", *IEEE Transactions on Neural Networks*, vol. 6, pp. 1542 - 1546, 1995.

[44] D. Northmore and J. Elias, "Temporal processing in artificial dendritic tree neuromorphs", *Proceedings of the Twenty-Ninth Conference on Information Sciences and Systems*, vol. , pp. 345 - 349, 1995.

[45] D. Northmore and J. Elias, "Directionally selective artificial dendritic trees", *Proceedings of the World Congress on Neural Networks, Portland*, vol. , pp. 503 - 508, 1993.

[46] R. Llinas and M. Sugimori, "Electrophysiological properties of in vitro purkinje cell dendrites in mammalian cerebellar slices", *Journal of Physiology*, vol. 305, pp. 197 - 213, 1980.

[47] H. Markram and B. Sakmann, "Calcium transients in dendrites of neocortical neurons evoked by single subthreshold excitatory postsynaptic potentials via low-voltage-activated calcium channels", *Proc. Natl. Acad. Sci*, vol. 91, pp. 5207 - 5211, 1994.

[48] N. Spruston, Y. Schiller, G. Stuart, and B. Sakmann, "Activity-dependent action potential invasion and calcium influx into hippocampal cal dendrites", *Science*, vol. 268, pp. 297 - 300, 1995.

[49] J. Magee and D. Johnston, "Synaptic activation of voltage-gated channels in the dendrites of hippocampal pyramidal neurons", *Science*, vol. 268, pp. 301 - 304, 1995.

[50] G. Stuart and B. Sakmann, "Active propagation of somatic action potentials into neocortical pyramidal cell dendrites", *Nature*, vol. 367, pp. 69 - 72, 1994.

[51] I. Levitan and L. Kaczmarek, *The Neuron: Cell and Molecular Biology*, OUP, Oxford, 1991.

[52] G. Yellen, "Calcium channels: Structure and selectivity", *Nature*, vol. 366, pp. 109 - 110, 1993.

[53] B. Hille, "Ionic selectivity, saturation and block in sodium channels. a four-barrier model", *Journal of General Physiology*, vol. 66, pp. 535 - 560, 1975.

[54] J. Zhang, P. Ellinor, R. Aldrich, and R. Tsien, "Molecular determinants of voltage-dependent inactivation in calcium channels", *Nature*, vol. 372, pp. 97 - 100, 1994.

[55] M. Sansom, "Twist to open", *Current Biology*, vol. 5, pp. 373 - 375, 1995.

[56] G. Yellen, "Premonitions of ion channel gating", *Nature Structural Biology*, vol. 5, pp. 421, 1998.

[57] A. Fox, M. Nowycky, and R. Tsien, "Kinetic and pharmacological properties distinguishing three types of calcium currents in chick sensory neurons", *Journal of Physiology*, vol. 394, pp. 149 - 172, 1987.

[58] R. Tsien, D. Lipscombe, D. Madison, K. Bley, and A. Fox, "Multiple types of neuronal calcium channels and their selective modulation", *Trends in Neurosciences*, vol. 11, pp. 431 – 438, 1988.

[59] D. Lovinger, A. Merritt, and D. Reyes, "Involvement of n- and non-n-type calcium channels in synaptic transmission at corticostriatal synapses", *Neuroscience*, vol. 62, pp. 31 – 40, 1994.

[60] O. Krasilnikov, P. Merzliak, L. Yuldasheva, R. Nogueira, and C. Rodrigues, "Non stochastic distribution of single channels in planar lipid bilayers", *Biochimica et Biophysica Acta*, vol. 1233, pp. 105 – 110, 1995.

[61] M. Leonetti and E. Dubois-Violette, "Pattern formation by electro-osmotic self-organisation in flat biomembranes", *Physical Review E*, vol. 56, pp. 4521 – 4525, 1997.

[62] T. Takahashi and A. Momiyama, "Different types of calcium channels mediate central synaptic transmission", *Nature*, vol. 366, pp. 156 – 158, 1993.

[63] Z. Sheng, J. Rettig, T. Cook, and W. Catterall, "Calcium-dependent interaction of n-type calcium channels with the synaptic core complex", *Nature*, vol. 379, pp. 451 – 454, 1996.

[64] J. Jing, P. Aitken, and G. Somjen, "Role of calcium channels in spreading depression in rat hippocampal slices", *Brain Research*, vol. 604, pp. 251 – 259, 1993.

[65] I. Segev and W. Rall, "Computational study of an excitable dendritic spine", *Journal of Neurophysiology*, vol. 60, pp. 499 – 523, 1988.

[66] R. Yuste and W. Denk, "Dendritic spines as basic functional units of neuronal integration", *Nature*, vol. 375, pp. 682 - 684, 1995.

[67] M. Segal, "Fast imaging of intracellular calcium reveals presence of voltage-gated calcium channels in dendritic spines of cultured hippocampal neurons", *Journal of Neurophysiology*, vol. 74, pp. 484 - 488, 1995.

[68] J. Miller, W. Rall, and J. Rinzel, "Synaptic amplification by active membrane in dendritic spines", *Brain Research*, vol. 325, pp. 325 - 330 , 1985.

[69] D. Rusakov, M. Stewart, M. Sojka, G. Richter-Levin, and T. Bliss, "Dendritic spines form "collars" in hippocampal granule cells", *Neuroreport*, vol. 6, pp. 1557 - 1561, 1995.

[70] G. Schultz, W. Rosenthal, J. Hescheler, and W. Trautwein, "Role of G proteins in calcium channel modulation", *Annual Review of Physiology*, vol. 52, pp. 275 - 292, 1990.

[71] C. Pribe, S. Grossberg, and M. Cohen, "Neural control of interlimb oscillations: Biped and quadruped gaits and bifurcations", *Biological Cybernetics*, vol. 77, pp. 141 - 152, 1997.

[72] S. Wolpert, "A parametric examination of VLSI-based neuronal models of cyclic and reciprocal inhibition", *IEEE Transactions on Biomedical Engineering*, vol. 43, pp. 1164 - 1175, 1996.

[73] M. Ashley Ross, "Metamorphic and speed effects on hindlimb kinematics during terrestrial locomotion in the salamander *dicamptodon tenebrosus*", *Journal of Experimental Biology*, vol. 193, pp. 285 - 305, 1994.

[74] C. Farley and T. Ko, "Mechanics of locomotion in lizards", *The Journal of Experimental Biology*, vol. 200, pp. 2177 - 2188, 1997.

[75] S. Reilly and M. Delancey, "Sprawling locomotion in the lizard *sceloporus clarkii*: Quantitative kinematics of a walking trot", *The Journal of Experimental Biology*, vol. 200, pp. 753 - 765, 1997.

[76] R. Douglas and M. Mahowald, "A construction set for silicon neurons", *in An Introduction to Neural and Electronic Networks.* Academic Press, 1995.

[77] C. Rasche, R. Douglas, and M. Mahowald, "Characterisation of a silicon pyramidal neuron", in S Smith, L and A Hamilton, editors, *Neuromorphic systems: engineering silicon from neurobiology.* World Scientific, Singapore, 1998.

[78] C. Koch and I. (Eds.) Segev, *Methods in Neuronal Modeling*, MIT Press, Cambridge, 1995.

[79] O. Hamill and D. McBride, "Mechanogated channels in xenopus oocytes: Different gating modes enable a channel to switch from a phasic to a tonic mechanotransducer", *Biological Bulletin*, vol. 192, pp. 121 -122 , 1997.

[80] R. Hume and P. Getting, "Motor organisation of tritonia swimming. iii. contribution of intrinsic membrane properties to flexion neuron burst formation", *The Journal of Physiology*, vol. 47, pp. 91 - 102, 1982.

[81] R. Butera, J. Clark, and J. Byrne, "Dissection and reduction of a modeled bursting neuron", *Journal of Computational Neuroscience*, vol. 3, pp. 199 – 223, 1996.

[82] A. Brown, P. Schwindt, and W. Crill, "Voltage dependence and activation kinetics of pharmacologically defined components of the high–threshold calcium current in rat neocortical neurons", *Journal of Neurophysiology*, vol. 70, pp. 1530 – 1543, 1993.

[83] A. Gillies, "Electrical properties of subthalamic nucleus projection neurons", in Bower J, editor, *Computational Neuroscience.* Academic Press, New York, 1996.

[84] D. Mayes, "Pulsed VLSI for RBF neural networks", *in In Proceedings. Microneuro 96*, pp. 177 – 184. 1996.

[85] D. Mayes, *Implementing Radial Basis Function Neural Networks in Pulsed Analogue VLSI*, Phd thesis, University of Edinburgh, 1997.

[86] A. Thompson, "An evolved circuit, intrinsic in silicon, entwined in physics", *Proc. 1st Int. Conf. on Evolvable Systems (ICES96)*, vol. , 1996.

[87] A. Thompson, "On the automatic design of robust electronics through artificial evolution", *Proc. 2nd Int. Conf. on Evolvable Systems: From Biology to Hardware*, vol. , 1997.

[88] C. Davidson, "Creatures from primordial silicon", *New Scientist*, vol. November, pp. 30 – 34, 1997.

[89] P. Allen and D. Holberg, *CMOS Analog Circuit Design*, Holt, Rinehart and Winston, New York, 1987.